1985

Fully resonant four-wave mixing spectroscopy of pentacene and dye molecules in condensed phases

Ta-Chau Chang
Iowa State University

INFORMATION TO USERS

This reproduction was made from a copy of a document sent to us for microfilming. While the most advanced technology has been used to photograph and reproduce this document, the quality of the reproduction is heavily dependent upon the quality of the material submitted.

The following explanation of techniques is provided to help clarify markings or notations which may appear on this reproduction.

1. The sign or "target" for pages apparently lacking from the document photographed is "Missing Page(s)". If it was possible to obtain the missing page(s) or section, they are spliced into the film along with adjacent pages. This may have necessitated cutting through an image and duplicating adjacent pages to assure complete continuity.

2. When an image on the film is obliterated with a round black mark, it is an indication of either blurred copy because of movement during exposure, duplicate copy, or copyrighted materials that should not have been filmed. For blurred pages, a good image of the page can be found in the adjacent frame. If copyrighted materials were deleted, a target note will appear listing the pages in the adjacent frame.

3. When a map, drawing or chart, etc., is part of the material being photographed, a definite method of "sectioning" the material has been followed. It is customary to begin filming at the upper left hand corner of a large sheet and to continue from left to right in equal sections with small overlaps. If necessary, sectioning is continued again—beginning below the first row and continuing on until complete.

4. For illustrations that cannot be satisfactorily reproduced by xerographic means, photographic prints can be purchased at additional cost and inserted into your xerographic copy. These prints are available upon request from the Dissertations Customer Services Department.

5. Some pages in any document may have indistinct print. In all cases the best available copy has been filmed.

University Microfilms International
300 N. Zeeb Road
Ann Arbor, MI 48106

Chang, Ta-Chau

FULLY RESONANT FOUR-WAVE MIXING SPECTROSCOPY OF PENTACENE AND DYE MOLECULES IN CONDENSED PHASES

Iowa State University PH.D. 1985

PLEASE NOTE:

In all cases this material has been filmed in the best possible way from the available copy. Problems encountered with this document have been identified here with a check mark __✓__.

1. Glossy photographs or pages _____
2. Colored illustrations, paper or print _____
3. Photographs with dark background _____
4. Illustrations are poor copy _____
5. Pages with black marks, not original copy _____
6. Print shows through as there is text on both sides of page _____
7. Indistinct, broken or small print on several pages ✓
8. Print exceeds margin requirements _____
9. Tightly bound copy with print lost in spine _____
10. Computer printout pages with indistinct print _____
11. Page(s) _____ lacking when material received, and not available from school or author.
12. Page(s) _____ seem to be missing in numbering only as text follows.
13. Two pages numbered _____. Text follows.
14. Curling and wrinkled pages _____
15. Dissertation contains pages with print at a slant, filmed as received _____
16. Other _____

_____

_____

University
Microfilms
International

Fully resonant four-wave mixing spectroscopy of pentacene and dye molecules in condensed phases

by

Ta-Chau Chang

A Dissertation Submitted to the
Graduate Faculty in Partial Fulfillment of the
Requirements for the Degree of
DOCTOR OF PHILOSOPHY

Department: Chemistry
Major: Physical Chemistry

Approved:

Signature was redacted for privacy.

In Charge of Major Work

Signature was redacted for privacy.

For the Major Department

Signature was redacted for privacy.

For the Graduate College

Iowa State University
Ames, Iowa

1985

TABLE OF CONTENTS

GENERAL INTRODUCTION

The first observation of nonlinear optical behavior was reported by Franken et al. [1] in 1961. In their experiments, a ruby laser at λ = 6942 A illuminating a quartz crystal was used to obtain second harmonic generation of ultraviolet light at λ = 3471 A. This discovery opened the field of nonlinear optics. A theoretical study for optical wave mixing was developed by Armstrong et al. [2] in 1962. In general, the nonlinear optical behavior can be described by a power expansion of the polarization, P, in terms of the radiation field E [3],

$$P = X^{(1)} \cdot E + X^{(2)} : EE + X^{(3)} \vdots EEE + \ldots,$$

where $X^{(n)}$ are the microscopic susceptibilities. In the weak field limit, the linear term, $X^{(1)} \cdot E$, is dominant, and is responsible for the phenomena of linear absorption and induced emission [4]. At high radiation field strengths, the nonlinear terms become important. The first nonlinear susceptibility is $X^{(2)}$, which describes the phenomena of second harmonic generation [1] and difference frequency generation between two waves [5]. The second nonlinear susceptibility is $X^{(3)}$, which delineates stimulated Raman emission [6], two-photon absorption [7,8] and four-wave mixing [9,10]. Since the generation

of nonlinear optical behavior requires high field intensities, the development of high peak power pulsed tunable lasers has encouraged the study of this behavior. In this dissertation, we focus on four wave mixing spectroscopy, which includes coherent anti-stokes Raman spectroscopy (CARS) and coherent stokes Raman spectroscopy (CSRS), to study the nonlinear optical behavior of pentacene (PT) doped in naphthalene (NPH), cresyl violet perchlorate (CV) in polyacrylic acid (PAA) and cresyl violet perchlorate in polyvinyl carbazole (PVK).

Normal incoherent Raman scattering is the result of the oscillating electric dipole, P, induced by an external radiation field, E, with the coupling governed by the polarizability tensor, α, as shown in the equation $P = \alpha \cdot E$. This linear relation causes the molecule to oscillate at the same frequency as the incident radiation. Further, the polarizability tensor varies constantly as the molecule vibrates. The beat frequencies between the radiation frequency, ω, and the vibrational frequency, ω_v, yield the stokes Raman scattering at $(\omega - \omega_v)$ and anti-stokes Raman scattering at $(\omega + \omega_v)$. It is noted that Raman scattering is a two-photon process, but is not a nonlinear process [11]. One can obtain fruitful information about vibrational energy levels, molecular structure, molecular motion, etc. from Raman spectroscopy. However, Raman signals have a low conversion and collection efficiency, due to incoherence and isotropic

scattering, and can be difficult to discriminate from luminescene.

Nonlinear four-wave mixing (FWM) in which two laser beams with different frequencies (ω_1 and ω_2) are utilized provides a powerful method to generate the CARS ($\omega_1 > \omega_2$) and CSRS ($\omega_1 < \omega_2$) emissions at $\omega_4 = 2*\omega_1 - \omega_2$ governed by $X^{(3)}$. The enhancement of intensities in normal CARS and CSRS results from the frequency difference $|\omega_1 - \omega_2|$ being on resonance with an active vibrational frequency. Further, the coherent and, therefore, collimated CARS or CSRS signals can be effectively separated from background fluorescence and other unwanted signals by using spatial filtering. Coherent anti-stokes Raman scattering was first observed by Terhune and Maker [9,10]. After the tunable laser was developed, Levenson et al. [12] used this method to investigate the interference between nonresonant mixing and CARS, and to measure the magnitude of nonresonant contributions in diamond. At the same time, similar studies were done on calcite by Akhmanov et al. [13] and on a single crystal $LiNbO_3$ by Wynne [14]. Because of the large nonresonant background signal in normal CARS spectra, the study of an impurity embedded in a host is limited. Chabay et al. [15] first observed that the signal was enhanced when ω_1 approached an electronic transition. Multi-resonant CARS can not only eliminate the nonresonant background, but can also provide a more selective method for

spectroscopy. In recent years, both dispersive [16-23] and picosecond [24-29] FWM (CARS and CSRS) spectroscopies have been used to probe vibrations in condensed phase molecular systems.

The study of relaxation processes may elucidate details of the molecular motion and structure of the system. In the condensed phase, molecules or ions in an ensemble usually do not have the same local environments because of crystal inhomogeniety. Thus an appreciable spread in resonant frequencies is observed, which is the sum of the lineshapes of all oscillators with different frequencies. The information for relaxation processes is lost. Resonant enhancement and site selection methods have been introduced to high resolution nonlinear optical spectroscopy in order to reduce the inhomogeneous broadening [30]. Recently, Druet et al. [31] and Oudar and Shen [32] have theoretically estabilished the line narrowing ability for multi-resonant CSRS to yield Doppler-free resonances in the gas phase.

In many cases for polyatomic molecules, the triply resonant condition with the two additional resonances being vibronic [22] will force a multi-level system into behaving like a four-level system [33]. Then if the inhomogeneous site excitation distributions associated with the pertinent vibrational and vibronic resonances are appropriately correlated, line narrowing can be attained. With Doppler

broadening, there is complete and positive correlation between the resonances which also leads to the result that CARS resonances are not line narrowed. In solids, the situation is more complicated, the requisite correlations for line narrowing may not exist or if they do only partially. Nevertheless, because of our interest in optical dephasing in amorphous solids like glasses and polymers [34-36], it was the line narrowing potential of fully resonant four-wave mixing which initially triggered this work.

Prior to initiating studies on amorphous solids, we felt it important first to understand the details of fully resonant FWM better in a simpler system. To this end, we chose PT/NPH, primarily because a considerable amount of work in the time domain has been done by Duppen et al. [37] and Hesselink and Wiersma [38,39] on vibrational and vibronic dephasing of pentacene in this medium. In addition, pentacene in benzoic acid has been extensively studied by dispersive four-wave mixing by Andrews and Hochstrasser [20-21] and Bozio et al. [22].

The purpose of this dissertation is two-fold. In the first part, we study the general features for the third order nonlinear susceptibility in the four-level system and perform a variety of multi-resonant CARS and CSRS experiments on PT/NPH to examine the line narrowing. Tuning ω_1 to a vibronic resonance at ω_{ij} and scanning ω_2 to a vibrational resonance

at $\omega_{vo} = \omega_1 - \omega_2$ provide a fully double resonant and nearly triply resonant condition which theory argues is necessary for the observation of line narrowing [23,32,40]. At the same time, care must be taken to limit laser pulse intensities to sufficiently low values so that the dynamic stark effect will not broaden the linewidth, especially when $\omega_1 - \omega_{ij} = 0$ [21,23]. In addition, temperature studies show that at sufficiently high temperatures the dephasing-induced coherent emission (DICE) [20,21] can be significant and make line narrowing more difficult to observe [23]. In the present work, care was taken to optimize the conditions for line narrowing and, as a result, line narrowing was observed for the ground state vibrational mode of pentacene at 755 cm^{-1} in the CSRS experiments, at the conditions of $\omega_1 - \omega_{v'v} = 0.5$ cm^{-1} and (ω_1,ω_2) pulse energies of (1,0.75) μJ at T = 4.5 K. However, the linewidth after correction for the laser contributions yields vibrational dephasing time somewhat shorter (~20%) then the value obtained from a time domain study.

Further, the study of PT/NPH system yields interesting behavior in population inversion and other phenomena. The PT/NPH system appears to be unusual in that excited electronic state CARS resonances are observed for negative detunings, i.e., $\omega_1 < \omega_{0'0}$, which are large relative to the inhomogeneous linewidth of the $\omega_{0'0}$ transition. The subscripts 0' and 0 denote the zero-point vibrational levels of the excited and

ground electronic states. The subscripts v' and v label the vibration in its excited and ground states, respectively. Temperature-dependent studies indicate that the excited state population mechanism involves phonon hotband absorption. Novel temperature-dependent CARS data for positive detuning are presented and tentatively interpreted in terms of the interplay between DICE and the temperature dependence of the phonon sideband absorption building on the (0',0) band. Power broadening data for the ground state vibrational resonance at 755 cm^{-1} obtained for negative detunings are discussed in terms of dynamic Stark shifts resulting from the site inhomogeneous line broadening of vibronic transitions.

In the second part, we apply FWM to study the nonlinear optical behavior of ionic dyes in polymers. Very little work has appeared on resonant FWM spectroscopy of molecules doped in amorphous solids such as polymers. The excellent optical quality of polymers makes them attractive candidates. We chose cresyl violet perchlorate (CV) in polyacrylic acid (PAA), primarily because the nonphotochemical hole burned (NPHB) spectra of CV/PAA provided us with information on individual vibronic transitions[1]. One of our motivations for studying FWM of CV/PAA was to see whether the CARS and CSRS spectra would reveal line narrowing. None was observed for

---

[1]Provided by B. L. Fearey, Dept. of Chemistry, Iowa State University.

the CV resonance at 593 cm^{-1}. The absence of line narrowing in the CARS and CSRS spectra for the CV 593 cm^{-1} ground state resonance in PAA may be due to the large inhomogeneous linewidths of CV/PAA, which make the assumption of a four-level system questionable. Further, it will be argued that the linear electron-phonon interaction is an important mechanism for producing an egalitarian distribution of excited dye sites with a population sufficiently high to permit observation of the excited state resonance at 585 cm^{-1} which is the counterpart of the 593 cm^{-1} mode. In addition, the hole burning effect is used to observe changes in the absolute CARS intensities which support the assignment of the 585 cm^{-1} resonance to an excited state mode. We remark that these observed phenomena in CV/PAA were also observed in nile blue perchlorate (NB) in PAA.

However, the study of CV in polyvinyl carbazole (PVK) presented different features in the CARS spectra. We chose CV/PVK because nonphotochemical hole burning does not occur to a significant extent in this system[2]. The differences include that nonresonant background interferences occur with PVK and, generally, the excited state CV resonance at 586 cm^{-1} is markedly weaker than in PAA where the frequency is 585 cm^{-1}.

---

[2]Obtained by B. L. Fearey and T. P. Carter, Dept. of Chemistry, Iowa State University.

The nonresonant CARS contribution is shown to depend on the location of ω_1 within the CV absorption profile. In addition, data are presented which suggest that the inhomogeneously broadened absorption profile of CV in PVK may be the superposition of overlapping spectra due to two chemically distinct species. Temperature dependent CARS spectra are presented. Finally, the observed linewidths for the 593 cm^{-1} resonance are compared for PAA and PVK.

The arrangement of this dissertation follows the alternate style format. It begins with a "general introduction" to the four-wave mixing techniques. Theoretical background for $X^{(3)}$ and theories developed for the experimental results are given in "theory". Sample preparation, experimental set-up for CARS and other techniques involved in this work are described in "experiments". "Paper I" is the study of multiresonant four wave mixing spectroscopy of pentacene in naphthalene, which will be published in the Journal Physical Chemistry, June 1985. "Paper II" is the study of fully resonant CARS of cresyl violet in polyacrylic acid polymer films, which has been accepted for publication in Chemical Physics. The study of resonant CARS of cresyl violet in polyvinyl carbazole (PVK) polymer films is discussed in the "additional results and discussions". The dissertation ends with the "conclusion".

THEORY

Four-Wave Mixing Coherent Emission

We begin by considering the generation of FWM signals. For FWM (CARS and CSRS) experiments in which three laser beams with different frequencies (ω_1, ω_2 and ω_3) intersect inside the sample, a coherent outgoing wave with frequency $\omega_4 = \omega_1 - \omega_2 + \omega_3$ is generated. The intensity of the ω_4 wave depends on the degree to which the phase-matching condition, $\underline{k}_4 = \underline{k}_1 - \underline{k}_2 + \underline{k}_3$, is satisfied. Additional enhancement in normal CARS or CSRS arises when the frequency difference $|\omega_1 - \omega_2|$ equals a Raman active vibration frequency, vide infra. It is noted that the vibrational symmetry selection rules for CARS or CSRS are the same as for Raman. The polarization, P, for the outgoing beam can be derived from the following Maxwell's equation

$$\nabla^2 \cdot \underline{E}(\omega) + \frac{\omega^2}{c^2} \varepsilon(\omega) \cdot \underline{E}(\omega) = - \frac{4\pi\omega^2}{c^2} \underline{P}(\omega) \qquad (1)$$

where

$$\underline{E}(\omega) = \frac{\hat{e}}{2} \{\xi \cdot \exp[i(\underline{k} \cdot \underline{r} - \omega \cdot t)] + c.c.\}, \qquad (2)$$

$\hat{e}$ is the polarization vector, $\varepsilon(\omega)$ is the dielectric tensor and ξ is the amplitude of the wave with frequency ω. For a nonmagnetic medium, the polarization induced by an intense

field can be expanded into a power series in the field [5]

$$\underline{P} = \underline{\underline{X}}^{(1)} \cdot \underline{E} + \underline{\underline{X}}^{(2)} : \underline{E}\,\underline{E} + \underline{\underline{X}}^{(3)} \vdots \underline{E}\,\underline{E}\,\underline{E} + \ldots, \qquad (3)$$

where $X^{(n)}$ are microscopic susceptibilities. In the electric-dipole approximation the first nonlinear order susceptibility $X^{(2)}$ vanishes by symmetry in crystals possessing a center of inversion. However, the second nonlinear term, $X^{(3)}$, does not vanish for any symmetry group [41,42]. That is, the third rank tensor associated with $X^{(3)}$ will always possess certain non-zero elements. For isotropic medium, the field intensity is related to the electric field by

$$I = \frac{nc}{2\pi} |\underline{E}|^2, \qquad (4)$$

where n is the refractive index at the field frequency. An equation for the intensity of the FWM signal, $I(\omega_4)$, can be obtained from Eqs. 1 to 4 [30,43],

$$I(\omega_4) = \frac{2\pi\omega_4^2}{n^2 c} |X^{(3)}(\omega_4)|^2 |\xi_1|^4 |\xi_2|^2 L^2 \left(\frac{\sin[\Delta k \cdot L/2]}{\Delta k \cdot L/2}\right)^2, \qquad (5)$$

where L is the length over which the two laser beams intersect in the sample and $\Delta k = 2*k_1 - k_2 - k_4$ is the phase-mismatch factor. In order to maximize the FWM signal, the interaction length, L_I, of the two laser beams should be larger than the

sample length, L_S. From Fig. 1, L_I is directly related to the phase-matching angle, θ, and the beam diameter, d, which is given by

$$L_I = \frac{d}{2 \sin(\theta/2)}. \qquad (6)$$

If d is a constant, a small angle θ favors a large L_I. For d = 0.03 cm and $\theta = 1.2^o$, the calculated value of L_I is 1.4 cm, which is much larger than the value for samples L_S used in the present studies. Further, the coherence length of the laser is calculated by the light velocity divided by the laser band width [44], which is 2.2 cm in our laser system.

The second factor which can be used to enhance the FWM intensity is the phase mismatch Δk. If Δk is not equal to zero, the FWM signal is proportional to $L^2 \sin^2(\Delta k\, L/2)$ which has a maximum when $\Delta k\, L/2 = \pi/2$. It is useful to define a coherence length, $L_C = \pi/\Delta k$ [43]. If $L_C > L_S$, the generated signal increases as L_S increases. If $L_S > L_C$, the signal strength may decrease as L_S increases because of saturation effects [30]. In order to maximize L_C, it is necessary to minimize Δk. This can be achieved by adjusting the phase-matching angle, θ. The adjustment of the phase-matching angle is a very important factor in FWM experiments.

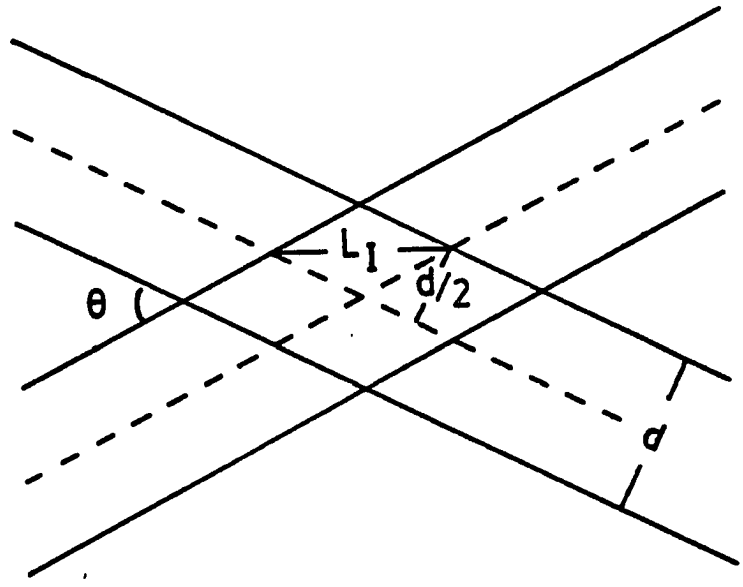

Figure 1. Phase-matching angle for the interaction of crossed beams.

Third-Order Nonlinear Susceptibility, $X^{(3)}$

The third factor involved in the FWM signal is the third order nonlinear susceptibility which describes the interaction between the fields and the medium. It depends, in part, on the details of the material resonances. Thus, experiments which probe the structure of $X^{(3)}$ can provide important spectroscopic information related to the energies and relaxation processes of excited states.

The nonlinear susceptibilities $X^{(n)}$ are frequency-dependent tensors which are defined by the constitutive relationship between the radiation field and the polarization, P. The determination of the constitutive relationship is based on the general principles of time-invariance with two restrictions, causality and reality, and intrinsic permutation symmetry [41,42]. For the n^{th}-order susceptibility tensor, the reality condition dictates that $[X^{(n)}(\omega;\omega_1,\omega_2,\ldots,\omega_n)]^* = X^{(n)}(-\omega^*;-\omega_1^*,-\omega_2^*,\ldots,-\omega_n^*)$. Causality ensures that $X^{(n)}(-t) = X^{(n)}(t=0)$ has a magnitude constant before the radiation field impinges on the medium. The intrinsic permutation symmetry property implies that $X_{u\alpha\beta\gamma\ldots}(\omega;\omega_1,\omega_2,\omega_3,\ldots)^{(n)}$ is invariant under all n! permutations of the pairs $\alpha\omega_1$, $\beta\omega_2$, $\gamma\omega_3,\ldots$, where $\alpha\beta\gamma$ are cartesian coordinates and ω_i are the frequencies of incident fields.

Nonlinear optical phenomena have been theoretically studied both by classical [41-43] and quantum mechanical

[3,30,41-43] approaches. Although the classical treatment suffices to illustrate the origin of nonlinear optical phenomena, the explicit derivation of expressions for $X^{(n)}$ requires a quantum mechanical approach. This is because the $X^{(n)}$ depend on the microscopic structure of the material resonances and the time-varying electromagnetic fields coupled with the time-varying fluctuations of the charge distribution in the medium. Thus, we reproduce the essential steps of the quantum mechanical calculation for the $X^{(n)}$ here by following the method of ref. [42] and expand on the discussion.

The calculation of $X^{(n)}$ begins by solving the equation of motion for the density matrix of the system

$$\dot{\rho} = -i\hbar^{-1}[H,\rho]. \tag{7}$$

The Hamiltonian H of the system is given by

$$H = H_0 + H_I, \tag{8}$$

where H_0 is the Hamiltonian for the unperturbed system with eigenstates $|j\rangle$ and eigenvalues W_j, i.e., $H_0|j\rangle = W_j|j\rangle$. H_I is the Hamiltonian for the interaction of radiation fields with the medium. In the electric dipole approximation, H_I is given by

$$H_I = \underline{u}\cdot\underline{E} \tag{9}$$

with $\underline{u}$ being the electric dipole moment operator. With adding the phenomenological damping term, Eq. 7 can be written as

$$\dot{\rho} = -i\hbar^{-1}[H_o+H_I,\rho] + (\dot{\rho})^R \tag{10}$$

In general, two different relaxation processes are involved in the damping term, which are pure dephasing and depopulation resulting from coupling to a thermal bath. Pure dephasing is analogous to transverse relaxation in nmr [45], which is a result of changes in phase coherence produced by fluctuations in the intermolecular potential. This is given by

$$(\dot{\rho})^R_{ij} = -\Gamma^*_{ij}\rho_{ij}. \tag{11}$$

Depopulation is analogous to longitudinal relaxation in nmr [45], which describes the processes of the population distribution from nonequilibrium to equilibrium. This is given by

$$(\dot{\rho})^R_{ii} = -\Gamma_{ii}\rho_{ii} + \sum_j \gamma_{ij}\rho_{jj}. \tag{12}$$

The phenomenological parameters for pure dephasing, depopulation and feeding are characterized by Γ^*_{ij}, Γ_{ii} and γ_{ij}, respectively. The phase relaxation between the states $|i\rangle$ and $|j\rangle$ is given by

$$\Gamma_{ij} = \frac{1}{2}\,(\Gamma_{ii} + \Gamma_{jj}) + \Gamma^{*}_{ij}. \tag{13}$$

In the absence of an external field, the system starts out in thermal equilibrium at temperature T. Thus, the density operator is given by

$$\rho_0 = \exp(-H_0/kT) \;/\; \mathrm{Tr}\{\exp(-H_0/kT)\}, \tag{14}$$

where k is the Boltzmann constant. When the radiation field interacts with the medium, the density operator ρ can be expressed in terms of a perturbation series analogous to the power expansion of the induced polarization in Eq. 3,

$$\rho = \rho^{(0)} + \rho^{(1)} + \rho^{(2)} + \ldots. \tag{15}$$

In general, Eq. 10 cannot be solved exactly. However, in the weak interaction limit, perturbation expansion of the density matrix in successive powers of H_I can be obtained by using a recursion relation and substituting Eq. 15 into Eq. 10,

$$\dot{\rho}^{(0)} = -i\hbar^{-1}[H_o,\rho^{(0)}] + (\dot{\rho}^{(0)})_R \tag{16a}$$

$$\dot{\rho}^{(1)} = -i\hbar^{-1}([H_0,\rho^{(1)}] + [H_I,\rho^{(0)}]) + (\dot{\rho}^{(1)})_R \tag{16b}$$

$$\dot{\rho}^{(2)} = -i\hbar^{-1}([H_0,\rho^{(2)}] + [H_I,\rho^{(0)}]) + (\dot{\rho}^{(2)})_R \tag{16c}$$

$$\ldots\ldots$$

$$\dot{\rho}^{(n)} = -i\hbar^{-1}([H_0,\rho^{(n)}] + [H_I,\rho^{(0)}]) + (\dot{\rho}^{(n)})_R. \tag{16d}$$

By introducing the unperturbed time-development operator,

$$U_0(t) = \exp[-iH_0 t/\hbar] \tag{17}$$

and defining

$$H_I(t) = U_0(-t)\cdot H_I \cdot U_0(t) \tag{18}$$

in the interaction picture, Butcher [42] employed an integrating factor to solve the density matrix as

$$\rho^{(n)}(t) = (i\hbar)^{-n} U_0(t)\cdot \int_{-\infty}^{t} dt_1 \int_{-\infty}^{t_1} dt_2 \cdots \int_{-\infty}^{t_{n-1}} dt_n \\ *[H_I(t_1),[H_I(t_2),[\ldots,[H_I(t_n),\rho_0]\ldots]]]\cdot U_0(-t). \tag{19}$$

Once the density matrix is known, the ensemble average of the electric polarization can be obtained as

$$\langle P\rangle = \mathrm{Tr}(\rho u), \tag{20}$$

which leads to

$$p^{(n)}(t) = (i\hbar)^{-n}\mathrm{Tr}\{U_0(t)\cdot \int_{-\infty}^{t} dt_1 \int_{-\infty}^{t_1} dt_2 \cdots \int_{-\infty}^{t_{n-1}} dt_n \\ *E(t_n)\ldots E(t_2)E(t_1)[u_\gamma(t_n),[\ldots,[u_\beta(t_2),[u_\alpha(t_1),\rho_0] \\ \ldots]]]\cdot U_0(-t)\ u\}, \tag{21}$$

where $\underline{u}$ is the electric dipole moment operator and $\alpha\beta\gamma$ are

cartesian coordinate indices. The n^{th}-order polarization can be expressed in the form

$$P^{(n)}(t) = \int_{-\infty}^{\infty} d\omega_1 \int_{-\infty}^{\infty} d\omega_2 \ldots \int_{-\infty}^{\infty} d\omega_n \, X^{(n)}(\omega;\omega_1,\omega_2,\ldots,\omega_n) \cdot E(\omega_1)E(\omega_2)\ldots E(\omega_n) \cdot \exp(-i\omega t). \tag{22}$$

By using a Fourier transformation

$$E(t) = \int_{-\infty}^{\infty} E(\omega)\exp(-i\omega t)\, d\omega, \tag{23}$$

the n^{th}-order susceptibility tensor can be calculated as

$$X^{(n)}(\omega;\omega_1,\omega_2,\ldots,\omega_n) = (-i\hbar)^{-n} \int_{-\infty}^{t} dt_1 \int_{-\infty}^{t_1} dt_2 \ldots \int_{-\infty}^{t_{n-1}} dt_n \, \mathrm{Tr}\{\rho_0[\ldots[[u,u_\alpha(t_1)],u_\beta(t_2)],\ldots,u_\gamma(t_n)]\}\exp[-i\sum_{m=1}^{n}\omega_m t_m]. \tag{24}$$

Bloembergen et al. [33] derived the expression of $X^{(3)}$ for a four-level system by using three radiation fields with frequencies ω_1, ω_2 and ω_3. A schematic diagram for the four-level system is shown in Fig. 2. Because of the time ordering in Eq. 24, $X^{(3)}$ contains six permutations of $E_1(t_i)$, $E_2(t_j)$ and $E_3(t_k)$. For $\rho_0 = 1$, $X^{(3)}$ contains 48 terms, which describe different physical nonlinear processes. Each term has three characteristic energy denominators which correspond to different resonant transitions.

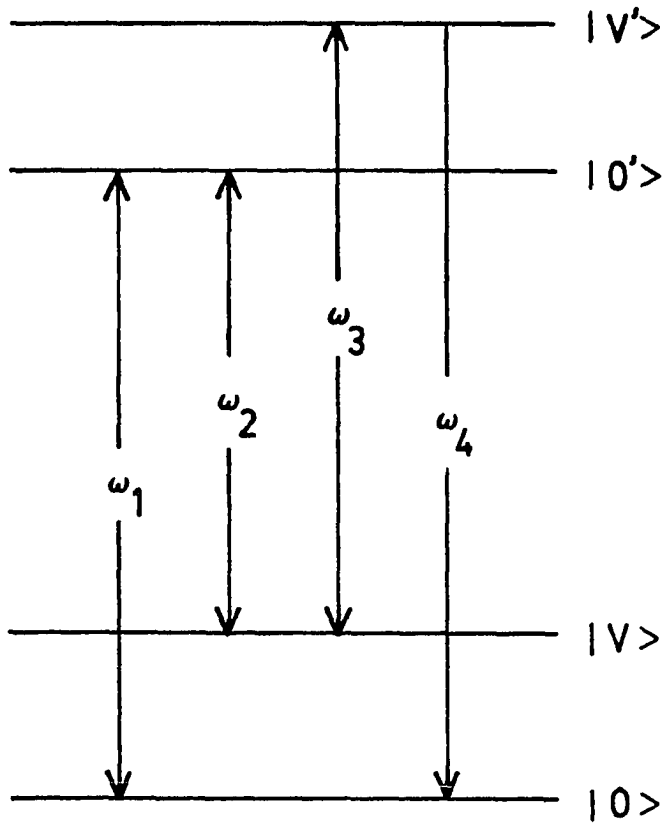

Figure 2. Energy diagram for a four level system.

$X^{(3)}$ for CARS ($\omega_1 > \omega_2$)

In this section we focus on the general features of $X^{(3)}$ in the four-level system for CARS. If one tunes $\omega_1 = \omega_{0',0}$, $\omega_2 = \omega_{0',v}$ and $\omega_3 = \omega_{v',v}$ as shown in Fig. 2, one obtains the most intense CARS signal; this condition is called fully (triply) resonant CARS. There is only one term out of 48 in the expression of $X^{(3)}$, which needs to be considered in the fully resonant CARS. This single term can be obtained from Appendix I of Ref. 33, and is given by

$$X^{(3)}(\omega_4) = \frac{C}{(\omega_{v',0}-\omega_4+i\Gamma_{v',0})\ (\omega_{v0}-\Delta+i\Gamma_{v0})\ (\omega_{0',0}-\omega_1+i\Gamma_{0',0})}, \quad (25)$$

where $C = -u^4_{0v'}u^3_{v',v}u^2_{v0'}u^1_{0',0}(6N^{-1}\hbar^3)^{-1}$ with u^{α}_{ij} being the vibronic transition moment between levels i and j associated with a photon of type α and N is a number density. It is defined that $\Delta = \omega_1 - \omega_2$. The three denominator terms correspond to different material resonances or transitions coupled to different fields, that is $\omega_{0',0}$ with ω_1, ω_{v0} with $(\omega_1 - \omega_2)$, and $\omega_{v',0}$ with the outgoing anti-stokes wave at $(2*\omega_1 - \omega_2)$.

For many molecules, the frequencies of corresponding vibrational modes in the ground and excited states are very similar; i.e., they usually agree to within a few wavenumbers. For a molecular mixed crystal like pentacene in naphthalene, where a specific ground state mode and its excited state

counterpart are probed, one can achieve further simplification by treating the problem in terms of a four-level system. Two laser beams with different frequencies ($\omega_1 = \omega_3$, and ω_2) were utilized in the present study to generate the CARS signals at $\omega_{as} = 2*\omega_1 - \omega_2$. By introducing the detuning parameter, $d = \omega_1 - \omega_{0',0}$, Eq. 25 can be rewritten in a more transparent way as

$$X^{(3)}(\omega_{as}) = \frac{C}{(-d+\omega_{v',0},-\Delta+i\Gamma_{v',0})\ (\omega_{v0}-\Delta+i\Gamma_{v0})\ (-d+i\Gamma_{0',0})}. \quad (26)$$

If ω_1 is fixed during the scan of ω_2, d is a constant but $(-d + \omega_{v',0},) - \Delta)$ and $(\omega_{v0} - \Delta)$ are variables. Further, if $-d = \omega_{v0} - \omega_{v',0},$, two resonant peaks should be observed with the linewidths governed by $2*\Gamma_{v0}$ and $2*\Gamma_{v',0}$ when ω_2 is scanned to generate the CARS resonances at $\Delta = \omega_{v0}$ and $\Delta = -d + \omega_{v',0},$, respectively. The ratio of their peak heights $I(\omega_{v0})$ / $I(-d + \omega_{v',0},)$ is approximately given by $(\Gamma_{v',0} / \Gamma_{v0})^2$, which is independent of the detuning. If $-d = \omega_{v0} - \omega_{v',0},$, two resonant peaks merge to yield a stronger line [31]. The peak position governed by the resonance at $(-d + \omega_{v',0},)$ is a result of the tuning of ω_1 and is referred to as a moveable peak or the moveable partner of the ω_{v0} resonance.

The above discussion of $X^{(3)}$ with $\rho_0 = 1$ is usually suitable for a large negative detuning (i.e., $\omega_1 < \omega_{0',0}$) in which the tuning of ω_1 is not able to build up the population

in the excited state. If $d \sim 0$, the population can be driven from the ground state to the excited state by the ω_1-field. For fully resonant CARS displayed in a discrete four-level system, a population redistribution among these four levels may occur. In order to examine this behavior, a kinetic approach with a steady-state approximation is used to determine the population among these four levels. A schematic diagram illustrating this is shown in Fig. 3. The rate equations are written as follows,

$$-\dot{\rho}_0 = R_1\rho_0 - R_1\rho_{0'} - \Gamma_{v0}\rho_v - R_4\rho_{v'} - k_{0',0}\rho_0, \tag{27a}$$

$$-\dot{\rho}_{0'} = -R_1\rho_0 + R_1\rho_{0'} - R_2\rho_v + R_2\rho_{0'} - \Gamma_{v',0'}\rho_{v'} + k_{0',v}\rho_{0'} + k_{0',0}\rho_{0'} \tag{27b}$$

$$-\dot{\rho}_v = R_2\rho_v - R_2\rho_{0'} + R_3\rho_v - R_3\rho_{v'} + \Gamma_{v0}\rho_v - k_{0',v}\rho_{0'} - k_{v',v}\rho_v, \tag{27c}$$

$$-\dot{\rho}_{v'} = -R_3\rho_v + R_3\rho_{v'} + \Gamma_{v',0'}\rho_{v'} + R_4\rho_{v'} + k_{v',v}\rho_{v'}, \tag{27d}$$

where R_i are induced rates which will be discussed later, $(\Gamma_{ij})^{-1}$ are vibrational relaxation times and $(k_{ij})^{-1}$ are fluorescence lifetimes. For PT/NPH, the fluorescence lifetime is about 20 ns and the vibrational relaxation time is about 100 ps, so k_{ij} can be neglected in Eq. 27. By using the steady-state approximation and $\rho_0 + \rho_v + \rho_{0'} + \rho_{v'} = 1$, Eq. 27

$$\rho_0 = [R_1(R_2+R_3+\Gamma_{v0})(R_3+\Gamma_{v',0'}) + R_2\Gamma_{v0}(R_3+\Gamma_{v',0'}) - R_1R_3^2] \,/\, \Lambda \tag{28a}$$

$$\rho_v = R_1R_2(R_3+\Gamma_{v',0'}) \,/\, \Lambda \tag{28b}$$

$$\rho_{0'} = [R_1(R_2+R_3+\Gamma_{v0})(R_3+\Gamma_{v'0'})-R_1R_3^2] \; / \; \Lambda \qquad (28c)$$

$$\rho_{v'} = R_1R_2R_3 \; / \; \Lambda \qquad (28d)$$

where

$$\Lambda = 2*R_1(R_2+R_3+\Gamma_{v0})(R_3+\Gamma_{v'0'})+(R_3+\Gamma_{v'0'})(R_2\Gamma_{v0}+R_1R_2)$$

$$+R_1R_2R_3-2*R_1R_3^2. \qquad (28e)$$

The calculated population distributions among these four levels for different R_i are given in Table 1. The results indicate that the populations ρ_v and $\rho_{v'}$ are negligible when $\Gamma_{ij} > R_1 > R_2$. Further, it is always true that $\rho_0 > \rho_{0'}$. In addition, an increase in the rate R_1 favors an increase in the $\rho_{0'}$, but an increase in the rate R_2 favors an increase in the ρ_0.

When the populations ρ_0 and $\rho_{0'}$ are both considered, the pertinent terms of $X^{(3)}(\omega_{as})$ which need to be addressed in the fully resonant condition are given by

$$X^{(3)}(\omega_{as}) = C \left[\frac{\rho_0}{(\omega_{v'0}-\omega_{as}+i\Gamma_{v'0})(\omega_{v0}-\Delta+i\Gamma_{v0})(\omega_{0'0}-\omega_1+i\Gamma_{0'0})}\right.$$

$$+ \frac{\rho_{0'}}{(\omega_{v'0}-\omega_{as}+i\Gamma_{v'0})} \left\{\frac{1}{(\omega_{v'0'}-\Delta+i\Gamma_{v'0'})(\omega_{0'v}-\omega_2-i\Gamma_{0'v})}\right.$$

$$- \frac{1}{(\omega_{v0}-\Delta+i\Gamma_{v0})(\omega_{0'0}-\omega_1+i\Gamma_{0'0})}$$

$$\left.\left. + \frac{1}{(\omega_{v0}-\Delta+i\Gamma_{v0})(\omega_{0'v}-\omega_2-i\Gamma_{0'v})} \right\}\right]. \qquad (29)$$

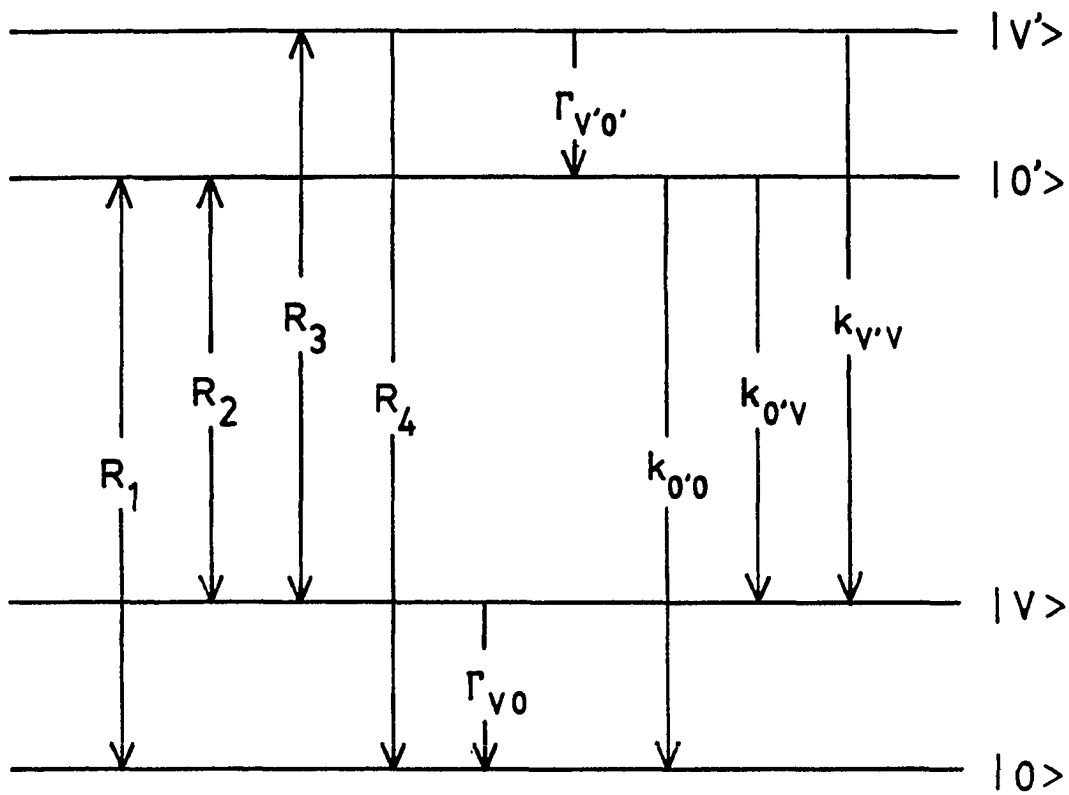

Figure 3. Energy levels and kinetics model used to calculate population distributions for a four level system.

Table 1. Theoretical calculation of population distributions for a four-level system

Cases	$R_1=R_3$	R_2	Γ_{ij}	ρ_0	ρ_v	$\rho_{0'}$	$\rho_{v'}$
	$x10^9$	$x10^9$	$x10^{11}$		%		
1	2	.1	1	51.17	0.05	48.78	~0
2	2	1	1	59.53	0.39	40.07	0.01
3	10	1	1	51.93	0.43	47.60	0.04
4	10	10	1	62.76	2.86	34.11	0.26
5	100	10	1	49.28	2.90	46.38	1.45

When the detuning parameter d is introduced, Eq. 29 can be rewritten in the form [22]

$$X^{(3)}(\omega_{as}) = \frac{C}{-d+i\Gamma_{0',0}}\left[\frac{\rho_0}{(\omega_{v',0}-d-\Delta+i\Gamma_{v',0'})(\omega_{v0}-\Delta+i\Gamma_{v0})}\right.$$

$$-\frac{\rho_{0'}}{(\omega_{v0}+d-\Delta+i\Gamma_{0',v})(\omega_{v',0}-\Delta+i\Gamma_{v',0'})}\left\{1+\frac{i\Gamma_1}{\omega_{v',0}-d-\Delta+i\Gamma_{v',0}}\right.$$

$$\left.\left.+\frac{i\Gamma_2(\omega_{v',0}-\Delta+i\Gamma_{v',0'})}{(\omega_{v',0}-d-\Delta+i\Gamma_{v',0})(\omega_{v0}-\Delta+i\Gamma_{v0})}\right\}\right], \qquad (30)$$

where $\Gamma_1 = \Gamma_{0'0} + \Gamma_{v'0'} - \Gamma_{v'0}$ and $\Gamma_2 = \Gamma_{0'v} + \Gamma_{0'0} - \Gamma_{v0}$. Two more resonances at $\Delta = \omega_{v'0'}$ and $\Delta = d + \omega_{v0}$ due to the addition of $\rho_{0'}$ are present. They correspond to the excited electronic state vibrational resonance at $\omega_{v'0'}$ which is the counterpart of the ground state mode at $\Delta = \omega_{v0}$ and its moveable partner at $\Delta = d + \omega_{v0}$. Their linewidths are $2*\Gamma_{v'0'}$ and $2*\Gamma_{0'v}$, respectively. Bozio et al. [22] have emphasized that in the low temperature limit, where pure dephasing is negligible, $\Gamma_1 = \Gamma_2 = \Gamma_{0'} \sim 0$. With reference to Eq. 30, it is suggested that the contributions to the peak intensities from ρ_0 to the resonances on $\Delta = \omega_{v'0'}$ and $\Delta = d + \omega_{v0}$ and from $\rho_{0'}$ to the resonances on $\Delta = \omega_{v0}$ and $\Delta = -d + \omega_{v'0'}$ can be neglected. Table 2 is given as confirmation of this result. Simulated calculations from Eq. 29 with varying ρ_0 and $\rho_{0'}$ are shown in Fig. 4. It is concluded that the peak heights for their peak positions are given by

$$I(\omega_{v0}) : I(-d + \omega_{v'0'}) : I(\omega_{v'0'}) : I(d + \omega_{v0})$$

$$= (\rho_0/\Gamma_{v0})^2 : (\rho_0/\Gamma_{v'0})^2 : (\rho_{0'}/\Gamma_{v'0'})^2 : (\rho_{0'}/\Gamma_{0'v})^2 \qquad (31)$$

for $d > \Gamma_{ij}$ in the low temperature limit.

Table 2. Examination of Γ_1 and Γ_2 contribution to Equation 30

CARS	[I]	[II][a]	[III][b]
Δ	ρ_0	$\rho_{0'}$	$\rho_{0'}$
ω_{v0} (GS)	$\frac{1}{d(\delta^{*}+d)\ i\Gamma_{v0}}$	$\frac{-1}{d(\delta+d)\ \delta}$	$\frac{-1}{d^2\ \delta}$
$\omega_{v'0'}$ (ES)	$\frac{1}{d^2\ \delta}$	$\frac{-1}{d^2(\delta+d)} + \frac{1}{d\ (\delta+d)\ i\Gamma_{v'0'}}$	$\frac{1}{d+(\delta+d)\ i\Gamma_{v'0'}}$
$-d+\omega_{v'0'}$ (GM)	$\frac{-1}{d(\delta+d)\ i\Gamma_{v'0}}$	0	$\frac{1}{d^2\ (\delta+2d)}$
$d+\omega_{v0}$ (EM)	$\frac{-1}{d^2(\delta+2d)}$	$\frac{1}{d^2(\delta+2d)} - \frac{1}{d(\delta+d)\ i\Gamma_{v0'}}$	$\frac{-1}{d(d+\delta)\ i\Gamma_{v0'}}$

CSRS	[I]	[II]	[III]
Δ	$\rho_{0'}$	ρ_0	ρ_0
$-\omega_{v0}$ (GS)	$\frac{-1}{d^2\ \delta}$	$\frac{-1}{d(d+\delta)\ i\Gamma_{v0}} + \frac{1}{d^2(d+\delta)}$	$\frac{-1}{d(d+\delta)\ i\Gamma_{v0}}$
$-\omega_{v'0'}$ (ES)	$\frac{-1}{d(\delta+d)\ i\Gamma_{v'0'}}$	$\frac{1}{d\ \delta(\delta+d)}$	$\frac{-1}{d^2\ \delta}$
$d-\omega_{v'0'}$ (GM)	$\frac{1}{d^2(2d+\delta)}$	$\frac{-1}{d^2(2d+\delta)} + \frac{1}{d(d+\delta)\ i\Gamma_{v'0}}$	$\frac{1}{d(d+\delta)\ i\Gamma_{v'0}}$
$-d-\omega_{v0}$ (EM)	$\frac{1}{d(d+\delta)\ i\Gamma_{0'v}}$	0	$\frac{-1}{d^2(2d+\delta)}$

[a] [I] x ρ_0 + [II] x $\rho_{0'}$ = Eq. 29 = Eq. 30.
[b] [I] x ρ_0 + [III] x $\rho_{0'}$ = Eq. 30 with $\Gamma_1 = \Gamma_2 = 0$.
* $\delta = \omega_{v0} - \omega_{v'0'}$.

Figure 4. Simulated calculation based on Eq. 29 to illustrate the prediction of Eq. 31 for the peak height. Profiles a - d were calculated with $(\rho_0,\rho_{0'})$ density matrix elements of (0.8,0.2), (0.7,0.3), (0.6,0.4) and (0.5,0.5), respectively. Damping parameters of Γ_{v0}, $\Gamma_{v'0'}$, $\Gamma_{0'0}$, $\Gamma_{v'0}$ and $\Gamma_{0'v}$ were 0.06, 0.08, 0.01, 0.12, 0.12 cm^{-1}, respectively.

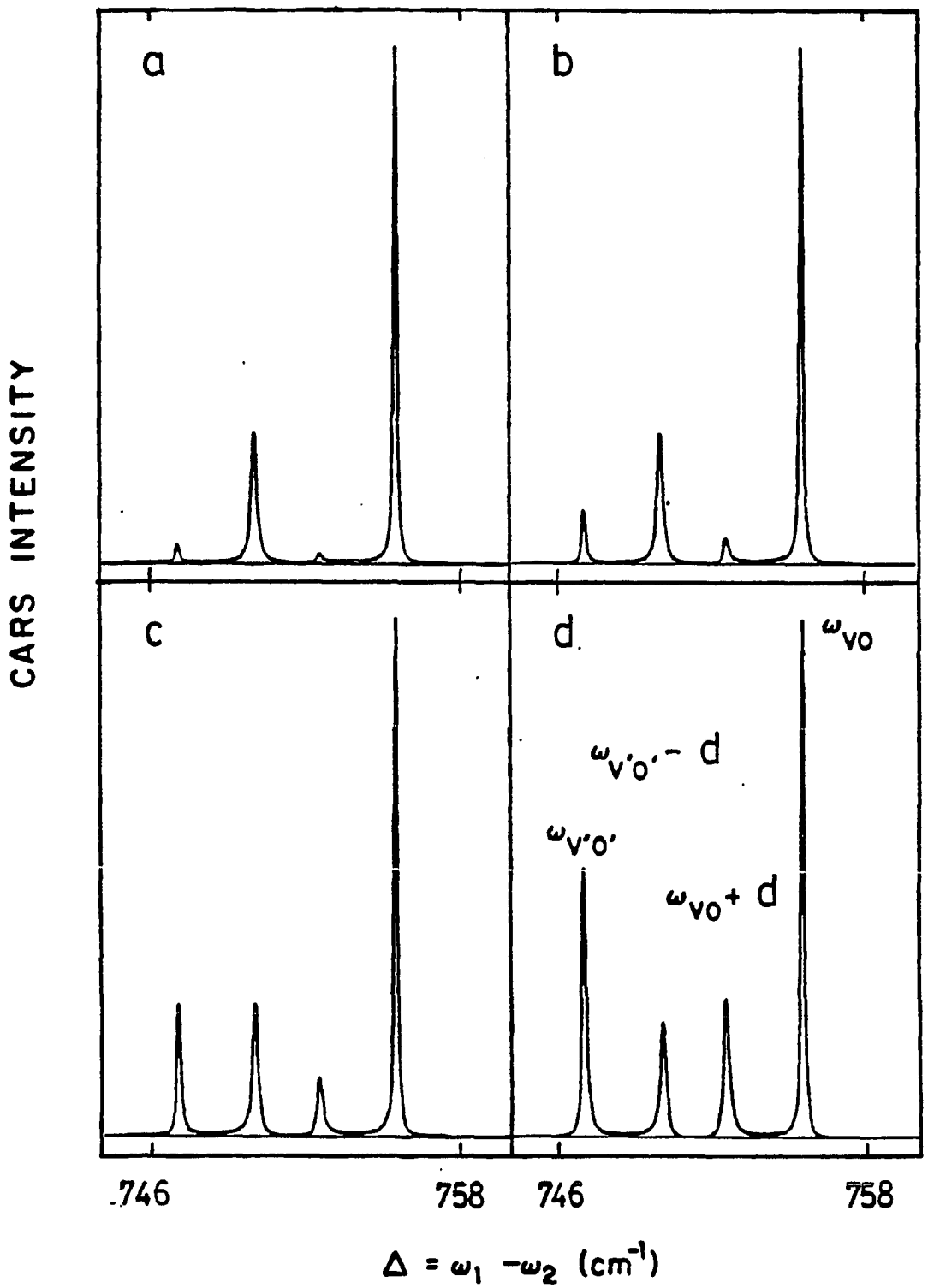
a
b
c
d
ω_{v0}
$\omega_{v'0'} - d$
$\omega_{v'0'}$
$\omega_{v0} + d$
CARS INTENSITY
746
758
746
758
$\Delta = \omega_1 - \omega_2$ (cm^{-1})

$X^{(3)}$ for CSRS ($\omega_1 < \omega_2$)

The same derivation and discussion are applied to $X^{(3)}(\omega_s)$ for the system of PT/NPH, where $\omega_s = 2*\omega_1 - \omega_2$ with $\omega_1 < \omega_2$ in CSRS. With the condition $\rho_0 + \rho_{0'} = 1$ for the four-level system, the equation for $X^{(3)}(\omega_s)$ is given by

$$X^{(3)}(\omega_s) = \frac{C'}{-d+i\Gamma_{0'0}} \left[\frac{\rho_{0'}}{(-d-\omega_{v0}-\Delta+i\Gamma_{0'v})(\omega_{v'0'}+\Delta-i\Gamma_{v'0'})} \right.$$

$$+ \frac{\rho_0}{(\omega_{v0}+\Delta+i\Gamma_{v0})(-d+\omega_{v'0'}+\Delta-i\Gamma_{v'0})} \left\{ 1 + \frac{i\Gamma_1'}{-d-\omega_{v0}-\Delta+i\Gamma_{0'v}} \right.$$

$$\left. \left. - \frac{i\Gamma_2'(\omega_{v0}+\Delta-i\Gamma_{v0})}{(\omega_{v'0'}+\Delta-i\Gamma_{v'0'})(-d-\omega_{v0}-\Delta+i\Gamma_{0'v})} \right\} \right], \qquad (32)$$

where $C' = -u^s_{v0}u^1_{0'0}u^2_{0v}u^1_{v'v}(6N^{-1}\hbar^3)^{-1}$, $\Gamma_1' = \Gamma_{0'v} - \Gamma_{v0} - \Gamma_{0'0}$ and $\Gamma_2' = \Gamma_{v'0} + \Gamma_{0'0} - \Gamma_{v'0'}$. According to Table 2 the same results for the peak heights are concluded for CSRS as for CARS. With reference to Eq. 32, it is noticed that the peaks at $-\Delta = \omega_{v'0'}$ and $-\Delta = d + \omega_{v0}$ may be present, even when $\rho_{0'}=0$ in CSRS, when temperature is increased. In the low temperature limit pure dephasing is negligible [22], which means that $\Gamma_1' = \Gamma_2' \sim 0$, and that the peaks at $-\Delta = \omega_{v'0'}$ and $-\Delta = d + \omega_{v0}$ will not be observed ($\rho_{0'} \sim 0$). However, $\Gamma_{0'0}$, $\Gamma_{v'0}$ and $\Gamma_{0'v}$ are quite sensitive to temperature, but Γ_{v0} and $\Gamma_{v'0'}$ are slowly varying functions of temperature in the temperature range studied here [39]. The increase of temperature

magnifies the value of Γ_2', which induces these two peaks. This phenomenon was observed and interpreted by dephasing-induced coherent emission (DICE) [20,21] which is analogous to PIER-4 in the gas phase [46-48].

Linewidths of Resonances

The contributions to the lineshape in the spectral sense are characterized by two categories; homogeneous and inhomogeneous broadening. Homogeneous lineshape broadening is primarily caused by two different processes. They are pure dephasing and depopulation. Since a molecule is weakly coupled to a thermal reservoir, intermolecular interactions may perturb the phase of the wave function of the excited molecule without changing its frequency. This process is called pure dephasing. Another process, depopulation, is due to the phase coherence loss arising from the population change between their transition levels. This process is also independent of frequency. The collection of these identical oscillators in absorption or emission of radiation yields a homogeneous line profile. However, crystal inhomogeneities provide different local fields surrounding the excited molecules. These produce different frequencies due to their different environments. The collection of lineshapes from these different frequencies forms an inhomogeneous line profile. Thus, the dynamic behavior of the field-matter

interaction is obscured. One of the purposes of this work is to examine whether the four-wave mixing technique would reveal line narrowing.

Druet et al. [31] and Oudar and Shen [32], using multi-resonant CSRS (or CARS) processes, have examined theoretically the possibility of line narrowing in order to reduce the Doppler broadening in the gas phase. They suggested that the signs of the damping parameters play an important role in determining which multi-resonant CSRS (or CARS) processes give Doppler-free line profiles. In the condensed phase, Dick and Hochstrasser [40] have studied the fully resonant $X^{(2)}$ spectroscopies to examine the possibility of narrowing inhomogeneous lineshapes. They have illustrated that line narrowing can be attained for the existence of special correlations between the resonances. Further, Bozio et al. [22] have utilized the time-ordered interaction sequences in Fig. 5 to illustrate that only those terms can be line narrowed which have both solid and dashed arrows.

We have extended their treatment [40] to $X^{(3)}$, especially when Lorentzians are used to describe the distributions for site excitation energies. $X^{(3)}$ can be calculated by averaging the susceptibility over the inhomogeneous distribution, $g(\omega)$. The ensemble average of $X^{(3)}$ is given by

$$\langle X^{(3)} \rangle = \int d\omega \, X^{(3)}(\omega) g(\omega), \qquad (33)$$

where

$$g(\omega) = \frac{\sigma}{\pi} \frac{1}{\omega^2+\sigma^2} , \quad \sigma > 0 \tag{34}$$

and σ is the half width of the distribution function. The residue method [31] is then applied to perform the integration over ω. According to the above discussion of Table 2, the contributions of Γ_1 and Γ_2 to CARS and Γ_1' and Γ_2' to CSRS are negligible in the low temperature limit. For simplicity, we utilize Eqs. 30 and 32 with $\Gamma_1 = \Gamma_2 = \Gamma_1' = \Gamma_2' = 0$ to investigate the possibility of line narrowing in the condensed phase.

Noting that $d = \omega_1 - \omega_{0'0}$, we define $x = \omega_{v0} - \omega_{v0}^0$, $y = \omega_{v'0} - \omega_{v'0}^0$ and $z = \omega_{0'0} - \omega_{0'0}^0$ as the shifts of the transition frequencies away from their mean values. In the absence of a correlation between these statistical variables, line narrowing in CARS (or CSRS) is not possible. The simplest situation is complete correlation where $y = \alpha x$ and $z = \beta x$, α and β are constants. It follows that the two remaining resonances are then automatically correlated; $\gamma x = (\alpha - \beta)x = \omega_{v'0'} - \omega_{v'0}^0$, and $(\beta - 1)x = \omega_{0'v} - \omega_{0'v}^0$. Whether or not a particular term of CARS or CSRS yields line narrowing depends on its pole structure and, therefore, the relative signs of its correlation coefficients.

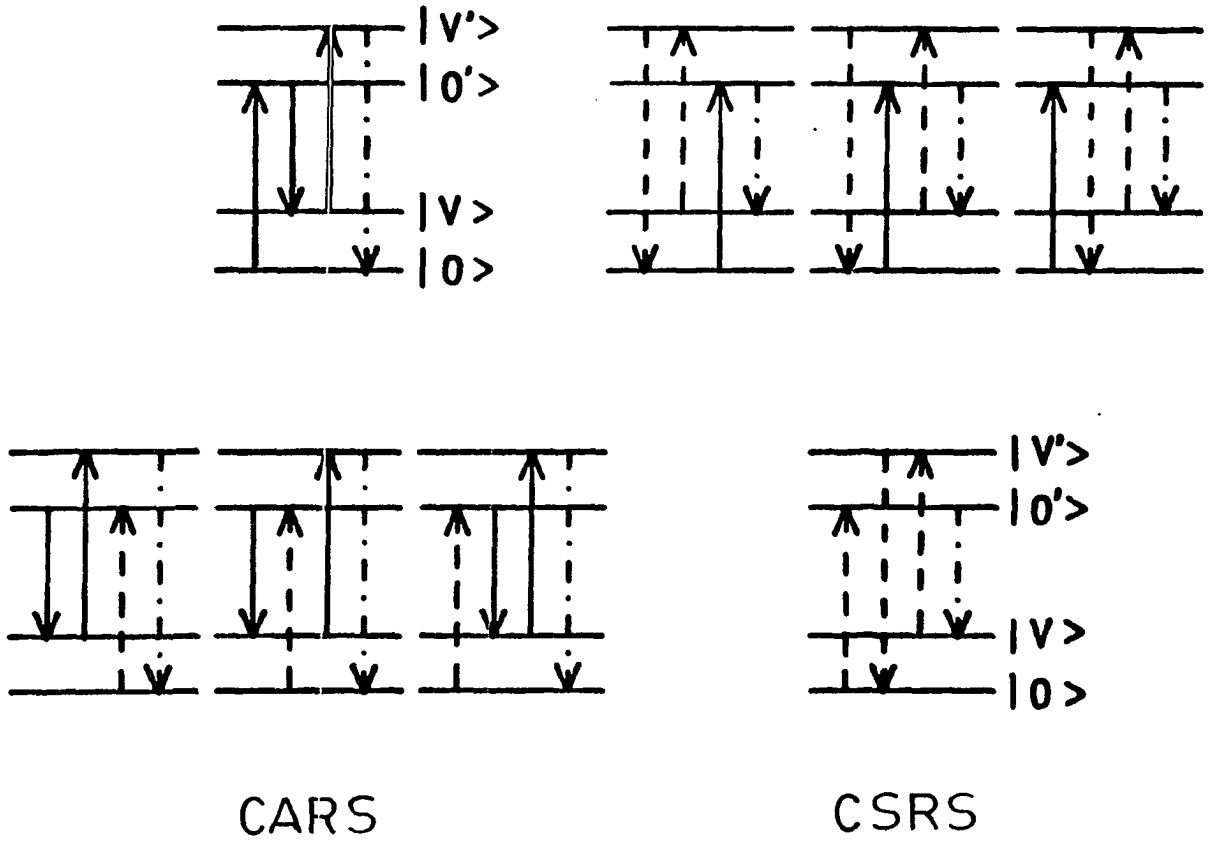

Figure 5. Schematic diagrams for time ordered interaction sequences for CARS and CSRS (Time ordering is from left to right in each spectrum).

There are a large number of possibilities for line narrowing. We intend to limit them by considering only the most likely ones for mixed molecular crystals and, specifically, the level structure of Fig. 5. First, if α, β, $\beta-1$, $\gamma > 0$ (complete positive correlation) and if we introduce for compactness the symbols S, S', M, M' as defined in Table 3, one finds that ($d^0 = \omega_1 - \omega^0_{0',0}$)

$$\langle X^{(3)}(\omega_{as})\rangle_I = C \{ \frac{-\rho_0}{[M+i(\Gamma_{v',0}+\alpha\sigma)][S+i(\Gamma_{v0}+\sigma)][d^0-i(\Gamma_{0',0}+\beta\sigma)]}$$

$$+ \frac{\rho_{0'}}{[M'+i(\Gamma_{0',v}-(\beta-1)\sigma)][S'+i(\Gamma_{v',0'}+\gamma\sigma)][d^0-i(\Gamma_{0',0}+\beta\sigma)]}$$

$$+ \frac{2i\sigma}{(\beta-1)^{-2}} \times \frac{\rho_{0'}}{[M'+i(\Gamma_{0',v}+(\beta-1)\sigma)][M'+i(\Gamma_{0',v}-(\beta-1)\sigma]}$$

$$\times \frac{1}{[\beta(\beta-1)^{-1}(M'+i\Gamma_{0',v})-d^0+i\Gamma_{0',0}]}$$

$$\times \frac{1}{[S'+i(\Gamma_{v',0'}+\gamma(\beta-1)^{-1}\Gamma_{0',v})+\gamma(\beta-1)^{-1}M']} \} \quad (35)$$

Thus, ω_{v0} from ρ_0 is not line narrowed while $\omega_{v',0'}$ from $\rho_{0'}$ is predicted to be narrowed to an extent governed by the magnitude of $\gamma(\beta - 1)^{-1}\Gamma_{0',v}$. For $\gamma(\beta - 1)^{-1} \ll 1$, and T sufficiently low to render pure electronic dephasing sufficiently small, the linewidth of the stationary resonance (S') $\omega_{v',0'}$ can yield $\Gamma_{v',0'}$, the vibrational dephasing. How

Table 3. Definition of terms for line narrowing expressions

Term	Definition[a]
S	$\omega^0_{v0} \mp \Delta$
S′	$\omega^0_{v'0'} \mp \Delta$
M	$\omega^0_{v'0'}-d^0 \mp \Delta$
M′	$\omega^0_{v0}+d^0 \mp \Delta$

[a]Minus and plus signs correspond to CARS and CSRS, respectively; $\Delta = \omega_1-\omega_2$; $d^0 = \omega_1-\omega^0_{0'0}$.

readily this occurs depends on the non-line narrowed $\omega_{v'0'}$ interference from the second term in Eq. 35. For $\gamma\sigma >> \Gamma_{v'0'}$, there would be no difficulty. We note that the moveable resonances (M, M′) are not line narrowed in CARS or CSRS, irrespective of the type of the correlation assumed.

If $\alpha,\beta < 0$ and $\gamma > 0$, we find

$$\langle x^{(3)}(\omega_{as})\rangle_{III} = C \{ \frac{-\rho_0}{[M+i(\Gamma_{v',0}-\alpha\sigma)][S+i(\Gamma_{v0}-\sigma)][d^0-i(\Gamma_{0',0}-\beta\sigma)]}$$

$$+ \frac{2i\sigma}{\alpha\beta} \times \frac{\rho_0}{[S+i(\Gamma_{v0}+\sigma)][S+i(\Gamma_{v0}-\sigma)]}$$

$$\times \frac{1}{[S+i(\Gamma_{v0}-\alpha^{-1}\Gamma_{v',0})-\alpha^{-1}M][S+i(\Gamma_{v0}-\beta^{-1}\Gamma_{0',0})+\beta^{-1}d^0]}$$

$$+ \frac{\rho_{0'}}{[M'+i(\Gamma_{v',0}-(\beta-1)\sigma)][S'+i(\Gamma_{v',0},+\gamma\sigma)][d^0-i(\Gamma_{0',0}+\beta\sigma)]}$$

$$+ \frac{2i\sigma}{\beta^{-2}} \times \frac{\rho_{0'}}{[d^0-i(\Gamma_{0',0}-\beta\sigma)][d^0-i(\Gamma_{0',0}+\beta\sigma)]}$$

$$\times \frac{1}{[\beta^{-1}(\beta-1)(d^0-i\Gamma_{0',0})-(M'+i\Gamma_{0',v})]}$$

$$\times \frac{1}{[S'+i(\Gamma_{v',0},-\gamma\beta^{-1}\Gamma_{0',0})+\gamma\beta^{-1}d^0]} \}. \qquad (36)$$

The situation is quite different from the previous case because there is line narrowing for ω_{v0} (to an extent limited by $\alpha^{-1}\Gamma_{v',0}$ and $\beta^{-1}\Gamma_{0',0}$, second ρ_0 term of Eq. 36). Again, line narrowing is predicted for the $\omega_{v',0}$, resonances. It is always the case that a line narrowed term is interfered by the corresponding non-line narrowed term and the moveable resonant terms. However, these will not pose a serious problem because the inhomogeneous vibronic linewidths are sufficiently broad

and the vibronic dephasing sufficiently small. It is noticed that $-(\alpha^{-1}M)$ and $\beta^{-1}d^0$ are line shifts for the line narrowed w_{v0} resonance in Eq. 36, which may cause a serious interference to obscure the line narrowing. For a specific case, $\alpha = \beta = 100$, $d^0 = 0$ so that $M = 8\ cm^{-1}$ in our system, and the difference between these two shifts is $0.08\ cm^{-1}$. This value is comparable to the value of the linewidth, which makes line narrowing ambiguous for the ω_{v0} resonance. Turning now to CSR S, we give here only the result for complete positive correlation, which is given by

$$\langle x^{(3)}(\omega_s)\rangle_I = C' \{ \frac{-\rho_0}{[M+i(\Gamma_{v',0}+\alpha\sigma)][S+i(\Gamma_{v0}+\sigma)][d^0+i(\Gamma_{0',0}-\beta\sigma)]}$$

$$+ \frac{2i\sigma}{\beta^{-2}} \times \frac{\rho_0}{[d^0+i(\Gamma_{0',0}+\beta\sigma)][d^0+i(\Gamma_{0',0}-\beta\sigma]}$$

$$\times \frac{1}{[S+i(\Gamma_{v0}+\beta^{-1}\Gamma_{0',0})+\beta^{-1}d^0][\alpha\beta^{-1}(d^0+i\Gamma_{0',0})+M+i\Gamma_{v',0}]}$$

$$+ \frac{\rho_{0'}}{[M'+i(\Gamma_{0',v}+(\beta-1)\sigma)][S'+i(\Gamma_{v',0'}-\gamma\sigma)][d^0+i(\Gamma_{0',0}+\beta\sigma)]}$$

$$- \frac{2i\sigma\gamma^4}{\beta(\beta-1)} \times \frac{\rho_{0'}}{[S'+i(\Gamma_{v',0'}-\gamma\sigma)][S'+i(\Gamma_{v',0'}+\gamma\sigma)]}$$

$$\times \frac{1}{[S'+i(\Gamma_{v',0'}+\gamma\beta^{-1}\Gamma_{0',0})+\gamma\beta^{-1}d^0]}$$

$$\times \frac{1}{[S'+i(\Gamma_{v',0'}+\gamma(\beta-1)^{-1}\Gamma_{0',v})+\gamma(\beta-1)^{-1}M']} \}. \qquad (37)$$

In contrast with CARS, line narrowing is predicted for the ω_{v0} resonance from ρ_0. The $\omega_{v',0}$, resonance from ρ_0, is also line narrowed. The line shifts for the line narrowed $\omega_{v',0}$, resonance, instead of the ω_{v0} resonance in Eq. 36, may provide a serious interference to obscure the line narrowing. If instead of $\gamma > 0$, $\gamma < 0$, the last term of Eq. 37 does not appear and line narrowing for $\omega_{v',0}$, is lost.

When the contributions of Γ_1 and Γ_2 to $X^{(3)}(\omega_{as})$ and $X^{(3)}(\omega_s)$ are taken into account as increasing temperature, new entries would appear. As an example for CARS, the Γ_2 term yields line narrowing for ω_{v0} for all cases. Clearly though, it is advantageous to work in the low temperature limit when attempting to identify line narrowing.

Dynamic Stark Effects

We have demonstrated that the population distribution is directly related to the induced transition rate which is given by the cross section multiplied by the photon flux. A strong radiation field induces not only changes in population distribution, but also changes in the energy levels and eigenfunctions. These produce Rabi splitting of the signal, Stark shifting of the peak, power broadening of the linewidth and even field inducing of new peaks because of higher order nonlinear resonances. Thus, the usual picture derived from the perturbation method is not valid. A general method in

determining the strength of the field is provided by the Rabi frequency ($W^{\alpha}_{ij} = u_{ij}.E_{\alpha}/\hbar$) and the tuning of the field from the material resonance ($\omega_{ij} - \omega_{\alpha} + i\Gamma_{ij}$), i.e., $|u_{ij}.E_{\alpha}/\hbar|^2 > [(\omega_{ij} - \omega_{\alpha})^2 + \Gamma^2_{ij}]$ for strong fields. Reversal of this inequality defines the weak field limit.

The field-induced effect for a two-level system has been widely investigated in a homogeneous medium [30,49-51]. The Stark shift due to an electric dipole interaction with an oscillating electric field can be calculated by using general second-order perturbation theory, and is given by

$$\Delta\delta = - \frac{|E_{\alpha}|^2}{4\hbar} \frac{u_{ij} \cdot u_{ji}}{\omega_{ij} - \omega_{\alpha}}. \qquad (38)$$

The change in the lineshape resulting from field-induced effect is that it is broadened from $\Gamma_{ij} = 1/T_2$ to

$$\Gamma^{b}_{ij} = \Gamma_{ij}(1 + W^{\alpha}_{ij} T_2 T_1)^{1/2} \qquad (39)$$

with $1/T_2 = 1/2T_1 + 1/T^{*}_2$, where $1/T_1 = \Gamma_{ii} + \Gamma_{jj}$ and $1/T^{*}_2 = \Gamma^{*}_{ij}$. Recently, Boyd et al. [52] have studied the four-wave parametric interactions by using three distinct frequencies interacting with a two-level system. They found that the generalized Rabi frequency produced in this process enables one to generate tunable radiation by changing the intensity of the driving lasers.

In a manner reminiscent of dressed atom effects in a two-level system, Ouellette and Denariez-Roberge [53] and Dick and Hochstrasser [54] have investigated theoretically the dynamic stark effect in CARS of a discrete four level system with monochromatic fields. The lengthy theoretical calculation, including the field-induced effect for the density matrix of a four-level system, is not reproduced here and can be found elsewhere [53-54]. If ω_1 is a strong field on resonance with an electronic transition (0',0), the population in the excited state should be included to calculate the density matrix element $\rho^1_{v',0}$. This is given by

$$\rho^1_{v',0} = \frac{\{(\rho_0-\rho_{0'})(\Omega^*_{0',0}\Omega^*_{0',v}\Omega_{v',0'}) + (\rho_{0'}|W^{(1)}_{0',0}|^2/2 - \rho_{0'}[|\Omega_{0',0}|^2 + |W^{(1)}_{0',0}|^2/2])(\Omega_{v',0'}+\Omega_{v0})\} * W^{(1)}_{00'}W^{(2)}_{0',v}W^{(3)}_{vv'}}{\{(|\Omega_{0',0}|^2+|W^{(1)}_{0',0}|^2/2)(\Omega_{v0}\Omega^*_{0',v}+|W^{(1)}_{0',0}|^2/4)(\Omega_{v',0}\Omega_{v',0'}-|W^{(1)}_{0',0}|^2/4)\}} \quad (40)$$

where

$$\Omega_{ij} = \omega_{ij}-\omega_\alpha+i\Gamma_{ij} = -\Omega^*_{ji}. \quad (41)$$

If ω_2 is a strong field on resonance with an electronic transition (v,0'), the population in the excited state can be neglected. The matrix element $\rho^2_{v',0}$ is given by

$$\rho^2_{v'0} = \frac{-W^{(1)}_{00'}W^{(2)}_{0'v}W^{(3)}_{vv'}}{8\Omega_{v'0}(\Omega_{v0}\cdot\Omega_{0'0}-|W^{(2)}_{v0'}|^2/4)}. \tag{42}$$

If ω_3 is a strong field on resonance with an electronic transition (v',v), the population in the excited state is negligible because d = -8.5 cm^{-1} in our work. The element $\rho^3_{v'0}$ is given by

$$\rho^3_{v'0} = \frac{W^{(1)}_{00'}W^{(2)}_{0'v}W^{(3)}_{vv'}}{8\Omega_{0'0}(\Omega_{v0}\cdot\Omega_{v'0}-|W^{(3)}_{v'v}|^2/4)} \tag{43}$$

For simplicity, Eq. 43 is utilized to demonstrate the dynamic Stark effect. From Eq. 43, the splitting between the stationary peak and the moveable partner peak is governed by

$$\delta = [(\omega_{v'v}-\omega_3)^2+|W^{(3)}_{v'v}|^2+4\Gamma_{v0}\Gamma_{v'0}]^{1/2}. \tag{44}$$

The linewidths of the stationary and the moveable bands are given by

$$\Gamma^b_{v0} = [\Gamma_{v0}\frac{|\omega_{v'v}-\omega_3|+\delta}{2} + \Gamma_{v'0}\frac{-|\omega_{v'v}-\omega_3|+\delta}{2}]/\delta \tag{45a}$$

$$\Gamma^b_{v'0} = [\Gamma_{v0}\frac{|\omega_{v'v}-\omega_3|-\delta}{2} + \Gamma_{v'0}\frac{-|\omega_{v'v}-\omega_3|-\delta}{2}]/-\delta \tag{45b}$$

In the case of $\Gamma_{v0} = \Gamma_{v'0}$, both linewidths are independent of $\omega_{v'v}$ as shown in ref. 53. For $\Gamma_{v0} = \Gamma_{v'0}$, Fig. 6 shows that

Figure 6. Simulated calculation based on Eq. 43 to demonstrate the Dynamic Stark effects. Profiles a - d were calculated with $W^{(3)}_{v'v} = 0.1, 1.0, 3.0, 10.0\ cm^{-1}$, respectively.

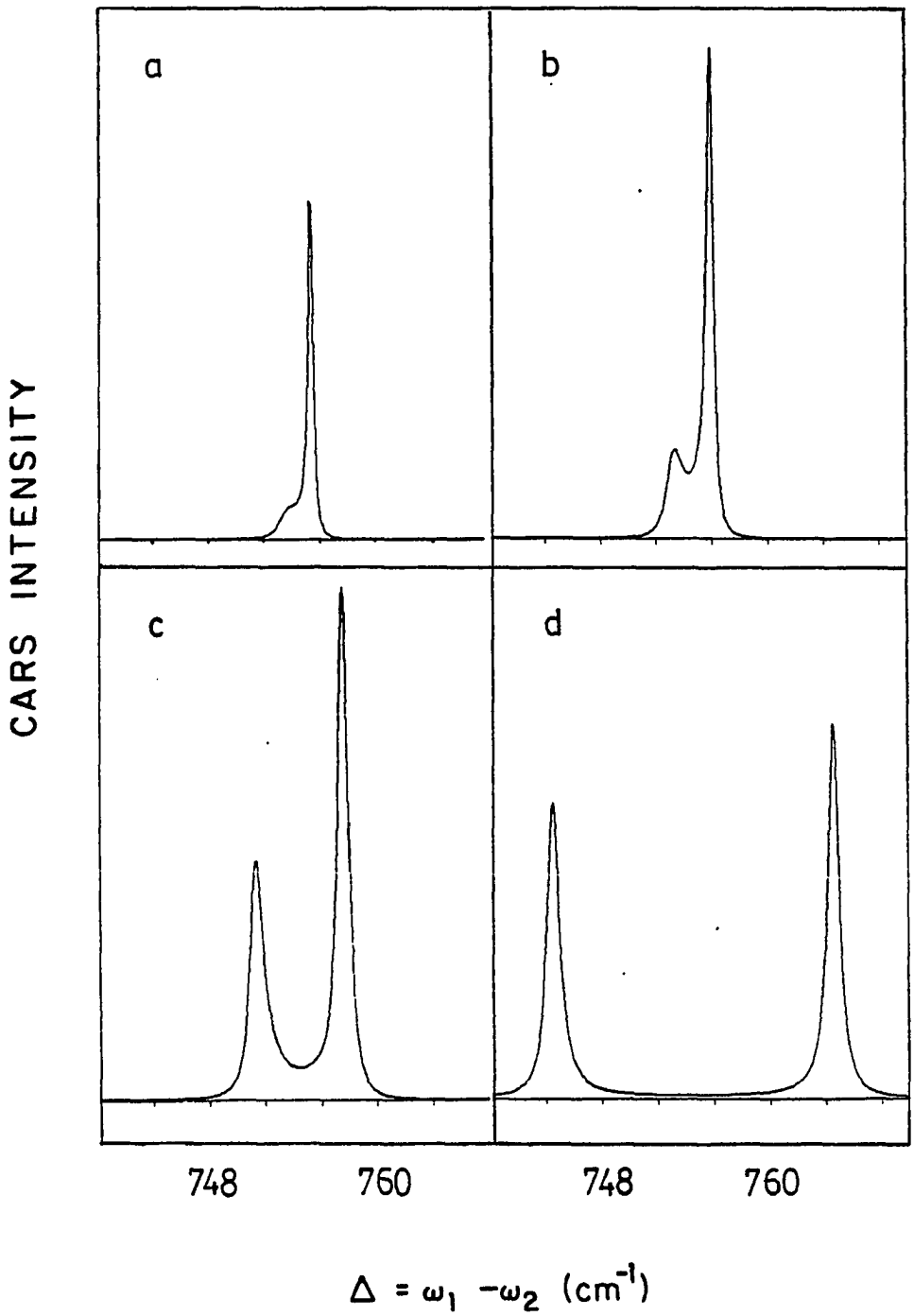
a
b
c
d
CARS INTENSITY
748
760
748
760
Δ = ω1 −ω2 (cm-1)

both linewidths depend upon the magnitudes of $W^{(3)}_{v'v}$ and converge to $\Gamma_{v0} = \Gamma_{v'0} = 1/2(\Gamma_{v0} + \Gamma_{v'0})$ when $W^{(3)}_{v'v} >> [(\omega_{v'v} - \omega_3) + 4\Gamma_{v0}\Gamma_{v'0}]$. It is noticed that the Rabi frequency, $W^{(3)}_{v'v}$, leads to broadening and also contributes to the Stark splitting. These phenomena are similar to the results from the multiphoton ionization and fluorescence excitation spectra using a weak field to couple the ground state and an intermediate excited-state and using another strong field on resonance with the higher excited state transition in the three-level system [55].

EXPERIMENTAL METHODS

Sample Preparation

Several samples which include an absorbing guest doped into an organic crystal, an organic glass, or a polymer have been used to perform the CARS experiments. A listing of the samples along with the temperature range used, the tuning region of the excitation frequency ω_1 and the observed peak frequencies for CARS are given in Table 1. Pentacene (PT) in p-terphenyl (PTP) was obtained from Dr. G. J. Small and cresyl violet perchlorate (CV) in polyvinyl alcohol (PVOH), CV in polyvinyl carbazole (PVK), nile blue perchlorate (NB) in polyacrylic acid (PAA) and oxazine 720 perchlorate (OX) in PAA were obtained from B. L. Fearey. Since the present work emphasizes the study of PT in naphthalene (NPH) and CV in PAA, the preparation of PT in NPH[1] and CV in PAA[2] are described in the following sections.

Naphthalene (Aldrich 98%) was purified[3] by sodium fusion followed by vacuum sublimation and zone refining (110 passes). Pentacene (Aldrich) was directly doped in naphthalene to make

---

[1]Followed the method from Dr. C. K. Johnson, Dept. of Chemistry, Iowa State University.

[2]Slightly modified version of the method in ref. 36.

[3]Purification by Dr. S. Stevenson, Dept. of Chemistry, Iowa State University.

Table 1. Samples investigated for FWM

Samples	T-range (K)	ω_1-range (A)	$\Delta = \omega_1 - \omega_2$ (cm^{-1})
Pentacene in P-terphenyl	4.5	5920-5928	747,755
Pentacene in Naphthalene	4.5-34	6020-6035	747,755
Perylene in Decalin	77 and 293	4360-4720	1372,1393
Cresyl violet perchlorate in glycerol : water	4.5 and 293	6260	594
Cresyl violet perchlorate in polyacrylic acid	4.5-293	5880-6500	585,593
Cresyl violet perchlorate in polyvinyl carbazole	4.5-293	5920-6260	593
Cresyl violet perchlorate in polyvinyl alcohol	293	6300	593
Nile blue perchlorate in polyacrylic acid	4.5-293	6320-6500	586,593
Oxazine 720 perchlorate in polyacrylic acid	4.5-293	6360-6500	594

a concentration of $5*10^{-5}$ to $1*10^{-5}$ mole/mole. Melt-grown crystals in a sealed tube under a low pressure (about 10 Torr) of nitrogen were grown in a temperature controlled Bridgeman furnace. The temperature gradient in the furnace was set about $10^{o}C$ above and below the melting point. The resulting high quality crystal was cleaved parallel to the ab plane and examined using conoscopic techniques. Typical sample thicknesses were ~1 mm. Crystal surfaces were polished with ethanol and soft tissue. All pentacene spectra and data in this work were obtained from samples held in a strain free mount. In the CARS experiments, both laser polarizations were parallel to the 2-fold screw axis (b) of the naphthalene unit cell.

The ionic dye CV (Exciton) was introduced into a polymer solution which was made by dissolving the PAA (Aldrich) polymer powder in hot purified water (kindly supplied by Dr. Lynch's group). The syrupy solution was first filtered by a filter syringe to remove undissolved material and was poured either onto a glass plate or into a cylindrical holder whose bottom consists of a thin microscope cover slip, which was then covered using another cover slip. The samples were placed into a desiccator with a slow flow of nitrogen gas over the solution and were allowed to dry into films. The cylindrical sample holder was usually employed for CV in PVK. The UV-Vis spectra of PAA and CV/PAA were recorded with a Perkin-

Elmer 320 UV-Vis spectrophotometer. It was noticed that high concentrations of CV in PAA produced additional band located at 315 nm in the UV spectra. High quality thin films (0.1 mm) with O.D.s of about 0.6 were selected to be mounted on a brass plate with appropriately drilled holes.

Cryogenic Equipments

A Janis Vari-Temp convection cooled liquid helium cryostat was used for the low temperature studies. Samples were mounted on a flat brass plate and were cooled by passing cold helium gas over the sample. A 20 Ω resistent heater was used to warm the cold helium gas for different temperatures. The temperature could also be adjusted by varying the flow rate of liquid helium into the sample chamber. A calibrated silicon diode temperature sensor (Lake Shore Cryotronics Model DTC-500) mounted next to the sample was used to measure the temperature in the region from 4.2K to 300K. The precision of the temperature measurement was ±0.5K and ±2K for the regions 4.2K-15K and 20K-80K, respectively.

Optics and Lasers for FWM

An actively Q-switched Nd:YAG laser (Quantel Yag 480) pumped a frequency doubler (KDP) to produce an average power of ~1.5 W at 532 nm with a pulse width of 8 ns. The pulse repetition rate was 10 Hz and the shot-to-shot intensity variations were typically ~±5%. A 50% beam splitter was

utilized to yield two excitation pulses which simultaneously pumped two tunable dye lasers (Quantel TDL-III). The TDL-III dye laser system was composed of an oscillator followed by two amplifiers with all dye cells designed to be transversely pumped. The dye-laser beam from the oscillator was passed through interference filters to remove amplified spontaneous emission (ASE). A number of dyes, including rhodamine 590, rhodamine 610, rhodamine 640, DCM, and oxazine 720, all in methanol, were used for the pentacene CARS and CSRS and cresyl violet CARS experiments. The stability of the dye laser was largely determined by the concentration of the dye solution and the alignment of the dye laser optics.

The experimental apparatus for the CARS experiments is shown in Fig. 1. Glan-Thompson polarizers, P, were used to attenuate the dye-laser beams and discriminate against ASE. A variable attenuator, A, (NRC model 935-5) and neutral density filters, F, provided variable attenuation of pulse energies. Pulse energies ranged from 0.3 to 25 μj and from 1 to 50 μj for pentancene and cresyl violet experiments, respectively. The quoted pulse energies were corrected for loss through the cryostat windows. Measurement of the linewidths of the dye-laser beams by a Fabry-Perot interferometer (Burleigh RC-150) or a confocal spectrum analyzer (Spectra Physics Model 470-04) yielded a value of ~0.14 cm^{-1}. The intensity profiles of the dye-laser beams were Gaussian.

Figure 1. The experimental apparatus. A: attenuator, B.S.: beam splitter, C: computer, C.R. chart recorder, D.P.: dichroic prism, F: filter, G.A.: gated amplifier, I: iris, I.F.: interference filter, K.E.: knife-edge, L: lens, M: mirror, Mo: monochromator, P: polarizer, Pr: prism, P.D.: photodiode, PMT: photo-multiplier tube, S: sample, S.C.: scanning controller, S.M.: stepping motor, W: wedged plate.

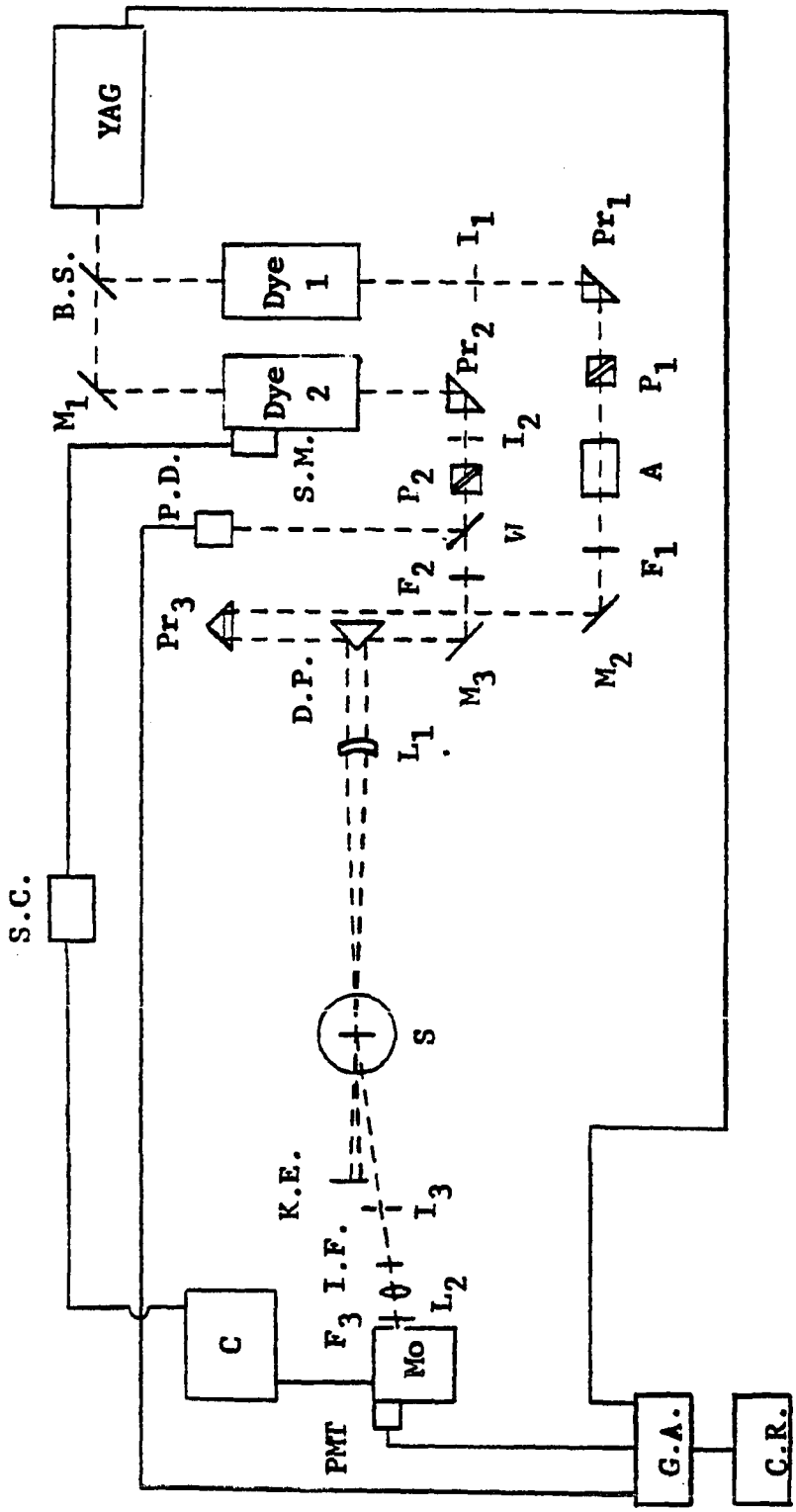
YAG
B.S.
Dye 1
Dye 2
M1
I1
Pr1
Pr2
P1
I2
P.D.
S.M.
P2
A
F1
F2
Pr3
D.P.
M3
M2
L1
S.C.
S
K.E.
I3
F3
I.F.
L2
C
Mo
PMT
G.A.
C.R.

The two laser beams were made collinear before inserting a dichroic prism, D.P., which was used to reflect both beams through a 50 cm focal length lens, L_1, focusing onto the sample. If both beams are collinear at the sample, the resulting phase mismatch can seriously degrade the magnitude of the CARS signal because dispersion is involved. Dewitt et al. [43] gave the equation for determining the phase-match angle, θ.

$$\cos\theta = \frac{4*\omega_1\omega_2 n_{as}^2 - 4*\omega_1^2(n_{as}^2 - n_1^2) - \omega_2^2(n_{as}^2 - n_2^2)}{4*\omega_1 n_1 \omega_2 n_2} \qquad (1).$$

In practice, determination of the phase-matching angle was accomplished by maximizing the CARS signal while translating the dichroic prism, D.P., and the lens, L_1, in Fig. 1. A typical phase matching angle was estimated at $\sim 1.2^{o}$. A melting point capillary tube [56] containing CV in a glycerol/water mixture was used to collimate the two laser beams which were then focused onto the sample. Utilization of the melting point capillary tube is definite aid to finding the CARS signal. The spot size radius on the sample was ~0.15 mm. Unless otherwise mentioned, the photon fluxes and Rabi frequencies given in this work were calculated using this radius. However, given the uncertainties in the transition dipoles and beam radius at the sample we estimated that the

fluxes and Rabi frequencies were uncertain by a factor of about 4 and 2, respectively.

The signal generated at $2*\omega_1 - \omega_2$ from the sample was spatially filtered by a knife-edge, K.E., [57] and frequency filtered by an interference filter, I.F., and McPherson 270 monochromator, Mo. A 10 cm focal length lens, L_2, collected the signal, which was passed through the monochromator whose slit widths typically were 500 microns corresponding to a bandpass of 10 A and was detected by a cooled RCA-C31034 photomultiplier tube, PMT. The neutral density filters, F_3, were utilized to avoid the saturation of the photomultiplier tube and to stay in the linear response region of the detection system. The presence of a CARS signal was easily demonstrated by blocking either one of the dye laser beams. A wedged plate, W, was used to partially reflect the output of the ω_2 laser to a photodiode, P.D., in order to produce a reference signal. Improvement in S/N was achieved by using a Quanta-Ray DGA-1 dual gated amplifier, G.A., to normalize the CARS signal to the reference beam. The normalized CARS spectra were recorded in real time by a Heath strip chart recorder, C.R.

The monochromator was calibrated using mercury and neon spectral calibration lamps and it was in turn utilized to calibrate the frequencies of the dye lasers. Experiments were performed by tuning ω_1 to a certain frequency and scanning ω_2

through the region of the Raman mode of interest (i.e., $\omega_{v0} = \omega_1 - \omega_2$). The dye-laser grating was tuned by a stepping motor, S.M., (Quantel SMI-1) combined with a scanning controller, S.C., (Quantel ASC-2) or by manual control. A computer program[4] was used to simultaneously scan the dye laser ω_2 and the monochromator, in opposite directions. The entire experiment was synchronized by the sync. output pulse from the Nd:YAG laser.

Experimental Techniques

Two different methods for investigating the electronic spectra of the impurity were used in this work. The transmission spectra of PT/NPH were obtained by focusing the output of a 120W tungston lamp onto the sample in the dewar. Transmitted light was focused onto the slits of a 1.5m Jobin-Yvon HR-1500 spectrometer equipped with a cooled photomultiplier detector. As the spectrometer was scanned, the detected signal was recorded on a strip chart recorder. Recently, T. Carter has improved the method of obtaining absorption spectra by constructing a double beam spectrometer which may probe samples mounted in a cryostat. Briefly, the absorption spectra of PT/NPH and CV/PAA were obtained by dispersing the output of a 450W Xenon arc lamp through a Jobin-Yvon spectro-

---

[4]Written by Dr. C. K. Johnson, Dept. of Chemistry, Iowa State University.

meter and then splitting the output into two beams. Both beams were mechanically chopped at different frequencies and passed through identical optics. One beam was used to produce a reference signal and another beam was focused onto the sample to produce a sample signal. Both signals were monitored by the same PMT whose output was sent to two lock-in amplifiers referenced to the chopping frequencies. The outputs of the lock-in amplifiers were processed by a logarithmic ratiometer which provided a signal directly proportional to the sample absorbance. In this way, contributions to the spectrum owing to lamp, monochromator and detector wavelength dependencies were eliminated.

Different types of CARS experiments included the tuning, temperature, power and time dependencies have been used to study line narrowing, population distribution, DICE effect, Stark and hole burning effects. It should be pointed out that the peak intensity of the CARS signal for CV in PAA decreased with irradiation time for room temperature CARS spectra. The rate of decrease was proportional to the pulse energies of the incident laser beams; therefore, lower pulse energies were used to take the CARS spectra. Since the relative intensity between the ground and the excited stationary peaks was sensitive to both pulse energies, temperature dependent spectra were obtained by fixing pulse energies and gain coefficients but varying the neutral density filters which

were placed in front of the monochromator slit. All CARS spectra for CV in PAA reported in this work were taken from fresh spots on the sample, except for the time dependent spectra. Furthermore, synchronous scanning of the ω_1 field and the monochromator with fixed ω_2 and synchronous scanning of both ω_1 and ω_2 and the monochronator have been initiated in this laboratory.

PAPER I.

MULTI-RESONANT FOUR WAVE MIXING SPECTROSCOPY OF PENTACENE IN NAPHTHALENE

MULTI-RESONANT FOUR WAVE MIXING SPECTROSCOPY OF PENTACENE IN NAPHTHALENE

TA-CHAU CHANG, CAREY K. JOHNSON* and GERALD J. SMALL

Ames Laboratory-USDOE and Department of Chemistry
Iowa State University, Ames, Iowa 50011

*Present address: Department of Chemistry, University of Pennsylvania, Philadelphia, PA 19104

ABSTRACT

Dispersive multi-resonant coherent anti-Stokes and Stokes (CARS and CSRS) data are reported for pentacene in naphthalene. The vibronic resonances are associated with the lowest excited singlet state of pentacene. Attention is focused on the 755 cm^{-1} ground state fundamental of pentacene, its excited state counterpart at 747 cm^{-1} and their two partners which move with the detuning, d, of the ω_1 laser away from the electronic origin transition at $\omega_{0',0}$ ($d = \omega_1 - \omega_{0',0}$). Pentacene in naphthalene appears to be unusual in that excited electronic state CARS resonances are observed for negative detunings which are large relative to the inhomogeneous linewidth of the $\omega_{0',0}$ transition. Temperature dependent studies indicate that the excited state population mechanism involves phonon hotband absorption. Power broadening data for the 755 cm^{-1} resonance obtained for negative detunings are discussed in terms of a distribution of dynamic Stark shifts resulting from the site inhomogeneous line broadening of vibronic transitions. Novel temperature dependent data for positive detuning ($d = 4\ cm^{-1}$) are presented and tentatively interpreted in terms of the interplay between dephasing induced coherent emission (DICE from the excited state population) and the temperature dependence of the phonon sideband absorption building on the (0',0) band. CARS and CSRS data are presented which are

consistent with line narrowing for the 755 cm^{-1} resonance. The observed linewidths for the 755 and 747 cm^{-1} resonances, when corrected for the laser contributions, yield vibrational dephasing times somewhat shorter (~20%) than the values obtained from time domain studies. In connection with the site inhomogeniety problem, some CARS and CSRS data are also presented for cresyl violet in polyacrylic acid.

INTRODUCTION

In recent years dispersive [1-7] and picosecond [8-13] four-wave mixing spectroscopies governed by $X^{(3)}$ (third order nonlinear susceptibility) have been used to probe vibrations in condensed phase molecular systems. Both coherent anti-Stokes (CARS) and Stokes (CSRS) Raman spectroscopies have been employed. For two color(laser) experiments, the intensity of the wave generated at $2\omega_1 - \omega_2$ is measured and is proportional to $|X^{(3)}|^2$; $\omega_1 > \omega_2$ and $\omega_1 < \omega_2$ for CARS and CSRS, respectively [14,15]. There are a number of reasons why it is advantageous in frequency domain experiments to operate in the triply resonant (or nearly so) mode with the two additional resonances being vibronic [16]. Besides very significant gains in sensitivity and selectivity, Raman resonances driven off the excited electronic state population as well as moveable resonances which accompany stationary resonances can be observed. The positions of the moveable resonances depend on the detuning d which for our purposes can be taken as $\omega_1 - \omega_{0'0}$, where $\omega_{0'0}$ is the frequency of the pure electronic origin transition. The "new" resonances provide information otherwise not attainable by conventional four-wave mixing, where only the vibrational resonance is driven. For example, the effect of pure dephasing associated with vibronic transitions on the vibrational resonances can be probed. Another reason is connected with the fact that in the frequency

domain, inhomogeneous broadening of the vibrational resonances can be significant. In many cases, the triply resonant condition will force a multi-level system into behaving like a four level system. Then if the inhomogeneous distributions associated with the pertinent vibrational and vibronic resonances are appropriately correlated, line narrowing can be attained. The ability of doubly and triply resonant CSRS (driven off the ground state population) to give Doppler-free resonances in the gas phase has been theoretically established [17,18]. With Doppler broadening there is complete and positive correlation between the resonances which also leads to the result that the CARS resonances are not line narrowed. In solids, the situation is far more complicated; the requisite correlations for line narrowing may not exist or if they do only partially. Because of our interest in the optical dephasing of impurities in glasses and polymers [19-21] it was the line narrowing potential of fully resonant four-wave mixing which initially triggered our interest.

In this paper, several facets of our studies on a crystalline system, pentacene in naphthalene, are discussed. This mixed crystal was chosen primarily because a considerable amount of dephasing data for it are available from the time domain studies of Duppen et al. [22] and Hesselink and Wiersma [23-24]. In addition, pentacene in benzoic acid has been extensively studied by Hochstrasser and his group using dispersive four-wave mixing. Here four-wave mixing spectra

are presented for the 755 cm^{-1} ground state fundamental of pentacene and its excited state counterpart at 747 cm^{-1} as well as their two moveable partners. The data show that pentacene in naphthalene is unusual in that excited electronic state CARS resonances are readily observed for negative detunings, d, large in comparison to the inhomogeneous linewidth of the (0',0) or origin transition of the $S_1 \leftarrow S_0$ absorption system. A population mechanism which is consistent with T-dependent data is proposed. Of more general interest are T-dependent CARS data obtained for small positive detuning which may be consistent with a novel interplay between DICE driven by the excited electronic state population and the T-dependence of the phonon side band intensity associated with the (0',0) transition. Power broadening data for the 755 cm^{-1} resonance obtained for negative detunings are discussed in terms of a distribution of dynamic Stark shifts afforded by the site inhomogeniety of vibronic transitions. In addition, data consistent with line narrowing for the 755 cm^{-1} resonance are given and discussed in terms of site excitation energy correlations.

EXPERIMENTAL

The four-wave mixing set up used was fairly conventional in design. Two grazing incidence dye lasers (ω_1, ω_2) pumped by the second harmonic of a Nd:YAG laser provided close to Gaussian frequency profiles with FWHM (full width of half maximum) of 0.14 cm^{-1}. For the pentacene CARS experiments rhodamine B and DCM were used for ω_1 and ω_2, respectively. Glan-Thompson polarizers were used to attenuate and purify the dye laser beams. Neutral density filters provided variable attenuation for power dependent studies. Pulse energies for ω_1 and ω_2 ranged from 0.3 ~ 25 μJ. The quoted pulse energies are corrected for losses through the cryostat windows. A melting point capillary tube [25] was used to collimate the two laser beams which were then focused onto the sample with a 50 cm focal length lens to a spot size of radius ~0.15 mm and with a phase-matching angle of about 1.2^{o}. Unless otherwise mentioned, the photon fluxes and Rabi frequencies given in this paper are calculated with this radius. However, given the uncertainties in the transition dipoles and beam radius at the sample we estimate that the fluxes and Rabi frequencies are uncertain by a factor of about 4 and 2, respectively. The signal generated at $2\omega_1 - \omega_2$ from the sample was spatially filtered by the knife-edge technique and frequency filtered by an interference filter and McPherson 270 monochromator. The monochromator was scanned synchronously with the ω_2 laser.

Pulse to pulse intensity jitter was typically ~±5%. Some improvement in S/N could be achieved by normalizing the four-wave mixing signal to the output of the ω_2 laser (using a Quanta-Ray DGA-1 dual gated amplifier). The four-wave mixing signal was detected by a RCA-C31034 photomultiplier tube in a cooled housing.

Crystals of naphthalene (extensively zone-refined) containing ~5 x 10^{-5} to 10^{-5} mole/mole pentacene were grown by the Bridgman technique and cleaved parallel to the a b plane. Typical sample thicknesses were ~1 mm. Crystal faces were polished with ethanol and soft tissue. A Janis vari-temp convection cooled liquid helium cryostat was used for low T studies. All pentacene spectra and data in this paper were obtained from samples held in a strain free mount. The ω_1 and ω_2 laser polarizations were parallel to the two-fold screw axis (b) of the naphthalene unit cell. Details pertaining to the preparation of the polyacrylic acid polymer films are given elsewhere [26].

RESULTS AND DISCUSSION

General Features of Detuning

Under the near triply resonant conditions of our experiments where two of the resonances are vibronic and the other vibrational, specific trems of a very large number [27] in $X^{(3)}$ are dominant for CARS and CSRS. This theoretical simplification is paralleled by an increase in the amount of vibrational and dynamical information which can be obtained [4-7,17,18]. For pentacene in naphthalene, where a specific ground state mode and its excited state counterpart are probed, one can achieve further simplification by treating the problem in terms of a four level system. Of particular interest is the four level system in Fig. 1. The $S_1 \leftarrow S_0$ origin transition lies at 16593.5 cm^{-1} and exhibits a linewidth (FWHM) of ~2 cm^{-1} at T = 5 K which is dominated by site inhomogeniety [22,28]. The 747 cm^{-1} $|v'\rangle$ level is the excited state analogue of the 755 cm^{-1} ground state a_{1g} fundamental [5-7]. Experiments have been performed for 16575 cm^{-1} - 16600 cm^{-1}. Illustrative spectra showing the effects of detuning are presented in Fig. 2 where the detuning $d = \omega_1 - \omega_{0'0}$. The pertinent terms of $X^{(3)}$ which need to be considered can be obtained from Appendix I of Ref. 27 and are:

Figure 1. Four level energy diagram for pentacene in naphthalene.

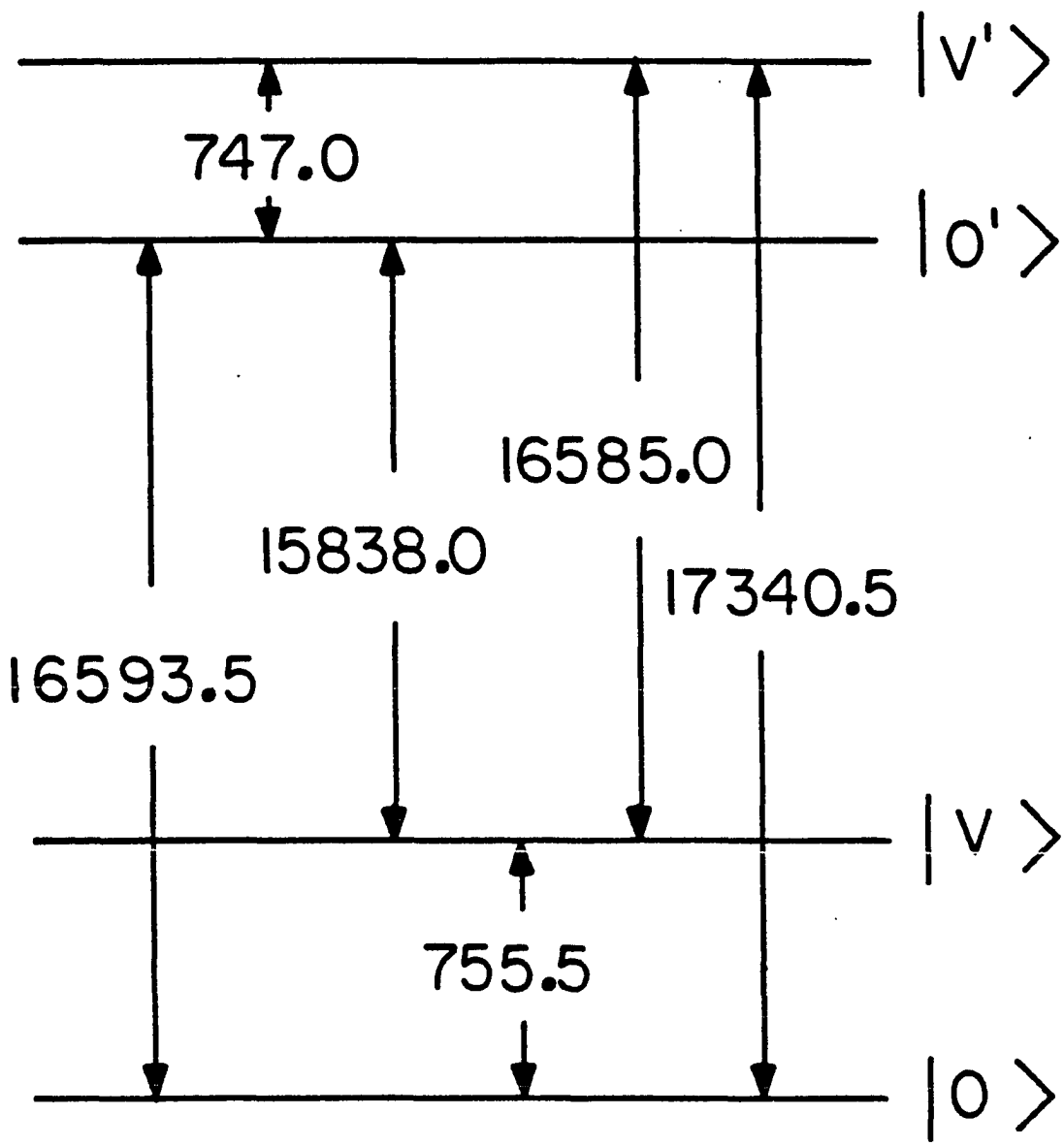
|v'>
747.0
|0'>
16585.0
15838.0
17340.5
16593.5
|v>
755.5
|0>

Figure 2. CARS spectra for pentacene in naphthalene as a function of detuning at T = 5K. Spectra a - d correspond to d = +4, 0, -2.5 and -6 cm^{-1} and were obtained with (ω_1,ω_2) pulse energies of (10,0.8), (5,0.8), (2.5,0.8) and (1,0.8) μJ, respectively.

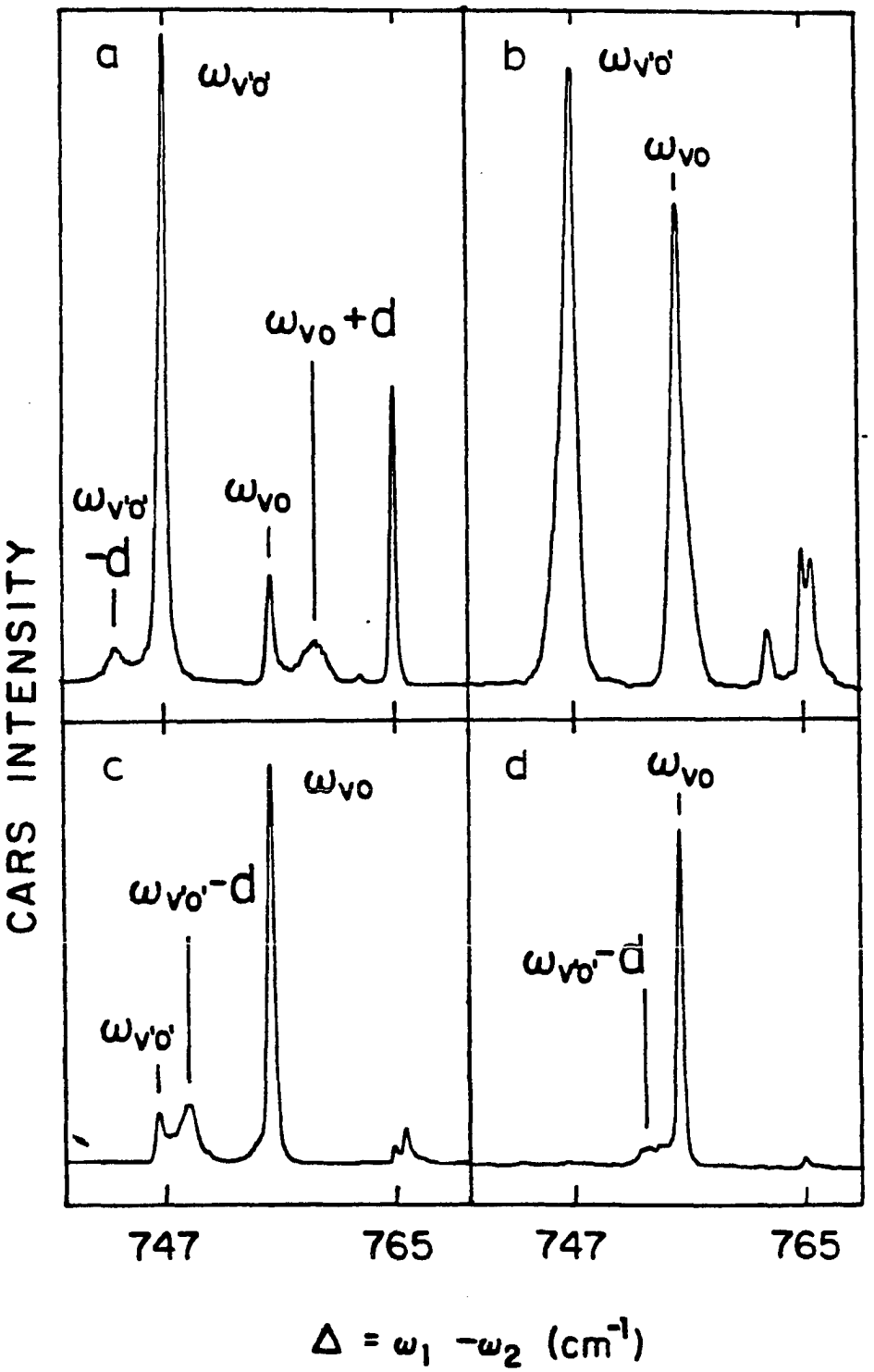
a
$\omega_{v'0'}$
b
$\omega_{v'0'}$
ω_{v0}
$\omega_{v0}+d$
$\omega_{v'0'}-d$
ω_{v0}
c
ω_{v0}
$\omega_{v'0'}-d$
$\omega_{v'0'}$
d
ω_{v0}
$\omega_{v'0'}-d$
CARS INTENSITY
747
765
747
765
$\Delta = \omega_1 - \omega_2$ (cm^{-1})

$$X^{(3)}(\omega_{as}) = C\left[\frac{\rho_0}{(\omega_{v'0}-\omega_{as}+i\Gamma_{v'0})(\omega_{v0}-\Delta+i\Gamma_{v0})(\omega_{0'0}-\omega_1+i\Gamma_{0'0})}\right.$$

$$+\frac{\rho_{0'}}{(\omega_{v'0}-\omega_{as}+i\Gamma_{v'0})}\left\{\frac{1}{(\omega_{v'0'}-\Delta+i\Gamma_{v'0'})(\omega_{0'v}-\omega_2-i\Gamma_{0'v})}\right.$$

$$-\frac{1}{(\omega_{v0}-\Delta+i\Gamma_{v0})(\omega_{0'0}-\omega_1+i\Gamma_{0'0})}$$

$$\left.\left.+\frac{1}{(\omega_{v0}-\Delta+i\Gamma_{v0})(\omega_{0'v}-\omega_2-i\Gamma_{0'v})}\right\}\right] \quad (1).$$

The damping constants associated with total dephasing are defined in the usual way as $\Gamma_{ij} = 1/2(\Gamma_i+\Gamma_j) + \Gamma^*_{ij}$, with Γ^*_{ij} the pure dephasing frequency. Further, $\omega_{ij} = \omega_i - \omega_j$, $\Delta = \omega_1 - \omega_2$, and $C = -u^1_{0',0}u^{as}_{0v'}u^1_{v',v}u^2_{v0'}(6N^{-1}\hbar^3)^{-1}$ with u_{ij} the vibronic transition moment between levels j and i associated with a photon of type α. Allowance has been made for CARS driven off the excited state population $\rho_{0'}$ ($\rho_{0'}+\rho_0 = 1$). Eq. (1) pertains to a discrete four level system and so to account for site inhomogeneous line broadening, it must be ensemble averaged utilizing site distribution functions for the pertinent resonances [18,29], vide infra. The nonresonant contribution to $X^{(3)}$ in Eq. 1 is not included since manifestations of it are not apparent in our spectra. The effects of detuning are more evident when the above expression is rewritten in the form [7]

$$X^{(3)}(\omega_{as}) = \frac{C}{-d+i\Gamma_{0'0}} \Big[\frac{\rho_0}{(\omega_{v'0'}-d-\Delta+i\Gamma_{v'0})(\omega_{v0}-\Delta+i\Gamma_{v0})}$$

$$- \frac{\rho_{0'}}{(\omega_{v0}+d-\Delta+i\Gamma_{0'v})(\omega_{v'0'}-\Delta+i\Gamma_{v'0'})} \Big\{ 1 + \frac{i\Gamma_1}{\omega_{v'0'}-d-\Delta+i\Gamma_{v'0}}$$

$$+ \frac{i\Gamma_2(\omega_{v'0'}-\Delta+i\Gamma_{v'0'})}{(\omega_{v'0'}-d-\Delta+i\Gamma_{v'0})(\omega_{v0}-\Delta+i\Gamma_{v0})} \Big\} \Big] \qquad (2),$$

Here $\Gamma_1 = \Gamma_{0'0} + \Gamma_{v'0'} - \Gamma_{v'0}$ and $\Gamma_2 = \Gamma_{0'v} + \Gamma_{0'0} - \Gamma_{v0}$. Bozio et al. [73] have emphasized that in the low T limit, where pure dephasing is negligible, $\Gamma_1 = \Gamma_2 = \Gamma_{0'}$, the inverse the 0′ level lifetime.

The four spectra (a-d) in Fig. 2 were obtained with (ω_1, ω_2) pulse energies of (10,0.8), (5,0.8), (2.5,0.8) and (1,0.8) μJ, corresponding to d = 4, 0, -2.5 and -6 cm^{-1}, respectively. At the outset, we note that the resonance at 765 cm^{-1} (barely observable in d) is a naphthalene fundamental whose intensity, to a very good approximation, is independent of d in this range (the lowest singlet exciton state of naphthalene lies at 31,475 cm^{-1}). Thus, the 765 cm^{-1} resonance can be used as an intensity marker to roughly gauge the relative degree of resonance enhancement for the pentacene resonances for the different d values. The resonance enhancement in spectrum d is significant because d = -6 cm^{-1} is close to $\omega_{v'0'}-\omega_{v0}$ = -8 cm^{-1}. From the ρ_0 term in Eq. 2, it can be seen that d = -8 cm^{-1} provides a double resonance [17]. Indeed, for this

reason a detuning of -8 cm^{-1} was generally used to find and optimize the CARS signals.

Turning to the other resonances in Fig. 2 (all due to pentacene), the 755 and 765.5 cm^{-1} bands are ground state fundamentals associataed with the ω_{v0}-Δ resonance (stationary) and have been previously observed in CARS and CSRS for pentacene in benzoic acid [3,7]. The relatively broad (~2 cm^{-1}) feature in spectrum d at 753 cm^{-1} is a ρ_0 resonance due to $\omega_{v'0'}$-d-Δ and one which moves with the detuning (moveable partner of ω_{v0}). With reference to Eq. 1, it is driven by the outgoing wave (ω_{as}) resonance. For ω_1 pulse energies of 10 μJ the excited state $\omega_{v'0'}$ = 747 cm^{-1} resonance has been observed for d as low as -6 cm^{-1}. It is not present in spectrum d because the pulse energy is only 1 μJ. However, in spectrum c it is readily apparent. For positive detuning, spectrum a, the $\omega_{v'0'}$ resonance is a factor of 6.5 times more intense than the ω_{v0} resonance, signifying a very significant excited state population ($\rho_{0'}$). The weak broader feature at 759 cm^{-1} is the moveable partner of $\omega_{v'0'}$ associated with the ω_{v0} + d - Δ resonance of Eq. 2, while the 743 cm^{-1} band is the moveable partner of ω_{v0}. The two unlabeled bands in spectrum b at 765.5 and 762.5 cm^{-1} correspond to another ground state-excited state pair of a pentacene fundamental.

Equation 2 predicts that for d = 0 the moveable partners of ω_{v0} and $\omega_{v'0'}$ should be coincident in energy with the stationary resonances at $\omega_{v'0'}$ and ω_{v0}, respectively. Spec-

trum b is in accord with this prediction although the power broadening is too large to allow the broad underlying moveable resonances to be discerned. Such on-resonance interferences present a potential complication for line narrowing experiments, vide infra.

Figure 3 summarizes the data from a series of detuning experiments. The solid and dashed lines are calculated and account quite well for the positions of the moveable resonances associated with the 755 and 747 cm^{-1} stationary resonances.

Linewidths of Resonances

Under triply resonance conditions, power broadening of CARS and CSRS resonances must be considered [30,31], cf. the section of Power Broadening. The extent of the power broadening depends not only on the field strengths and vibronic transition moments with which they interact but <u>also</u> on the field-vibronic transition detunings. With our experimental geometry it was found that for ω_1- and ω_2-pulse energies of <1 μJ and <5 μJ the power broadening was usually negligible. Under low power conditions the CARS linewidths (FWHM) observed for the $\omega_{v'0'}$ = 747 and ω_{v0} = 755 cm^{-1} resonances are 0.35 and 0.32 cm^{-1} at 5K, Fig. 4. Very recent CSRS experiments have yielded a linewidth for the ω_{v0} resonance of 0.28 cm^{-1}. An example of a CSRS scan is shown in Fig. 5. At the 1 μJ ω_1-pulse energy required to eliminate power broadening, the underlying fluo-

Figure 3. Pentacene in naphthalene CARS frequencies as a function of detuning. Solid circles and X's are experimental points with the latter obtained at higher powers. Solid line: calculated stationary peak frequencies. Dashed line: calculated moveable peak frequencies.

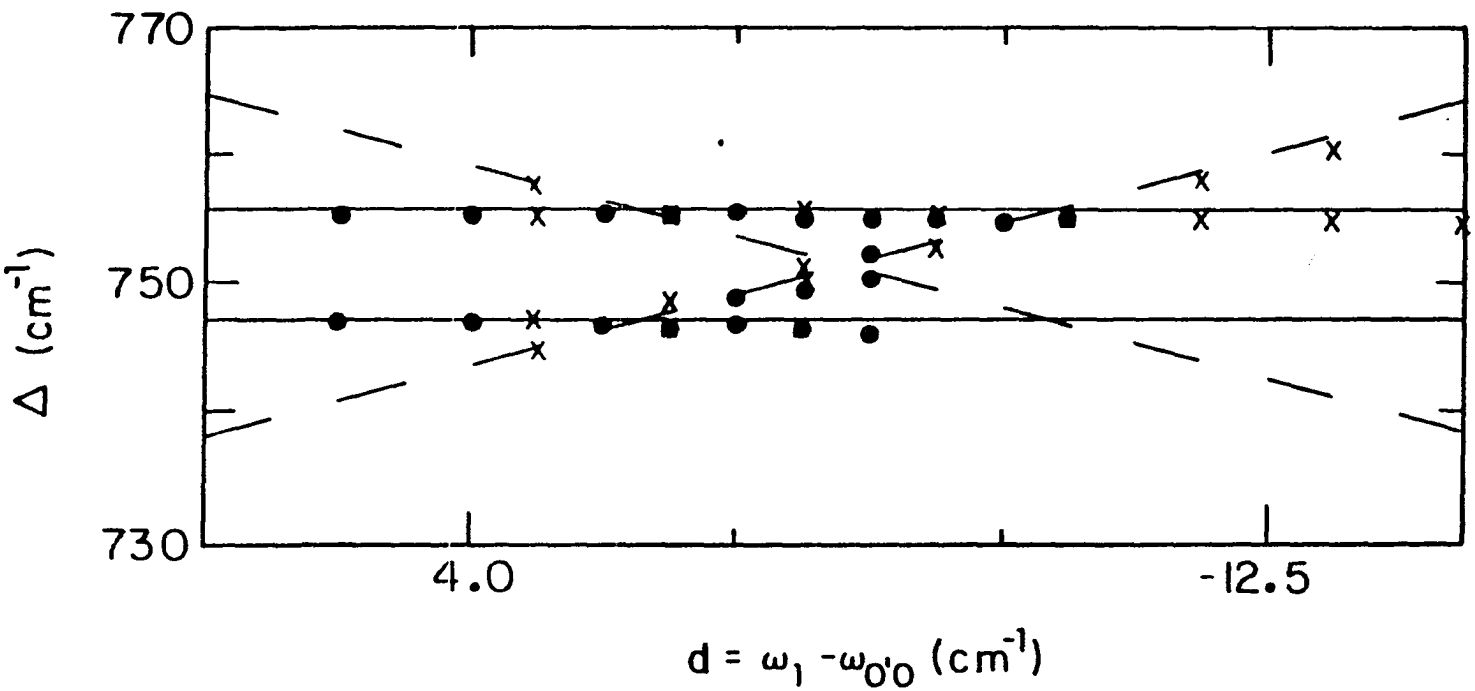
770
750
730
Δ (cm⁻¹)
4.0
-12.5
d = ω1 -ω0'0 (cm⁻¹)

Figure 4. Pentacene stationary resonances at low pulse energies. Profiles a and b correspond to the 747 and 755 cm^{-1} resonances in the CARS spectra obtained for d = +4 and -15 cm^{-1}, respectively.

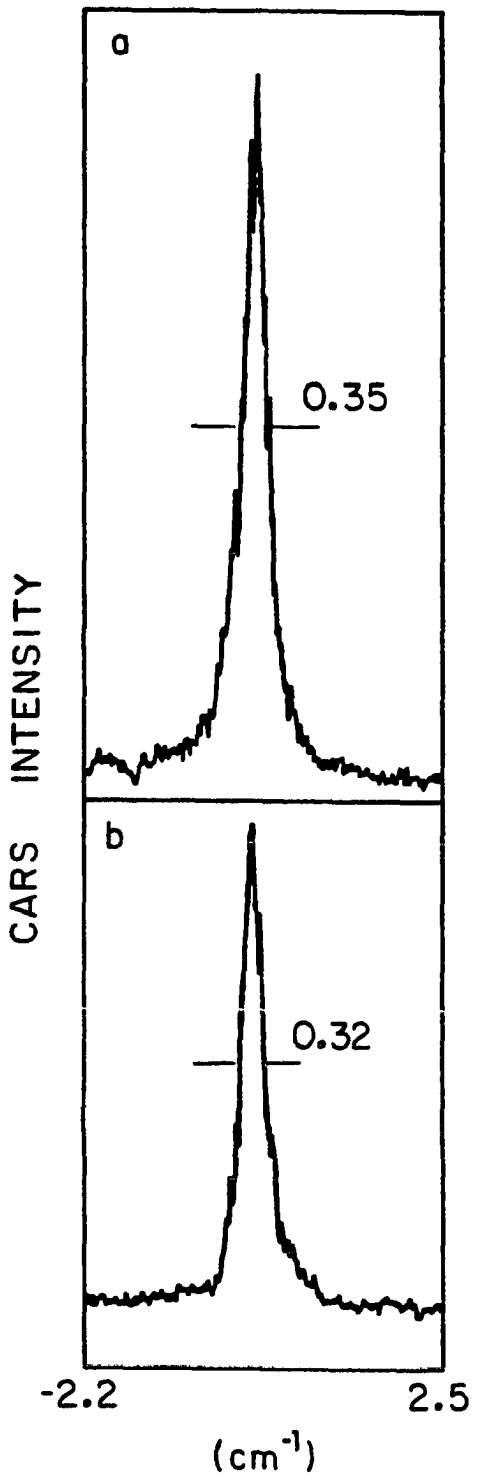
a
0.35
b
0.32
CARS INTENSITY
-2.2
2.5
(cm^{-1})

Figure 5. The pentacene in naphthalene ω_{v0} = 755 cm^{-1} stationary resonance in CSRS at T = 5K (spectrum a). Spectrum b is the fluorescence background obtained with the ω_1-field blocked, see text. The (ω_1,ω_2) pulse energies are (1,0.75) μJ.

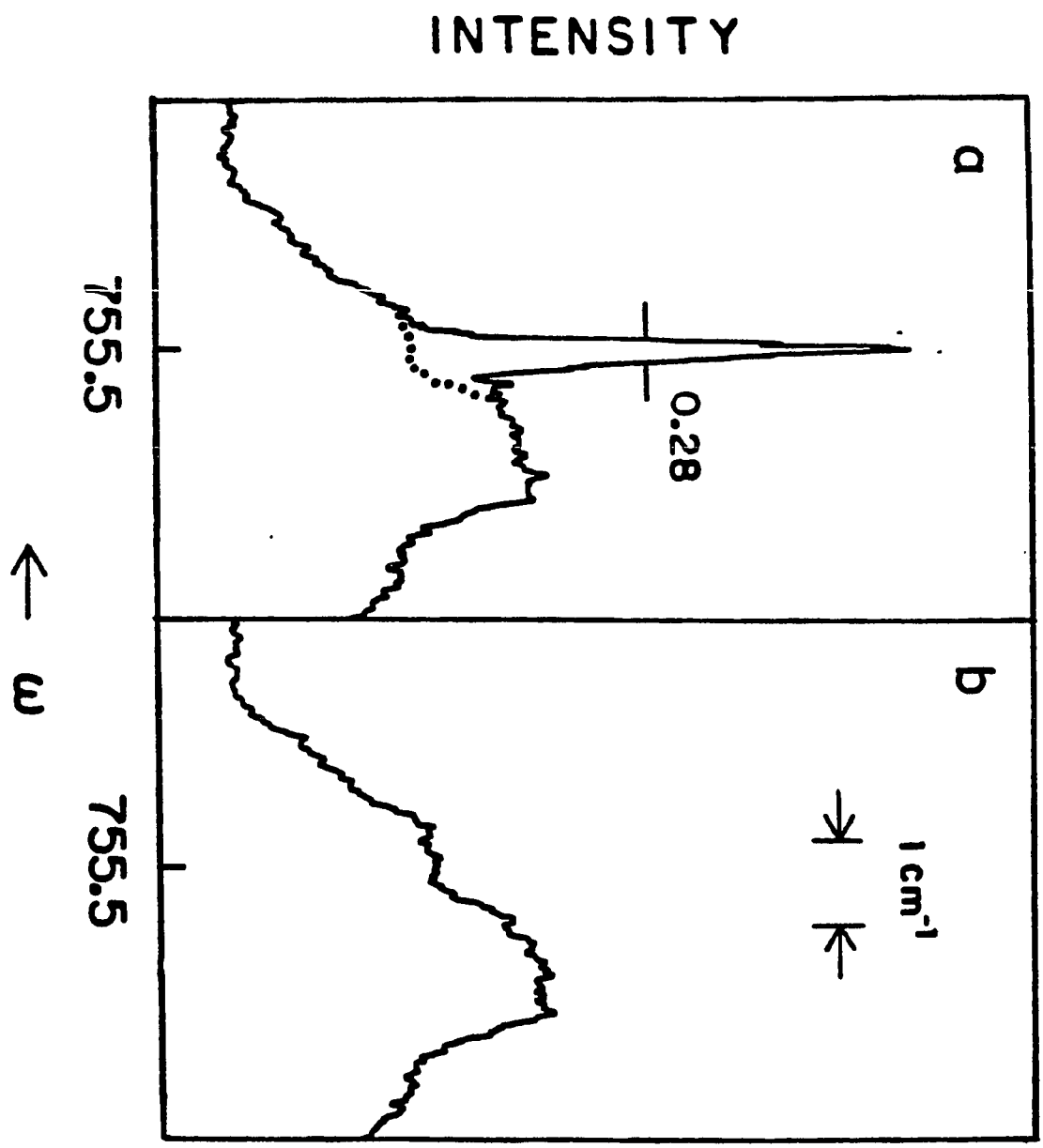
INTENSITY
a
b
755.5
755.5
0.28
1 cm⁻¹
ω

rescence background (due to ω_2-excitation of the S_1 state) is, unfortunately, significant. The right trace shows the fluorescence background obtained with the ω_1-field blocked and was used to determine the 0.28 cm^{-1} linewidth. For ω_1- and ω_2-pulse energies of 0.25 and 0.75 μJ, the linewidth observed was also 0.28 cm^{-1}. Thus, the CARS and CSRS results suggest that line narrowing is operative. The linewidth data and the time domain measurements of the pertinent T_2 dephasing times from the studies of Wiersma and coworkers are given in Table 1.

However, the lasers utilized here are characterized by FWHM of 0.14 cm^{-1} and are major contributors to the observed linewidths, vide infra. Thus, we emphasize that the question of line narrowing for the ω_{v0} resonance deserves further study with narrower lasers (not available in our laboratory).

Nevertheless, we proceed with the assumption that line narrowing is operative and a brief discussion of this phenomenon. Recently, Dick and Hochstrasser have considered the conditions under which fully resonant $\chi^{(2)}$ dispersive spectroscopies can yield line narrowing [29]. Their treatment is readily extended to $\chi^{(3)}$ especially when Lorentzians are used to describe the distributions for site excitation energies. For this case, the ensemble averages can be performed analytically using residue theory [17]. The linewidths obtained do not depend significantly on whether Lorentzian or Gaussian (more realistic) distribution functions are utilized [29].

Table 1. Linewidths and relaxation time for pentacene in naphthalene at 5K

Resonance	Expt. FWHM (cm^{-1})	corrected[a] FWHM (cm^{-1})	T_2[b] (ps)	T_2 (ps)
ω_{v0}=755	0.28[c]	0.14	76	101[d]
$\omega_{v'0'}$=747	0.35[e]	0.21	50	66[f]
$\omega_{v'0'}-d=\omega_{v'0}-\omega_1$	1.5[e]	1.5	NO	~660[g]
$\omega_{v0}+d=\omega_1-\omega_{0'v}$	1.5[e]	1.5	NO	~101[d]
$\omega_{0'0}$	---	---	---	~550[g]

[a]Corrected for laser linewidth, cf. text.

[b]At 5K the pure dephasing (T_2^*) contribution to $1/T_2 = 1/2T_1 + 1/T_2^*$ is negligible [22,23]; FWHM (cm^{-1}) = $(\pi c T_2)^{-1}$ with c the speed of light. NO ≡ not obtainable since the moveable resonance is inhomogeneously broadened, cf. text.

[c]CSRS work.

[d]Ref. 22.

[e]CARS.

[f]Ref. 23.

[g]Ref. 24.

We, therefore, use the former and present only a few results germane to this paper and which, hopefully, will prove useful for future studies. Since in our experiments we are in the low T limit where the contributions of Γ_1 and Γ_2 to Eq. 2 are negligibly small (as confirmed by calculations with the data

from Table 1), we utilize Eq. 2 with $\Gamma_1 = \Gamma_2 = 0$ for simplicity and space considerations. Noting that $d = \omega_1 - \omega_{0',0}$, we define $x = \omega_{v0} - \omega^0_{v0}$, $y = \omega_{v',0} - \omega^0_{v',0}$ and $z = \omega_{0',0} - \omega^0_{0',0}$ as the shifts of the transition frequencies away from their mean values. In the absence of correlation between these statistical variables, line narrowing in CARS (or CSRS) is not possible. The simplest situation (and the one one would hope for) is complete correlation where $y = \alpha x$ and $z = \beta x$, α and β constants. It follows that the two remaining resonances are then automatically correlated; $\gamma x \equiv (\alpha-\beta)x = \omega_{v',0'} - \omega^0_{v',0'}$ and $(\beta-1)x = \omega_{0',v} - \omega^0_{0',v}$. Whether or not a particular term of CARS or CSRS yields line narrowing depends on its pole structure and, therefore, the relative signs of correlation coefficients.

There are a large number of possibilities which we seek to limit by considering only the most likely ones for mixed molecular crystals and the level structure of Fig. 1. It seems reasonable to assume [2,28] that the magnitudes of the vibronic α and β coefficients are given <u>roughly</u> by the ratio of the gas to solid dispersion shift of a pure vibrational transition (like ω_{v0}) to the corresponding shift for a vibronic transition (like $\omega_{0',0}$). Then $|\alpha|$, $|\beta| > 1$ and the sign of $(\beta-1)$ is determined by the sign of β for β positive. Furthermore, it is most reasonable to consider that α and β carry the same sign. For $\alpha,\beta > 0$ or < 0, one should consider both $\gamma > 0$ or $\gamma < 0$ ($\gamma = \alpha-\beta$).

Table 2. Definition of terms for line narrowing expressions

Term	Definition[a]
S	$\omega_{v0}^{0} \mp \Delta$
S′	$\omega_{v',0'}^{0} \mp \Delta$
M	$\omega_{v',0'}^{0}-d^{0} \mp \Delta$
M′	$\omega_{v0}^{0}+d^{0} \mp \Delta$

[a]Minus and plus signs correspond to CARS and CSRS, respectively; $\Delta = \omega_1-\omega_2$; $d^0 = \omega_1-\omega_{0',0}^{0}$.

We treat first case I: $\alpha,\beta,\beta-1,\gamma > 0$ (complete positive correlation) and introduce for compactness the symbols S, S′, M and M′ as defined in Table 2. In what follows, σ is the half-width of the ω_{v0} resonance due to inhomogeneous broadening. One finds that ($d^0 \equiv \omega_1-\omega_{0',0}^{0}$)

$$\langle X^{(3)}(\omega_{as})\rangle_I = C\{\frac{-\rho_0}{[M+i(\Gamma_{v',0}+\alpha\sigma)][S+i(\Gamma_{v0}+\sigma)][d^0-i(\Gamma_{0',0}+\beta\sigma)]}$$

$$+\frac{\rho_{0'}}{[M'+i(\Gamma_{0',v}-(\beta-1)\sigma)][S'+i(\Gamma_{v',0'}+\gamma\sigma)][d^0-i(\Gamma_{0',0}+\beta\sigma)]}$$

$$+\frac{2i\sigma}{(\beta-1)^{-2}}\times\frac{\rho_{0'}}{[M'+i(\Gamma_{0',v}+(\beta-1)\sigma)][M'+i(\Gamma_{0',v}-(\beta-1)\sigma]}$$

$$\times\frac{1}{[\beta(\beta-1)^{-1}(M'+i\Gamma_{0',v})-d^0+i\Gamma_{0',0}]}$$

$$\times\frac{1}{[S'+i(\Gamma_{v',0'}+\gamma(\beta-1)^{-1}\Gamma_{0',v})+\gamma(\beta-1)^{-1}M']}\}. \quad (3)$$

Thus, ω_{v0} from ρ_0 is not line narrowed while $\omega_{v',0'}$ from $\rho_{0'}$ is predicted to be to an extent governed by the magnitude of $\gamma(\beta-1)^{-1}\Gamma_{0',v}$. For $\gamma(\beta-1)^{-1} \ll 1$ and T sufficiently low to render pure electronic dephasing sufficiently small, the linewidth of the stationary (S') $\omega_{v',0'}$ resonance can yield $\Gamma_{v',0'}$, the vibrational dephasing. How readily depends on the non-line narrowed $\omega_{v',0'}$ interference from the second term in Eq. 3. For $\gamma\sigma \gg \Gamma_{v',0'}$, there would be no difficulty. We note that the moveable resonances (M,M') are not line narrowed in CARS or CSRS, irrespective of the type of correlation assumed. They carry, in part, the inhomogeneous widths of vibronic transitions, i.e. $\alpha\sigma$ or $(\beta-1)$, and present potential interferences for the stationary resonances, e.g., when $d^0 = 0$.

We view $\gamma(\beta-1)^{-1}M' = \gamma(\beta-1)^{-1}(\omega_{v0}+d^0-\Delta)$ as a line shift for the line narrowed $\omega_{v'0'}$ resonance. Its magnitude for $\Delta \sim \omega_{v'0'}$ depends on $\omega_{v0} - \omega_{v'0'}$ (8 cm^{-1} for our system) and is controllable, to some extent, through d^0. If $\gamma(\beta-1)^{-1} \sim 0.01$, this line shift would be very small.

Expressions analogous to Eq. 3 have been derived for both CARS and CSRS for the four cases defined in the caption to Table 3. For space considerations, they are not given here [32]. In this table, entries with dephasing constants define the cases for which the ground and excited state stationary resonances in CARS or CSRS can be line narrowed. For example, for case I and case II, Table 3 shows that the ω_{v0} resonance can be line narrowed in CSRS but not CARS. The entry $\Gamma_{v0} + \beta^{-1}\Gamma_{0'0}$ determines the linewidth so that if $\beta^{-1}\Gamma_{0'0} << \Gamma_{v0}$, the dephasing constant of interest, Γ_{v0}, can be determined.

With this in mind, an interpretation of why the CSRS ω_{v0} linewidth is narrower than in CARS is that the ω_{v0}, $\omega_{v'0}$ and $\omega_{0'0}$ site excitation energy distributions are positively correlated. With reference to cases I and II for CARS and the $\rho_{0'}$ column, it is seen that the $\omega_{v'0'}$ resonance is also predicted to be line narrowed. Thus, the measured linewidth of 0.35 cm^{-1} for the $\omega_{v'0'}$ = 747 cm^{-1} resonance may be line narrowed value. We note that for the four-level system of Fig. 1 but with benzoic acid as host, Bozio et al. [7] and Hochstrasser [33] have observed line narrowing consistent with negative correlation.

Table 3. Line narrowing conditions

CASE[a]	BAND	CARS[b]	
		ρ_0	$\rho_{0'}$
I	ω_{v0}	n.l.n[c]	n.l.n.
I	$\omega_{v'0'}$	---[d]	$\Gamma_{v'0'}+\gamma(\beta-1)^{-1}\Gamma_{0'v}$
II	ω_{v0}	n.l.n.	n.l.n.
II	$\omega_{v'0'}$	---	$\Gamma_{v'0'}+\lvert\gamma\beta^{-1}\rvert\Gamma_{0'0}$
III	ω_{v0}	$\Gamma_{v0}+\lvert\alpha^{-1}\rvert\Gamma_{v'0}$;[e] $\Gamma_{v0}+\lvert\beta^{-1}\rvert\Gamma_{0'0}$	---
III	$\omega_{v'0'}$	---	$\Gamma_{v'0'}+\lvert\gamma\beta^{-1}\rvert\Gamma_{0'0}$
IV	ω_{v0}	$\Gamma_{v0}+\lvert\alpha^{-1}\rvert\Gamma_{v'0}$; $\Gamma_{v0}+\lvert\beta^{-1}\rvert\Gamma_{0'0}$	---
IV	$\omega_{v'0'}$	---	$\Gamma_{v'0'}+\lvert\gamma(\beta-1)^{-1}\rvert\Gamma_{0'v}$

[a]Cases I-VI correspond to $\alpha,\beta,\gamma > 0$; $\alpha,\beta > 0$, $\gamma < 0$; $\alpha,\beta < 0$, $\gamma > 0$; and $\alpha,\beta,\gamma < 0$, respectively (see text). It is assumed that $|\alpha|, |\beta| > 1$.

[b]The low temperature limit where the Γ_1 and Γ_2 terms are negligible is assumed, cf. text. Relaxation of this assumption only affects the --- entries.

[c]n.l.n. ≡ non-line narrowed resonance.

[d]No contribution.

[e]Entries with damping constants imply line narrowing. In this case, there are two line narrowed resonant denominator terms, cf. Eq. 4, with the extent of line narrowing dictated by $|\alpha^{-1}|\Gamma_{v'0}$ and $|\beta^{-1}|\Gamma_{0'0}$. Line narrowed terms suffer interference from non-line narrowed terms, cf. text.

		CSRS[b]	
		ρ_0	$\rho_{0'}$
I	ω_{v0}	$\Gamma_{v0}+\beta^{-1}\Gamma_{0'0}$	---
I	$\omega_{v'0'}$	---	$\Gamma_{v'0'}+\gamma\beta^{-1}\Gamma_{0'0}$; $\Gamma_{v'0'}+\gamma(\beta-1)^{-1}\Gamma_{0'v}$
II	ω_{v0}	$\Gamma_{v0}+\beta^{-1}\Gamma_{0'0}$	---
II	$\omega_{v'0'}$	---	n.l.n.
III	ω_{v0}	$\Gamma_{v0}+\lvert\alpha^{-1}\rvert\Gamma_{v'0}$	---
III	$\omega_{v'0'}$	---	n.l.n.
IV	ω_{v0}	$\Gamma_{v0}+\lvert\alpha^{-1}\rvert\Gamma_{v'0}$	---
IV	$\omega_{v'0}$	---	$\Gamma_{v'0'}+\gamma(\beta-1)^{-1}\Gamma_{0'v}$; $\Gamma_{v'0'}+\gamma\beta^{-1}\Gamma_{0'0}$

In all the CARS spectra obtained, the moving resonances associated with the 755 and 747 cm^{-1} modes exhibit FWHM of ~1.5 cm^{-1} corresponding to the inhomogeneous broadening of the $0' \leftarrow 0$ and and $v' \leftarrow 0$ vibronic absorption transitions (note from Table 1 that the widths for these transitions from dephasing are negligible at 5K). Data are presented later which illustrate that the moveable resonances become broader with increasing temperature due to increasing vibronic dephasing.

If ω_{v0} and $\omega_{v'0'}$ linewidths of 0.28 and 0.35 cm^{-1} are considered to contain a negligible contribution from site inhomogeneous line broadening. Deconvolving out the laser contributions will provide dephasing times which can be compared with the time domain values. Following Yuratich [34] and taking both the ω_1 and ω_2 lasers as gaussian with full-widths of 0.14 cm^{-1} (the Δ driving field width = $\sqrt{2}(0.14)$), we find for the half-widths that Γ_{v0} (755) = 0.07 cm^{-1} and $\Gamma_{v'0'}$ (747) = 0.11 cm^{-1}. These translate to dephasing times of 76 ps and 50 ps which compare reasonably well with but are shorter than the time domain measurements of 101 and 66 ps [22,23]. Considering the fact that our laser widths are comparable to the dephasing widths. This is not surprising.

The question of how large the coefficients α and β are relative to unity for the level structure of Fig. 1 is important because it speaks to the degree of line narrowing which

is achievable. For mixed molecular crystals $|\alpha|\sigma \sim |\beta|\sigma \sim 1\ cm^{-1}$. Assuming [2,28] that $\sigma/|\alpha|\sigma$ scales as the gas to solid dispersion shifts for the vibrational and vibronic transitions, leads to the estimate $10 < |\alpha| < 100$ (based on one-photon absorption and fluorescence spectra). For pentacene in naphthalene, the above 1 cm^{-1} value is appropriate for the $\omega_{v'0}$ and $\omega_{0'0}$ transitions, Fig.1. If the difference between the observed CARS and CSRS half-widths for ω_{v0}, 0.02 cm^{-1}, is σ, then $\alpha \sim \beta = 50$. In this connection, our CARS and CSRS data [35] in cresyl violet in polyacrylic acid and polyvinyl carbazole indicate that $\alpha, \beta \sim 100$. For these systems, the inhomogeneous vibronic linewidths are ~500 - 1000 cm^{-1} while the same for the vibrational resonances are ~4 cm^{-1}. Fig. 6 shows some of the T-dependent four-wave mixing data for the 594 cm^{-1} fundamental of cresyl violet in polyacrylic acid. The profile from CSRS is no sharper than that from CARS. This, together with the fact that the widths do not increase with increasing temperature indicate that the low T width of ~4 cm^{-1} is a good measure of inhomogeneous broadening for the ω_{v0} resonance. Thus, a value of $\alpha \sim \beta \sim 50$ for pentacene in naphthalene is reasonable provided transferability is valid.

Figure 6. CARS and CSRS spectra for cresyl violet in polyacrylic acid. Profiles a - e are from CARS for the 593 cm^{-1} ground state mode of cresyl violet at temperatures of ~ 5, 20, 40, 60 and 300 k, respectively. The frequency corresponds to 630.0 nm (low energy tail of the $S_1 \leftarrow S_0$ cresyl violet absorption profile). Profile f is CSRS at room temperature with ω_1 at 640.0 nm. Power broadening was confirmed to be negligible for these spectra.

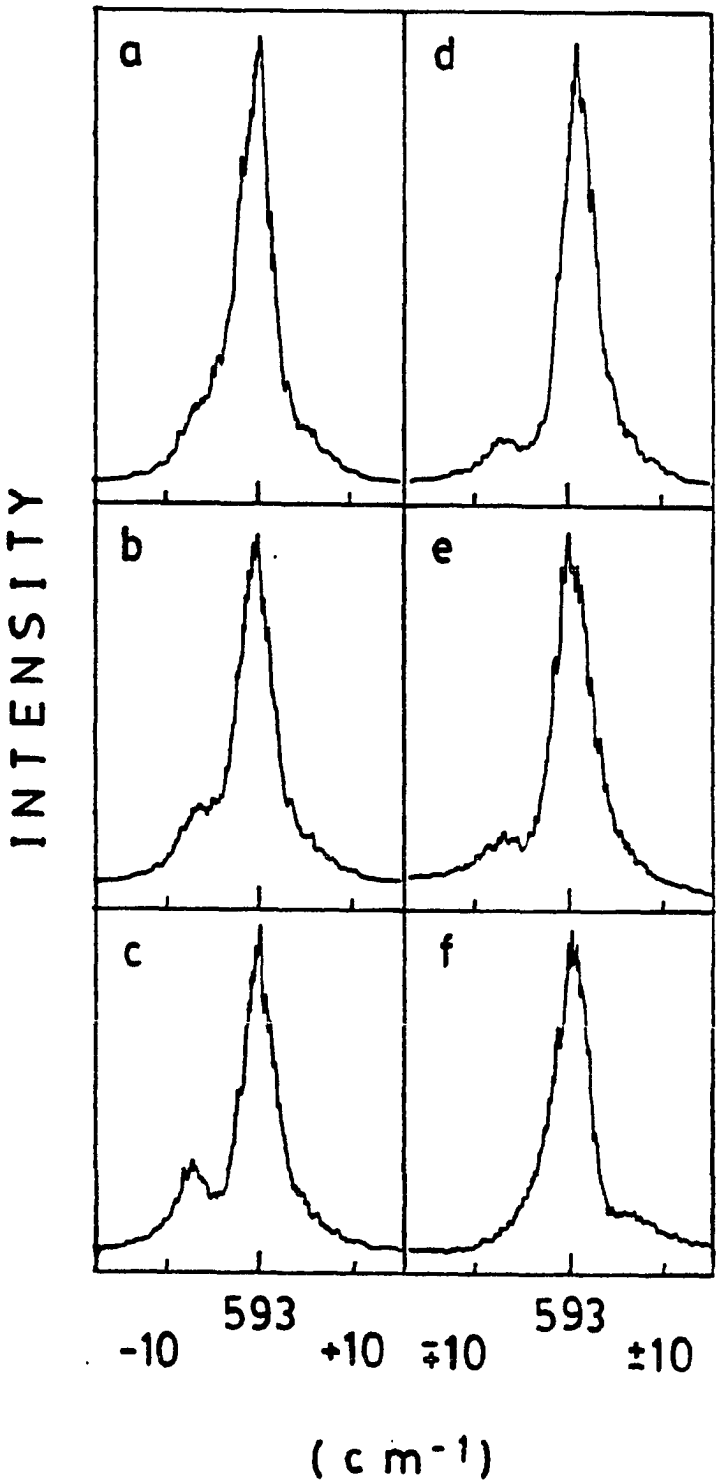
a
d
b
e
c
f
INTENSITY
593
-10
+10
∓10
593
±10
(c m⁻¹)

Mechanism for Excited Resonance for Negative Detuning

As noted earlier the pentacene in naphthalene system is unusual in the sense that the excited state resonance $\omega_{v'0'}$ and its moveable partner can be observed with modest pulse energies for negative detunings, d, which are large relative to the inhomogeneously broadened (0',0) transition. This behavior is apparently not observed for pentacene in benzoic acid [7]. Furthermore, we have performed negative detuning experiments for pentacene in p-terphenyl [36] and for d = -4.5 cm^{-1} and pulse energies about an order of magnitude higher than those used in Fig. 2, the $\omega_{v'0'}$ = 747 cm^{-1} resonance could not be observed (the inhomogeneous (0',0) linewidth is very nearly the same as for the naphthalene host). Thus, the mechanism for creating an excited population which depends on excitation of a narrow isochromat (~0.14 cm^{-1}) in the far red wing of the gaussian (0',0) absorption profile can be discounted. Nor is a mechanism based on phase disruption of the coherent CARS process a viable candidate. First, there is no apparent reason why this mechanism should not be operative for pentacene in p-terphenyl or benzoic acid. Second, in our experiments a detuning of d = -8 cm^{-1} (747-755) was always used to initially find and optimize the 755 cm^{-1} resonance. This detuning drives the ρ_0 term of Eq. 1 doubly resonant and the resulting signal is about as intense as the signal for d=0 (also doubly resonant), in accord with Eq. 1. Nevertheless,

ρ_0, resonances could not be observed for d = -8 cm^{-1} and pulse energies comparable to and greater than those in Fig. 2. another possibility is suggested by the recent work of Duppen et al. [22]. They presented fluorescence line narrowing data which indicate that a weak and broad (inhomogeneous linewidth 10 cm^{-1}) pentacene (0',0) absorption profile underlies the principal origin at 16593.5 cm^{-1}. They suggested that the broad absorption is associated with pentacene at crystal defects. Judging from their absorption spectra and ours this absorption is very weak. This, together with the fact that this absorption is inhomogeneously broadened, make it difficult to understand how narrow line (ω_i) laser excitation can create sufficient ρ_0, population to account for the intensities of the excited state resonances. That additional enhancement of the $\omega_{v',0'}$ = 747 cm^{-1} resonance from ρ_0, derives from higher excited electronic states can be excluded since the observed intensity of $\omega_{v',0'}$ relative to its moveable partner is well accounted for by Eq. 1, i.e., the $s_n \leftarrow s_1$ absorption systems are very broad meaning that a $s_n \leftarrow s_1$ resonance via ω_1 or ω_2 would impart a linewidth to the moveable resonance too large to allow for its observation. A fourth possibility is that two-photon absorption (TPA) by the naphthalene host and subsequent energy transfer to pentacene creates excited state population. However, a comparison of the published TPA spectra [37] with the range of ω_1 and ω_2 frequencies used here exclude this possibility.

The T-dependent data in Fig. 7 provide, in part, the key for determination of the mechanism. The ratio of the intensity of $\omega_{v'0'}$ = 747 cm^{-1} to ω_{v0} = 755 cm^{-1} increases with increasing temperature in CARS. At the outset we emphasize that this is <u>not</u> a dephasing-induced coherent emission (DICE) effect as observed by Andrews and Hochstrasser in <u>CSRS</u> for pentacene in benzoic acid [5]. This follows from Eq. 2 ($\rho_{0'}$ term) which shows that DICE from the Γ_2 contribution affects the ω_{v0} resonance and not the $\omega_{v'0'}$ resonance. The interplay between this contribution and the ρ_0 term would lead to a T-dependence <u>opposite</u> to that observed. We proceed now to show how the T-dependence can be explained in terms of Eq. 2 and a mechanism for creating excited state population which is generally not available in mixed crystals.

Pentacene in naphthalene differs from the same in banzoic acid and p-terphenyl in that it exhibits a phonon hot band in absorption which lies 4 cm^{-1} to the red of the (0',0) origin. Hesselink and Wiersma [24] have studied this transition in considerable detail and concluded that the hot band is a sequence transition involving a u-type pseudo-localized phonon of 18 cm^{-1} in the ground state and its excited state counterpart with a frequency of 14 cm^{-1} [24]. Our own T-dependent absorption studies [36] are in agreement with theirs. Thus, the possibility that the creation of $\rho_{0'}$ population occurs via the phonon hot band needs to be considered. To this end the

Figure 7. Temperature dependence of the pentacene in naphthalene ω_{v0} = 755 and $\omega_{v'0'}$ = 747 cm^{-1} CARS resonances for a detuning d = -5 cm^{-1} and (ω_1,ω_2) pulse energies of (0.8,0.5) μJ. Spectra a-d correspond to T = 5, 8.5, 15 and 23K, respectively.

INTENSITY
Δ = ω1 − ω2 (cm-1)
747
755.5
747
755.5
c
d
a
b
ωv'0
ωv'0−D
ωv0

simple four level system in Fig. 8 is utilized with levels 1 and 1' corresponding to the ground and excited state phonon levels, respectively. The kinetic equations can be written down immediately and, for space considerations, are not given here. For the laser pulsewidths and energies used in our experiments they may be solved using the steady state approximation for the populations of the pseudo-localized phonon levels (i.e. $\rho_0 + \rho_{0'} = 1$). We note that the induced absorption rate R, Fig. 8, is calculated from

$$R = \frac{(2\pi e)^2}{n_b c\hbar^2} \; |\underline{D}_{11'} \cdot \underline{b}|^2 \int d\omega \; g(\omega) I(\omega), \qquad (4)$$

and that $D_{1'1} = D_{0'0} \sim 0.3$ A as calculated from the absorption spectra of ref. [24]. The unit vector $\underline{b}$ is parallel to the $\underline{b}$-axis of the naphthalene unit cell while $\underline{D}_{11'}$ is parallel to the short axis of pentacene. The appropriate direction cosine squared for the projeaction is 0.57 [38]. The phonon hot band absorption profile has been analyzed by Hesselink and Wiersma [24] and found to be characterized by a Lorentzian contribution to the FWHM of 2 cm^{-1}. Thus, the line shape function $g(\omega)$ is considerably broader than the laser ($I(\omega)$) so that the integral in Eq. 4 reduces to $I_{TOTAL}/(2^{-1}\pi \cdot FWHM)$. Because the relaxation mechanism for the pseudo-localized phonons is harmonic [24], we make the reasonable approximation that R is

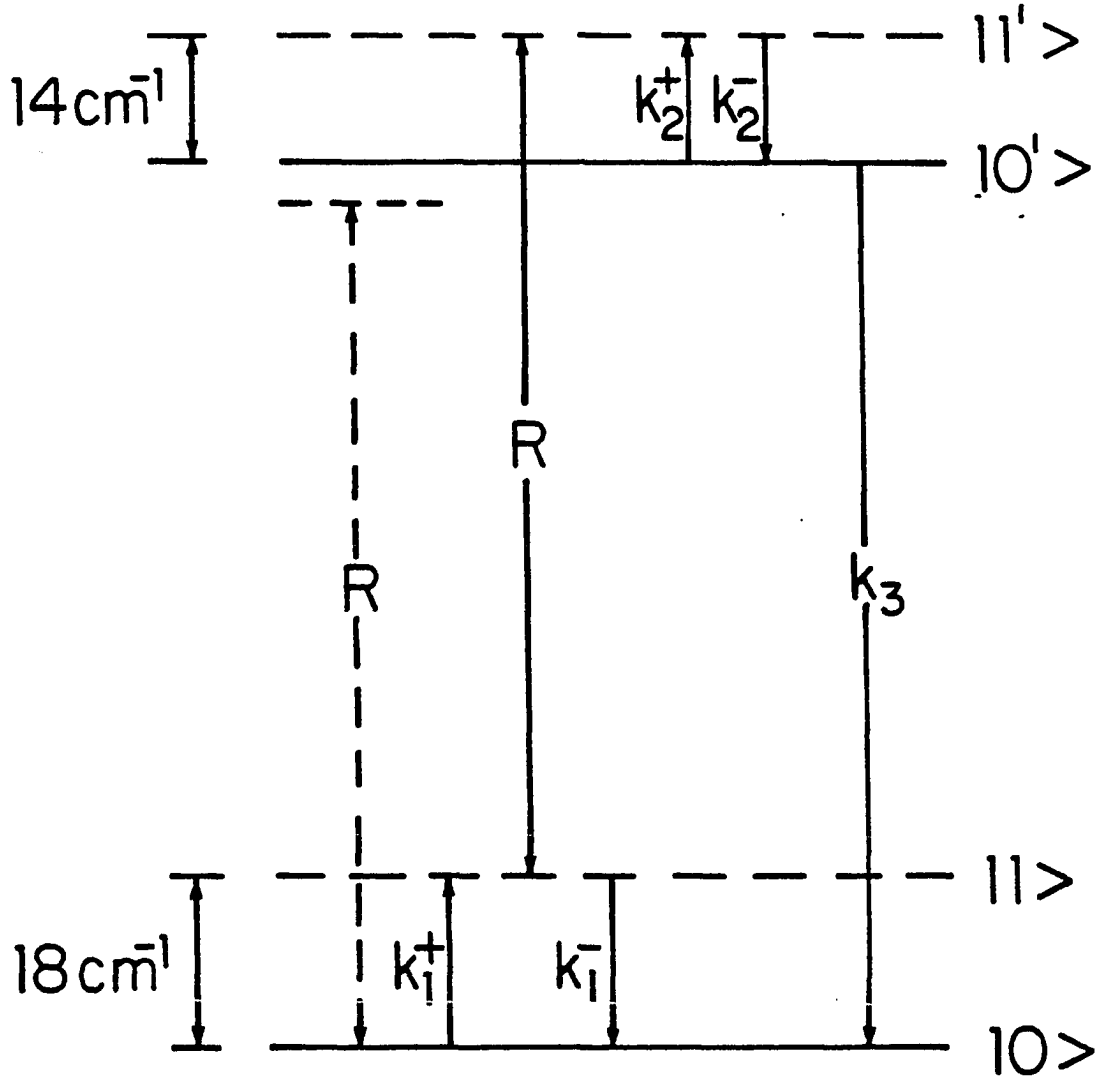

Figure 8. Energy level and kinetics model used to calculate excited state population, $\rho_{0,,}$ arising from phonon hotband absorption lying 4 cm^{-1} to the red of $\omega_{0,0}$ = 16593.5 cm^{-1}, see text for details.

not strongly dependent on temperature over the range studied. Finally, $n_b = 1.78$ is the refractive index of naphthalene for b-naphthalene polarization. The calculation yields $R_1 = 1.7 \times 10^9\ s^{-1}$. The above line shape analysis can be used to estimate that $k_1^- \sim k_2^- \sim (2.5\ ps)^{-1}$. However, the calculated populations, ρ_0 and $\rho_{0'}$, are insensitive to this value provided it is significantly larger than the induced absorption rate (as is the case here). The k_3 decay constant equals $(20\ ns)^{-1}$ [24]. The rate constants $k_i^+ = k_i^- \exp(-\varepsilon_i/kT)$ with $(\varepsilon_1,\varepsilon_2) = (18,14)\ cm^{-1}$ and alone determine the T-dependence of ρ_0 and $\rho_{0'}$. Once these values are determined they are used with Eq. 2 and the dephasing constants given in Table 4 to calculate the intensity ratio $I_{v'0'}/I_{v0}$ as a function of temperature.

The observed values for the ratio at T = 5, 8.5, 15 and 23K are ---, 1/17, 1/5.5 and 1/3.5, respectively. At the highest gains employed the $\omega_{v'0'}$ resonance could not be observed at 5K. Reasonable agreement between the observed and calculated ratios are obtained with $R = 1.7 \times 10^9\ s^{-1}$; the calculated ratios for 8.5, 15 and 23K agree with the above experimental values to within 15%. The calculated value of the ratio for 5K is ~1/600. Given that the calculated value of R carries a considerable uncertainty (cf. the section of Linewidths of Resonances), we conclude that the phonon hot band absorption is the mechanism responsible for the obser-

Table 4. Dephasing constants

T (K)	$\Gamma_{v'0}$	Γ_{v0}	$\Gamma_{0'0}$	$\Gamma_{v'0'}$	$\Gamma_{v'v}$	$\Gamma_{0'v}$
			(cm^{-1})			
5	0.08[a]	0.06[a]	0.01[b]	0.08[b]	0.14[c]	0.06[d]
8.5	0.12[a]	0.06[a]	0.06[a]	0.08	0.18	0.10
15	0.24[a]	0.06[a]	0.18[b]	0.08	0.30	0.22
23	0.34	0.06	0.26	0.08	0.40	0.32

[a] Obtained from Ref. 22.
[b] Obtained from Ref. 24.
[c] $\Gamma_{v'v} = \Gamma_{v'0} + \Gamma_{v0}$.
[d] $\Gamma_{0'v} = \Gamma_{v'v} - \Gamma_{v'0'}$.

vation of the $\omega_{v'0'}$ resonance at significant negative detunings. We point out that the large homogeneous contribution to the phonon hot band profile ensures that the excited electronic state ($\rho_{0'}$) site distribution is a reasonably faithful representation of the ground state (ρ_0) site distribution.

Finally, in Fig. 7 the moveable partner of ω_{v0} at $\omega_{v'0'}$-d is discernable in spectra a and b, barely so in c, and absent in d (T = 23K). This is consistent with broadening of the moveable resonance with increasing T due to vibronic dephasing ($\Gamma_{v'0}$), cf. ρ_0 term of Eq. 3. At 23K, $\Gamma_{v'0} \sim 0.34$ cm^{-1} [22] and, again, $\alpha\sigma \sim 1$ cm^{-1}.

Observation of DICE by Phonon Sideband Absorption

For CSRS an expression analogous to Eq. 2 exists and predicts that the excited state resonance $\omega_{v'0'}$ from ρ_0 should vanish in the limit of zero pure dephasing [5]. Its intensity is proportional to the square of $\Gamma_2 = \Gamma_{v'0'} - \Gamma_{0'0} - \Gamma_{v'0}$ which is different than Γ_2 of Eq. 2 for CARS. The latter equals the inverse of the 0' level lifetime in the limit of zero pure dephasing. The pure dephasing induced effect in CSRS has been observed for $\omega_{v'0'} = 747\ cm^{-1}$ of pentacene in benzoic acid through variation of the temperature (electron-phonon scattering) [5]. It has also been observed in the gas phase and referred to as PIER-4 (pressure-induced extra resonances in four-wave mixing) by Bogdan et al. [39,40] and Prior et al. [41].

The ability to readily create significant excited state populations in CARS experiments of the type described here opens up the possibility of observing DICE effects in CARS via the Γ_2 term of Eq. 2. For example, in spectrum a of Fig. 2, the intensity of $\omega_{v'0'}$ relative to ω_{v0} is ~6.5:1 for an ω_1-pulse energy of 10 μJ and $d = +4\ cm^{-1}$. This detuning corresponds to an ω_1 excitation into the low energy tail of the phonon sideband [24] and creates an acoustic phonon wavepacket. The wavepacket propagates away from an initial site of excitation in a time $\tau \sim 1$ ps (the order of a lattice spacing divided by the acoustic velocity). This time can be

associated with the phonon relaxation time which governs population of the zero-point level (0') of the S_1 state. For $d = +4\ cm^{-1}$ and an ω_1-pulse energy of 10 μJ, is the 6.5:1 intensity ratio qualitatively consistent with phonon side band pumping? We present a rough calculation to argue that it is. At 5K the phonon sideband absorption cross-section at $d = +4\ cm^{-1}$ is ~ 1/50th [24] that of the (0',0) transition (which has a transition dipole of 0.3 A). Equation 4 yields an induced phonon sideband absorption rate of $2.6 \times 10^8\ s^{-1}$ for $\tau = 2.8$ ps. Now, consider a simple three-level system consisting of the two zero-point levels, 0 and 0', and a $+4\ cm^{-1}$ effective phonon level building on 0'. For the above absorption rate and $\tau = 2.8$ ps, the kinetic equations yield $\rho_{0'}/\rho_0 \sim 3.3$. With this value and the pertinent dephasing constants from Table 4, Eq. 2 predicts a $\omega_{v'0'}/\omega_{v0}$ intensity ratio of 6.3/1. Thus, it is not unreasonable to suggest that phonon sideband pumping is the excited state population mechanism.

With this in mind an interesting question arises: how might the ratio of the $\omega_{v'0'}$ intensity to the ω_{v0} intensity respond to increasing temperature from the low T limit (~5K) where $\Gamma_2 \sim \Gamma_{0'}$, cf. Eq. 2. A key point is that the total induced absorption rate for phonon sideband pumping can increase with increasing T since the linear electron-phonon coupling dictates that the phonen sideband absorption inten-

sity will initially increase [42,43]. Thus, for a fixed pulse energy, ρ_0, can increase with increasing T. Provided the onset of this increase occurs at a lower T than that for a significant increase in Γ_2, the form of Eq. 2 suggests that the intensity ratio $\omega_{v'0'}/\omega_{v0}$ can reach a maximum value at some $T = T_{max}$. By significant is meant that the γ_2 source of ω_{v0} intensity becomes significant in comparison with the ρ_0 term. For $T > T_{max}$ the intensity ratio would decrease. To test this idea, an experiment with $d = +4\ cm^{-1}$ and (ω_1,ω_2) pulse energies of (2,1.5) μJ was performed at T = 4.5, 13, 23 and 34K. The observed values for the intensity ratio at these temperatures are 1.1, 1.7, 1.9 and 1.0, Fig. 9. This type of T-dependence has not been previously reported and is consistent with an interplay between DICE from ρ_0, and the T-dependence of the phonon sideband absorption intensity. It is not possible at this time to discuss these results more quantitatively since the T-dependence of the Debye-Waller factor for pentacene in naphthalene has not been determined. Such a study is planned along with detailed studies of the proposed DICE effect as a function of positive detuning into the phonon sideband of the (0',0) transition.

Figure 9. Temperature dependence of the pentacene in naphthalene ω_{v0} = 755 and $\omega_{v'0'_{-1}}$ = 747 cm^{-1} CARS resonances for detuning d = +4 cm^{-1}. Spectra a-d correspond to T = 4.5, 13, 23 and 34K, respectively. In spectrum a, the band labeled by N corresponds to a naphthalene fundamental, cf. Fig. 2.

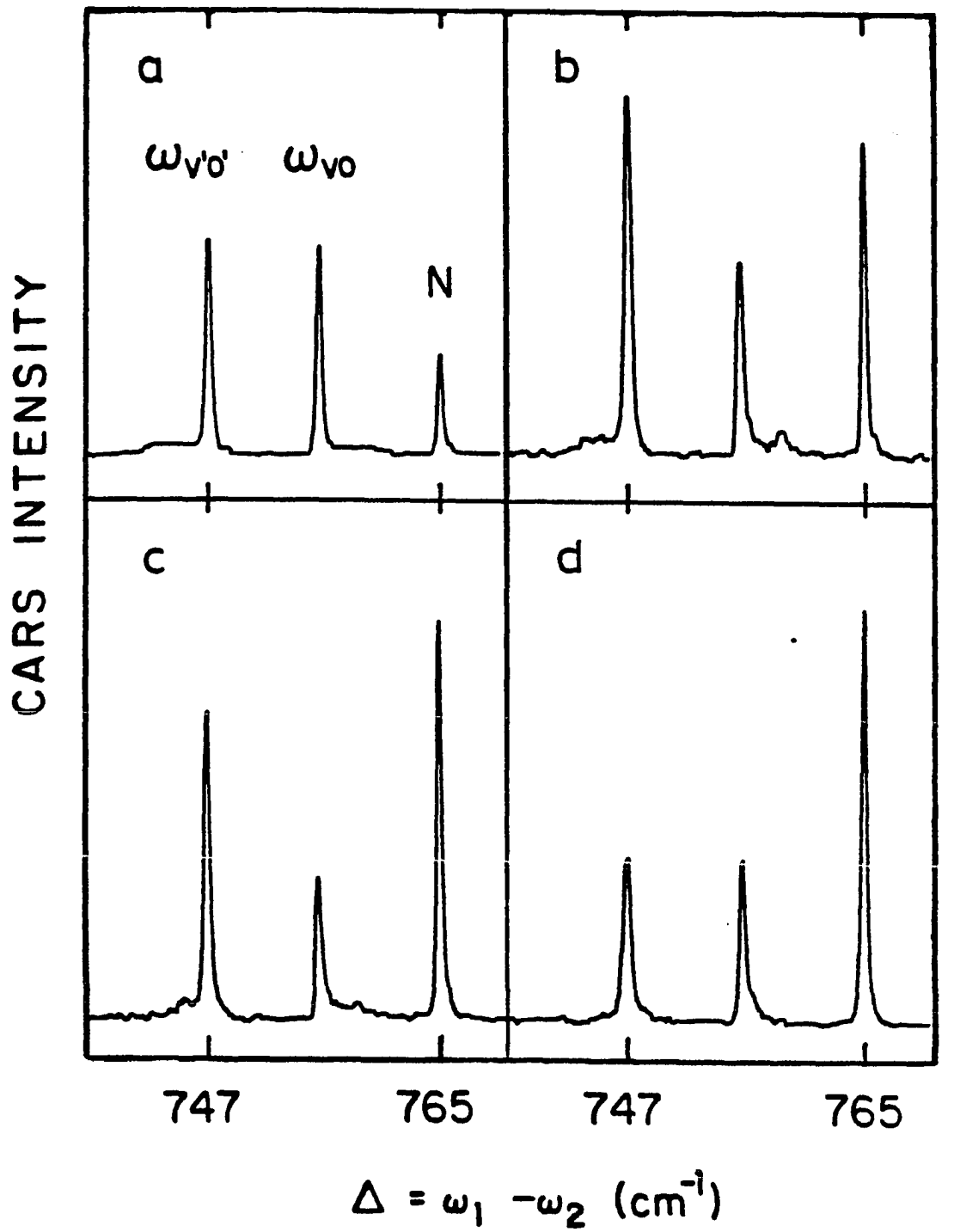
a
b
c
d
$\omega_{v'0'}$
ω_{v0}
N
CARS INTENSITY
747
765
747
765
$\Delta = \omega_1 - \omega_2$ (cm^{-1})

Power Broadening

Here we discuss experimental data on power broadening of the stationary ω_{v0} = 755 cm^{-1} resonance for pentacene in naphthalene. Earlier work by Andrews and Hochstrasser [6] had noted that power broadening for mixed molecular crystals is readily observable in nearly fully resonant four-wave mixing spectra with pulse energies of only a few μJ.

Ouellette and Denariez-Roberge (hereafter OD) [31] and Dick and Hochstrasser [30] have investigated theoretically the dynamic Stark effect in CARS of a discrete four level system interacting with monochromatic fields. In a manner reminiscent of dressed atom effects in a two level system [44], one or more strong fields can produce a Stark multiplet structure for a stationary CARS resonance (the moveable resonances can also be affected but this is not our concern here). The Stark component intensities depend on the detunings of the fields from the pertinent material resonances while the detunings and Rabi frequencies ($W_i = \mu E_i/\hbar$) govern the splittings. However, the component linewidths are generally not significantly power broadened.

In OD three incoming fields ($\omega_1, \omega_2, \omega_3$) are considered with $\underline{k}_{as} = \underline{k}_1 - \underline{k}_2 + \underline{k}_3$, and a number of cases of interest are treated (in our experiments $\omega_3 = \omega_1$). The cases are distinguished by the strengths of fields (strong vs. weak). The

strength is governed by the Rabi frequency and the detuning of the field from the material resonance. The resulting expressions for the density matrix element which governs the CARS spectrum are lengthy and are not reproduced here.

It is instructive to consider the case of a strong ω_1-field (ω_2- and ω_3-fields weak) and d = 0 which is described by Eq. 24 of OD. For the value of 0.3 A for the pentacene (0',0) transition dipole and a pulse energy of 10 μJ (focused to 0.15 mm), the ω_{v0} resonance should appear as a symmetric doublet with a Stark splitting of 0.4 cm^{-1} (equal to the Rabi frequency) [45]. This result can be obtained in a more transparent manner by noting that in the derivation of the ρ_0 term of Eq. 1, the pertinent term for the ω_1 strong field case yields the $\omega_{v0} - \Delta$ resonance through the equality $\omega_{0'0} - \omega_{0'v} = \omega_{v0}$. The ω_1 field interacting only with the $\omega_{0'0}$ resonance via the matrix element $u_{0'0} \cdot E_0/2\hbar$ splits this resonance into a doublet, $\omega_{0'0} \pm u_{0'0} \cdot E_0/2\hbar$. Each component for d = 0 contributes equally in four-wave mixing resulting in the aforementioned doublet. The calculated results presented below are obtained using this simple approach and agree with those obtained from the appropriate equations of OD. Now, although pulse energies of 10 μJ and greater have been used in a few d = 0 experiments, no discernible splitting was observed, only a power broadening comparable to the Rabi frequency. The reasons for this are that the inhomogeneous linewidth of the (0',0) absorption transition is greater than the field-resonance Rabi

frequency and our lasers are multi-mode. The theory is strictly applicable only to a discrete four-level system interacting with monochromatic fields.

We have studied in most detail the power dependence of the ω_{v0} resonance for negative detunings, d = -2.5 and -6.0 cm^{-1}. For a fixed ω_2 pulse energy of 0.8 μJ and ω_1 pulse energies of 1.0, 2.5, 5.0 and 10 μJ the observed ω_{v0} linewidths are 0.35, 0.45, 0.55 and 0.65 cm^{-1}, respectively, and are the same for both detunings. The narrowest linewidth observed for the resonance is 0.32 cm^{-1} (in CARS for d = -15 cm^{-1}, vide supra). Rough estimates of the power broadenings are 0.03, 0.13, 0.23 and 0.33 cm^{-1}. However, for a fixed ω_1 pulse energy of 1 μJ and d = -6 cm^{-1}, the linewidths for ω_2 pulse energies of 0.2, 0.8, 2.0 and 8.0 μJ were observed to be identical (0.35 cm^{-1}). In considering this result it is important to note that the transition dipole for the $\omega_{0,v}$ resonance interacting with the ω_2-field is ca. 1/5th of that for the $\omega_{0,0}$ and $\omega_{v,v}$ resonances [24]. The latter provide the important interactions with the ω_1-fields.

At detunings of -2.5 cm^{-1} and -6 cm^{-1} and with the Rabi frequencies employed, vide infra, it is readily shown, for the discrete four-level system of Fig. 1, that only one of the ω_{v0} Stark shifted components would carry sufficient intensity to be observable. Further, with the pulse energies employed and the ~ ± 1 cm^{-1} uncertainty in our measured vibrational fre-

quencies, one could not expect to measure the Stark shifts. The most likely explanation for the power broadening observed from the ω_1 field is that it is a manifestation of the distribution of Stark shifts stemming from the fact that the vibronic resonances are inhomogeneously broadened (~2 cm^{-1}). That is, the magnitude of the Stark shift for a particular impurity site depends on the detunings of <u>its</u> resonances away from ω_1. Consider first the d = -2.5 cm^{-1} case with the reasonable approximation that ω_1 <---> $\omega_{0',0}$ represents the only strong coupling ($\omega_3 = \omega_1$ being detuned from $\omega_{v',v}$ by ~6 cm^{-1}). The secular determinant (2x2) for the strong interaction is readily solvable (off-diagonal matrix element = $u_{0',0} \cdot E_0/2\hbar = (2\pi)^{1/2} n_b^{-3/2} (u_{0',0}/\hbar)(I/c)^{1/2}$, where I is the intensity of the ω_1-field measured outside the crystal). The solution yields the Stark shift for the allowed component of the CARS resonance since in Eq. 1 $\omega_{v0} = \omega_{0',0} - \omega_{0',v}$. To estimate the "power broadening" due to the inhomogeneous broadening of the (0',0) transition, the calculated Stark shifts for d = -2.5 and -2.5 ± 1.0 cm^{-1} (corresponding to the FWHM points of the (0',0) profile) are given in Table 5. The Rabi frequencies corresponding to the ω_1 pulse energies of 1.0, 1.5, 5.0 and 10 μJ (beam radius of 0.1 mm) are 0.18, 0.28, 0.4 and 0.58 cm^{-1}. Subtraction of the d = -1.5 and -3.5 cm^{-1} entries in Table 5 for a given Rabi frequency provides an estimate of the power broadening. Thus, the estimated power broadenings for the

Table 5. Stark shifts as a function of detuning and Rabi frequency

W (cm^{-1})	d (cm^{-1})		
	-1.5	-2.5	-3.5
0.1	0.01	0	0
0.15	0.02	0.01	0.01
0.2	0.03	0.02	0.01
0.25	0.04	0.03	0.02
0.3	0.06	0.04	0.03
0.35	0.08	0.05	0.04
0.4	0.10	0.06	0.05
0.5	0.15	0.10	0.07
0.6	0.21	0.14	0.10
0.7	0.28	0.18	0.14
0.8	0.35	0.23	0.17
1.0	0.50	0.35	0.27

experimental Rabi frequencies are sufficiently close to the observed values to assert that a distribution of Stark shifts is a likely explanation for the power broadening. We point out that the calculated values in Table 5 are in very good agreement with those calculated with Eq. 24 of OD. At present we are developing a more formal theory for the dynamic Stark effect which is to be applicable to a four-level system pos-

sessing inhomogeneously broadened resonances.

With our simple model one can understand why the power broadenings for d = -6 and -2.5 cm^{-1} are equal within experimental uncertainty. For d = -6 cm^{-1}, $\omega_3 = \omega_1 \langle\text{---}\rangle \omega_{v'v}$ is the strong interaction since its detuning is +2.5 cm^{-1} and $u_{v'v} = u_{0'0}$. The $\omega_1 \langle\text{---}\rangle \omega_{0'0}$ interaction is approximated as weak since its detuning is -6 cm^{-1}. The pertinent term for the ω_3 strong field case contributes to the $\omega_{v0} - \Delta$ resonance of Eq. 1 (ρ_0 term) by virtue of the equality $\omega_{v0} = \omega_{v'0} - \omega_{v'v}$. Thus, Stark shifting of $\omega_{v'v}$ leads directly to Stark shifting of the CARS ω_{v0} resonance. As expected, our calculations show that the power broadening from the distribution of Stark shifts for d = -6 cm^{-1} is, for all intent and purposes, identical to that for d = -2.5 cm^{-1}.

In the above Stark shift calculations, it has been assumed that the ω_2-field is weak. This is reasonable since in the $\omega_1(\omega_3)$-power dependence studies an ω_2-pulse energy of 0.8 μJ was used and, furthermore, power broadening of the ω_{v0} resonance was not observed for ω_2-pulse energies as high as 8 μJ (ω_1-pulse energy of 1 μJ, d = -6 cm^{-1}), vide supra. This absence of power broadening is understandable since the transition dipole of the $\omega_{0'v}$ resonance is 1/5th that of the $\omega_{0'0}(\omega_{v'v})$ resonance and also for d = -6 cm^{-1} the average detuning of ω_2 from the $\omega_{0'v}$ resonance is large, ~ -6 cm^{-1}.

ACKNOWLEDGEMENT

Ames Laboratory is operated for the U.S. Department of Energy by Iowa State University under Contract No. W-7405-Eng-82. This research was supported by the Director for Energy Research, Office of Basic Energy science. Funding for the Laser system used was provided by NSF.

Useful discussions with Robin M. Hochstrasser pertaining to line narrowing and dynamic Stark effects are gratefully acknowledged.

REFERENCES

1. R. M. Hochstrasser; G. R. Meredith; H. P. Trommsdorff, J. Chem. Phys. 73, 1009 (1980).

2. P. L. DeCola, R. M. Hochstrasser and H. P. Trommsdorff, Chem. Phys. Lett. 72, 1 (1980).

3. P. L. DeCola, J. R. Andrews, R. M. Hochstrasser and H. P. Trommsdorff, J. Chem. Phys. 73, 4695 (1980).

4. J. R. Andrews, R. M. Hochstrasser and H. P. Trommsdorff, Chem. Phys. 62, 87 (1981).

5. J. R. Andrews and R. M. Hochstrasser, Chem. Phys. Lett. 82, 381 (1981).

6. J. R. Andrews and R. M. Hochstrasser, Chem. Phys. Lett. 83, 427 (1981).

7. R. Bozio, P. L. DeCola and R. M. Hochstrasser, in "Time Resolved Vibrational Spectroscopy", G. H. Atkinson, Ed., Academic Press: New York, 1983.

8. B. H. Hesp, and D. A. Wiersma, Chem. Phys. Lett. 75, 423 (1980).

9. F. Ho, W.-S. Tsay, J. Trout and R. M. Hochstrasser, Chem. Phys. Lett. 83, 5 (1981).

10. K. Duppen, B. Hesp and D. A. Wiersma, Chem. Phys. Lett. 79, 399 (1981).

11. F. Ho, W.-S. Tsay, J. Trout, S. Velsko and R. M. Hochstrasser, Chem. Phys. Lett. 97, 141 (1983).

12. E. L. Chronister and D. D. Dlott, J. Chem. Phys. 79, 5286 (1983).

13. C. L. Schlosser and D. D. Dlott, J. Chem. Phys. 80, 1394 (1984).

14. M. D. Levenson, "Introduction to Nonlinear Laser Spectroscopy", Academic Press: New York, 1982.

15. R. M. Hochstrasser and H. P. Trommsdorff, Acc. Chem. Res. 16, 376 (1983).

16. See Refs. 7 and 15 and references therein.

17. S. A. J. Druet, J.-P. E. Taran and Ch. J. Borde', J. Phys. (Paris) 40, 819 (1979).

18. J. L. Oudar and Y. R. Shen, Phys. Rev. A22, 1141 (1980).

19. J. M. Hayes, R. P. Stout and G. J. Small, J. Chem. Phys. 74, 4266 (1981).

20. G. J. Small, in "Molecular Spectroscopy", V. M. Agranovich and R. M. Hochstrasser, Eds. North Holland Publishing Co.: Amsterdam, 1983.

21. T. P. Carter, B. L. Fearey, J. M. Hayes and G. J. Small, Chem. Phys. Lett. 102, 272 (1983).

22. K. Duppen, D. P. Weitekamp and D. A. Wiersma, J. Chem. Phys. 79, 5835 (1983).

23. W. H. Hesselink and D. A. Wiersma, J. Chem. Phys. 74, 886 (1981).

24. W. H. Hesselink and D. A. Wiersma, J. Chem. Phys. 73, 648 (1980).

25. L. A. Carreira, T. C. Maquire and T. B. Malloy, Jr., J. Chem. Phys. 66, 2621 (1977)

26. B. L. Fearey, T. P. Carter ands G. J. Small, J. Phys. Chem. 87, 3590 (1983).

27. N. Bloembergen, H. Lotem and R. T. Lynch, Indian J. Pure Appl. Phys. 16, 151 (1978).

28. P. DeBree and D. A. Wiersma, Chem. Phys. Lett. 88, 17 (1982).

29. B. Dick and R. M. Hochstrasser, J. Chem. Phys. 78, 3398 (1983).

30. B. Dick and R. M. Hochstrasser, Chem. Phys. 75, 133 (1983).

31. F. Ouellette and M. Denariez-Roberge, Can. J. Phys. 60, 877 (1982).

32. Available upon request, Dept. of Chemistry, Iowa State University.

33. R. M. Hochstrasser, Dept. of Chemistry, University of Pennsylvania, Private communication.

34. M. A. Yuratich, Mol. Phys. 38, 625 (1979).

35. T-C. Chang and G. J. Small, Chem. Phys. to be published.

36. T-C. Chang and G. J. Small, Dept. of Chemistry, Iowa State University, unpublished results.

37. R. M. Hochstrasser and H. N. Sung, J. Chem. Phys. 66, 3276 (1977).

38. A. N. Winchell, "The Optical Properties of Organic Compounds", Academic Press: New York, 1954; 78.

39. A. R. Bogdan, Y. Prior and N. Bloembergen, Opt. Lett. 6, 82 (1981).

40. A. Bogdan, M. Downer and N. Bloembergen, Phys. Rev. A24, 623 (1981).

41. Y. Prior, A. R. Bogdan, M. Dagenais and N. Bloembergen, Phys. Rev. Lett. 46, 111 (1981).

42. See, for example, F. P. Burke and G. J. Small, Chem. Phys. 5, 198 (1974) and references cited therein.

43. At sufficiently high T 2- and higher-phonon transitions can become more probable than 1-phonon transitions and, thus, the absorption intensity from the latter could maximize and then decrease.

44. H. Haken, "Light", North-Holland Publishing Company, Amsterdam, 1981.

45. Because the calculations which follow are only approximate, the direction cosine correction for the Rabi frequencies is not made since the correction reduces the frequencies by only 25%.

PAPER II.

FULLY RESONANT CARS OF CRESYL VIOLET IN POLYACRYLIC ACID POLYMER FILMS

FULLY RESONANT CARS OF CRESYL VIOLET IN POLYACRYLIC ACID POLYMER FILMS

TA-CHAU CHANG and GERALD J. SMALL

Ames Laboratory-USDOE and Department of Chemistry
Iowa State University, Ames, Iowa 50011

ABSTRACT

Multi-resonant CARS data for ground and excited electronic state resonances (585,593 cm^{-1}) of cresyl violet perchlorate in polyacrylic acid are reported. The intensity of the excited state resonance (585 cm^{-1}) depends on the location of the ω_1-field ($\omega_{as} = 2\omega_1 - \omega_2$) within the severely inhomogeneously broadened absorption profile of the dye. Nonphotochemical hole burning is used to determine the vibronic transitions which contribute to the absorption profile. It is argued that the linear electron-phonon interaction is an important mechanism for producing an egalitarian distribution of excited dye sites with a population sufficiently high to permit observation of the excited state resonance. A marked nonphotochemical hole burning effect on the intensities of the CARS resonances is used for the assignment of 585 cm^{-1} as an excited state resonance. The absence of line narrowing in the CARS and CSRS spectra is reported and discussed. Finally, a novel narrowing of the 593 cm^{-1} ground state resonance with increasing temperature is reported and shown to only occur for restricted values (frequency) of ω_1.

INTRODUCTION

Dispersive fully resonant four-wave mixing spectroscopy (CARS, CSRS) of mixed molecular crystals has been the subject of several investigations. Pentacene in benzoic acid has been studied most thoroughly [1-5], although pentacene in naphthalene has been recently investigated [6]. In the former studies, Hochstrasser and his coworkers have shown how to exploit the fact that, in the fully resonant mode, the guest molecule can be modeled as a four level system. For example, dephasing induced coherent emission or DICE (analogous to PIER-4 in the gas phase [7-9]) has been observed in the ground and excited electronic states of pentacene [3-5,6] as has line narrowing [5,6]. The latter phenomenon occurs if the site inhomogeniety distribution functions associated with the pertinent vibrational and vibronic resonances are appropriately correlated [6,10,11].

Very little work, however, has appeared on resonant four-wave mixing spectroscopy of molecules imbedded in amorphous or highly disordered hosts such as polymers. While the excellent optical quality of polymers make them attractive candidates, the large inhomogeneous broadening their disorder imparts on the vibronic transitions of the guest molecule introduces obvious complexities. Pertinent for this work is the fact that the low temperature optical absorption spectra of ionic

laser dyes in polymers are extremely broad and exhibit little discernable vibronic structure [12].

In this letter we present, for the first time, resonant CARS ($\omega_{as} = 2\omega_1 - \omega_2$) data from an ionic dye in a polymer matrix; cresyl violet perchlorate (CV) in polyacrylic acid (PAA). Prior to initiating the CARS studies it was important to have a reasonable understanding of which vibronic transitions, in addition to the origin, contribute to the broad absorption profile of CV in a polymer. Fortunately, the non-photochemical hole burned (NPHB) spectra of CV in polyvinyl alcohol provided us with such [12]. It is shown here that the vibronic satellite hole structure of CV in PAA is very similar to that for polyvinyl alcohol. Because the 585 cm^{-1} excited state mode of CV is an intense feature in the hole burned spectrum it was decided to focus attention on the ~590 cm^{-1} region for the CARS studies. This proved to be a good choice. Several resonances in this region have been observed. We focus here on two resonances at 585 and 593 cm^{-1} which are readily observable with modest pulse energies (a few μJ). They are assigned as the excited and ground electronic state counterparts of the same mode. The data which, in addition to the NPHB results, lead to this assignment include those from experiments in which the ω_1-field is tuned over a considerable portion of the CV absorption profile, and in which the intensities of the two resonances are monitored as a function of

ω_1-irradiation time. The latter experiments reveal a pronounced hole burning effect. Possible reasons for the case with which the excited state resonance is observed in such a severely inhomogeneously broadened system are considered. In addition, T-dependent data are presented which establish, for the first time, that a CARS resonance (593 cm^{-1}) can undergo a decrease in linewidth with increasing T in a polymer. Importantly, the extent of this narrowing depends on the location of ω_1 within the absorption profile. It is suggested that the narrowing is not the result of configurational motion intrinsic to the polymer but, rather, motion along a coupled polymer - CV coordinate. Finally, the absence of any apparent line narrowing [6,10,11] in the CARS spectra is reported and discussed.

EXPERIMENTAL

The four-wave mixing experimental system used is fairly conventional in design and has been discussed elsewhere [6]. Briefly, two grazing incidence dye lasers (ω_1 and ω_2) pumped by the second harmonic of a Q-switched Nd:YAG laser provided close to Gaussian profiles with FWHM of 0.14 cm^{-1}. In the ω_1-tuning experiments on CV/PAA, ω_1 was varied from near the peak of the absorption profile at 17,010 cm^{-1} to 15,625 cm^{-1} on the low energy tail (with R610, R640, DCM dyes). For each value of ω_1, the ω_2-field was tuned to generate the CARS resonances. For ω_1 and ω_2 pulse energies ranging from 2 to 50 μJ (spot size ~0.3 mm) no significant power broadening of the resonances was observed. This is not surprising since the resonances reported here have FWHM ~4 cm^{-1}, an order of magnitude greater than those observed for mixed crystals [6]. A Janis vari-temp convection cooled liquid helium cryostat was used for the T-dependent studies. Details pertaining to the preparation of the polymer films are given elsewhere [12]. Although we do not report here the results of CV experiments in which polyvinyl carbazole was used as the polymer host, it should be noted that the non-resonant CARS background from this polymer is much greater than that from PAA.

RESULTS

The low T absorption spectrum of CV in PAA is given as the upper curve in Fig. 1. The lower trace is the NPHB spectrum obtained with a burn frequency, ω_B, close to the absorption maximum. Details of the experimental hole burning apparatus and procedure are given elsewhere [12,13]. Of concern here is that the displacements from ω_B of the vibronic satellite holes lying to lower energy of ω_B, yield the frequencies of the active excited state vibrations of CV. Note the prominent satellite hole at 585 cm^{-1}. The interpretation or analysis of vibronic satellite hole structure is straightforward [14] so we only point out that the hole at 585 cm^{-1} is due to CV sites whose zero-phonon origin transition frequency lines at ω_B - 585. These sites absorb ω_B via the 585 cm^{-1} vibronic transition and subsequently, following vibrational relaxation, undergo hole burning. Despite the richness of the satellite hole sturcture, NPHB studies with ω_B situated on the low energy tail of the absorption profile indicate that the origin transition of CV is considerably more intense than the vibronic transitions [14]. Further discussion of the NPHB spectrum is deferred until the following section.

Resonant CARS spectra of the 590 cm^{-1} region revealed two resonances at 585 and 593 cm^{-1}. Independent of the temperature (~5 - 300 K), their relative intensities exhibit a strong

Figure 1. Hole burning for CV in PAA at ~5 K. Spectrum a is the inhomogeneous profile before hole burning, trace b shows the same sample after burning with the dye laser for 8 min with 5 mW/cm^{-1} at 596.0 nm. Frequency displacements of the satellite holes from the burn frequency are given in cm^{-1}. The broad hole to the red of ω_B at 32 cm^{-1} is a pseudo-phonon sideband hole.

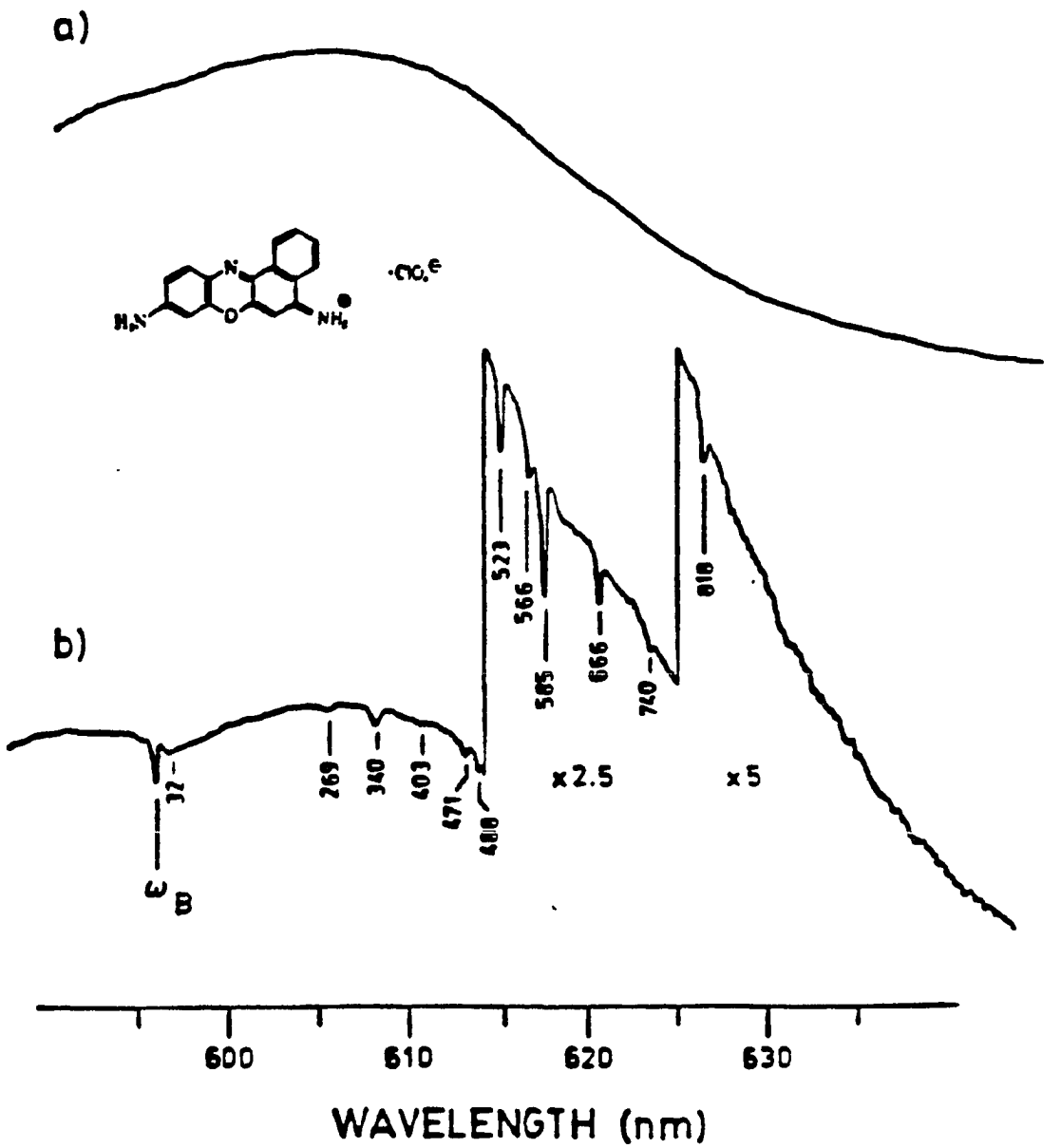
a)
b)
ω_B
332
269
340
403
471
488
523
566
585
666
740
818
x2.5
x5
600
610
620
630
WAVELENGTH (nm)

dependence on the ω_1 frequency. As an example, Fig. 2 shows T = 80 K spectra corresponding to ω_1 values ranging from 608.0 nm near the absorption maximum to 638.0 nm on the low energy tail. The picture which emerges is that the intensity of the 585 cm^{-1} resonance maximizes when ω_1 is close to the maximum of the absorption profile and decreases as ω_1 is tuned to the high and low energy sides of the maximum. We note that at the elevated temperature of 80 K used to obtain the spectra in Fig. 2, nonphotochemical hole burning is not a complication. At the outset we considered the possibility that the 585 and 593 cm^{-1} resonances might be the same ground state mode due to CV occupying amorphous and crystalline regions of the polymer. As a check, samples were annealed at 105°C (close to the glass transition temperature) for four days and then quenched to 77 k. Spectra were then obtained at 77 K and liquid helium temperatures. No significant effect on the relative intensities of the 585 and 593 cm^{-1} resonances due to annealing was observed. Annealing should increase the degree of crystallinity. Thus, although crystalline regions of PAA should exist since PAA possesses H-bonding, the annealing experiment argues against the above interpretation.

Given the existence of the 585 cm^{-1} hole in the NPHB spectrum, a more likely possibility is that the 585 cm^{-1} CARS resonance is the excited electronic state counterpart of the CV ground state mode at 593 cm^{-1}. That is, absorption by (and

Figure 2. CARS spectra for CV in PAA as a function of ω_1 at T = 80 K (except profile f at T = 65 K and profile g at T = 70 K). Profiles a-h correspond to ω_1 = 608.0, 614.0, 618.0, 622.0, 626.0, 630.0, 634.0 and 638.0 nm obtained with (ω_1,ω_2) pulse energies of (24,24), (40,17),(30,18), (15,18), (13,9), (13,20), (25.20), and (14,20) μJ, respectively.

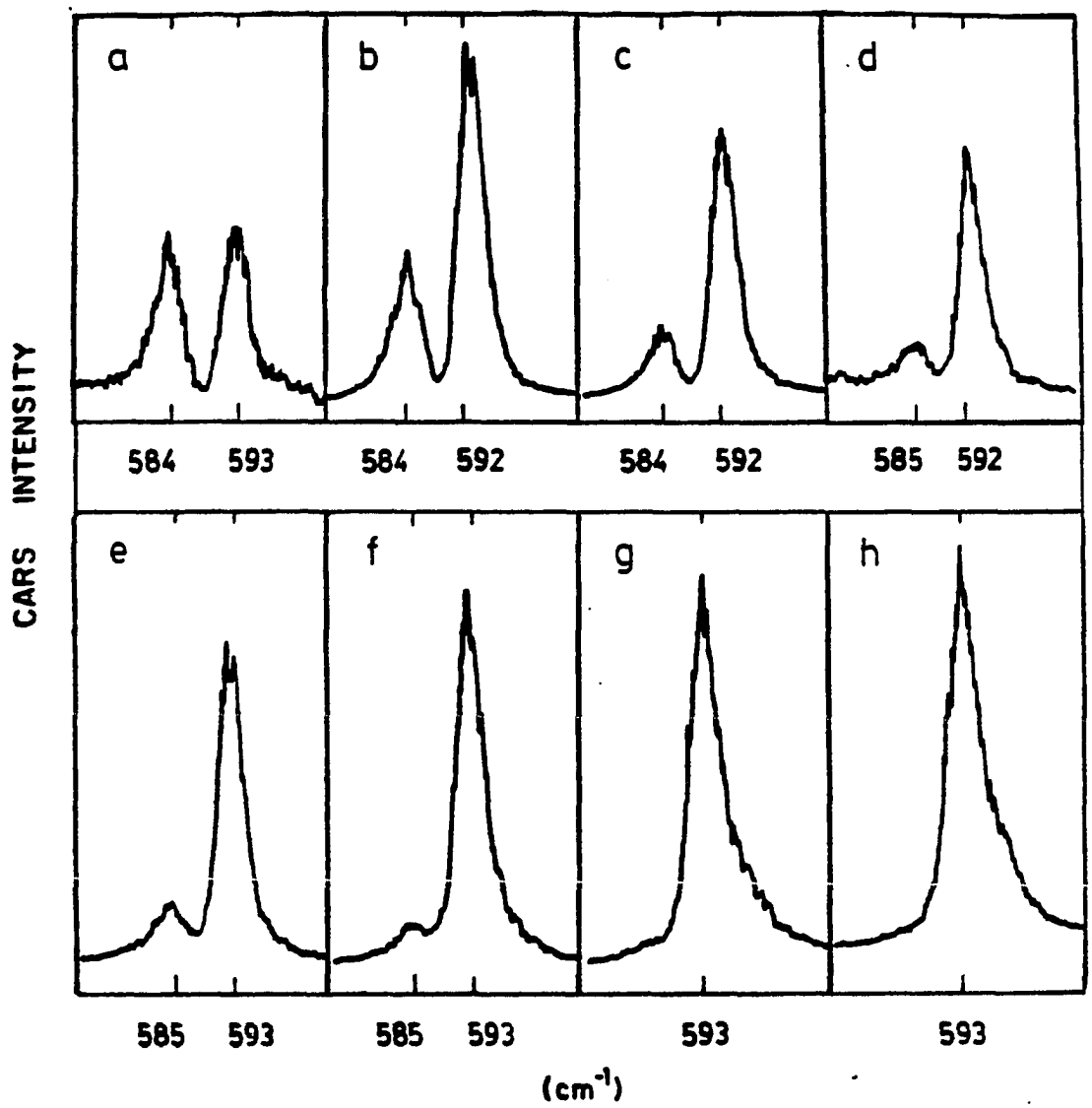
a
b
c
d
584 593
584 592
584 592
585 592
e
f
g
h
585 593
585 593
593
593
CARS INTENSITY
(cm⁻¹)

ω_2) results in a significant population of the S_1 state of CV. Data are now presented which support this interpretation. The three sets of spectra for the 585 and 593 cm^{-1} resonances shown in Fig. 3 were obtained with (ω_1,ω_2) pulse energies of 5.2 and 1.6 μJ, T = 4.6 K. The average ω_1-field intensity is 75 mW/cm^2, considerably greater than that used to obtain the hole burned spectrum of Fig. 1. Prior to the scan for spectrum a, a different sample spot was used to optimize the phase-matching condition. Translation to a fresh spot could be achieved without significant loss of phase-matching. Thus, a fresh spot was used to obtain spectrum a with the (ω_1, ω_2) irradiation time given by the scan time (~4 min). Immediately, following this scan the ω_2-beam was blocked and the same spot irradiated for 1.5 min by ω_1 (5.2 μJ). Spectrum b was obtained directly after this irradiation. Spectrum c was obtained following an additional irradiation with ω_1 of 5 min. Spectra a-c were recorded with the same gain and so it is apparent that the dependence (decrease) of the intensity of the 585 cm^{-1} resonance on increasing ω_1-irradiation time is stronger than the dependence for the 593 cm^{-1} resonance. This type of behavior was observed for several other ω_1 frequency values.

To conclude this section we present Fig. 4 which shows the T-dependence of the 593 cm^{-1} CARS profile for ω_1 = 15723 cm^{-1} (636.0 nm). The apparent narrowing behavior with in-

creasing T was reproducible from sample to sample but, interestingly, is confined to ω_l values lying to lower energy of 633.0 nm. For example, for ω_l = 630.0 nm the FWHM of the 593 cm^{-1} resonance is constant at ~4.1 cm^{-1} between 5 K and room temperature. The above narrowing behavior is reversible, i.e. the original broad low T linewidth is recovered upon recycling back to 4.6 K.

Figure 3. CARS spectra for CV in PAA as a function of irradiation time of ω_1 at 596.0 nm. Spectra were obtained with (ω_1,ω_2) pulse energies of (5.2,1.6) μJ at T = 4.6 K. See text for details.

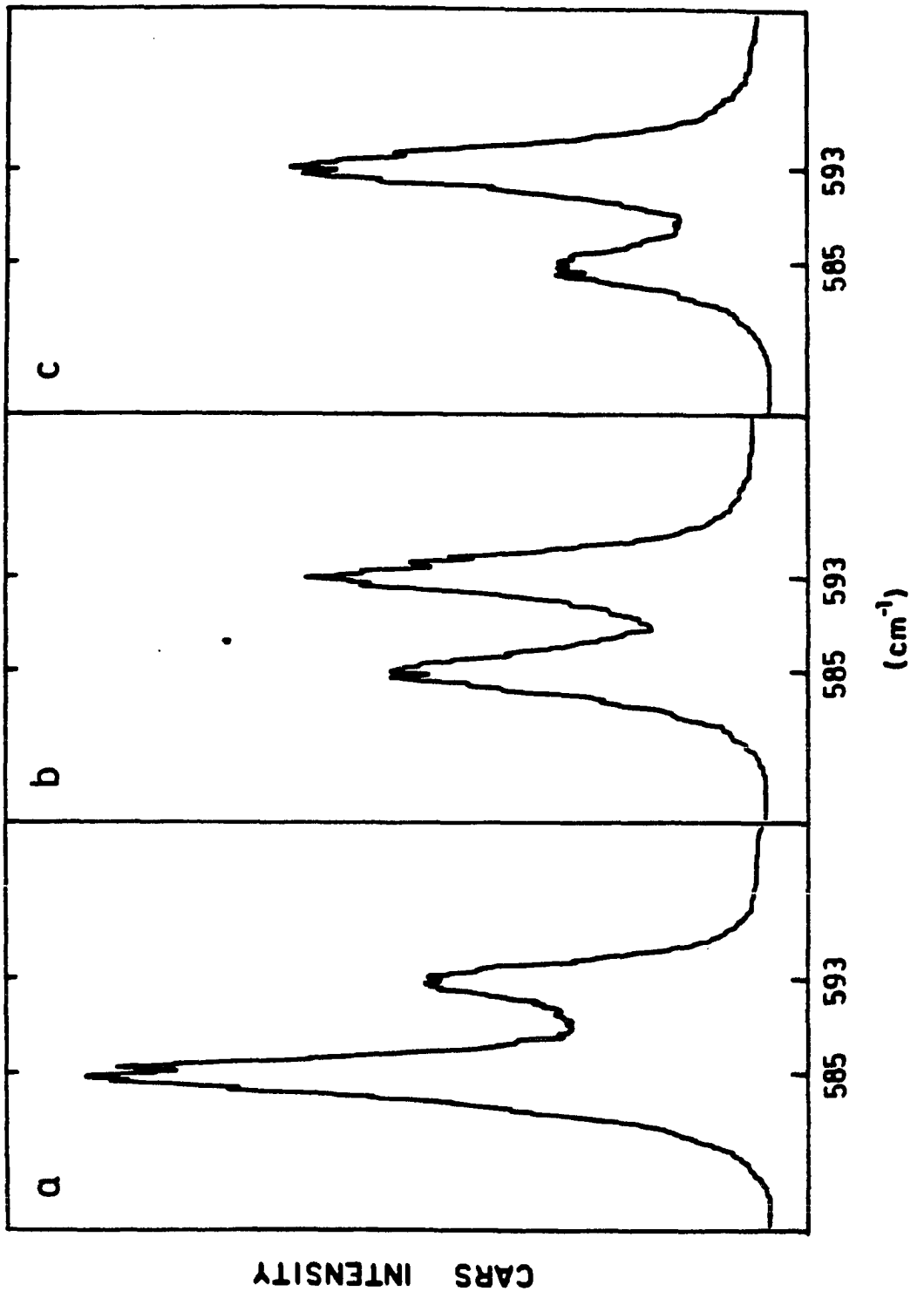
a
b
c
585
593
585
593
585
593
(cm⁻¹)
CARS INTENSITY

Figure 4. Temperature dependence of the ω_{v0} = 593 cm^{-1} CV/PAA CARS resonance for ω_1 = 636.0 nm. Spectra a-f correspond to T = 4.6, 11, 19, 30, 48 and 74 K obtained with (ω_1,ω_2) pulse energies of (6,1.5) μJ, respectively.

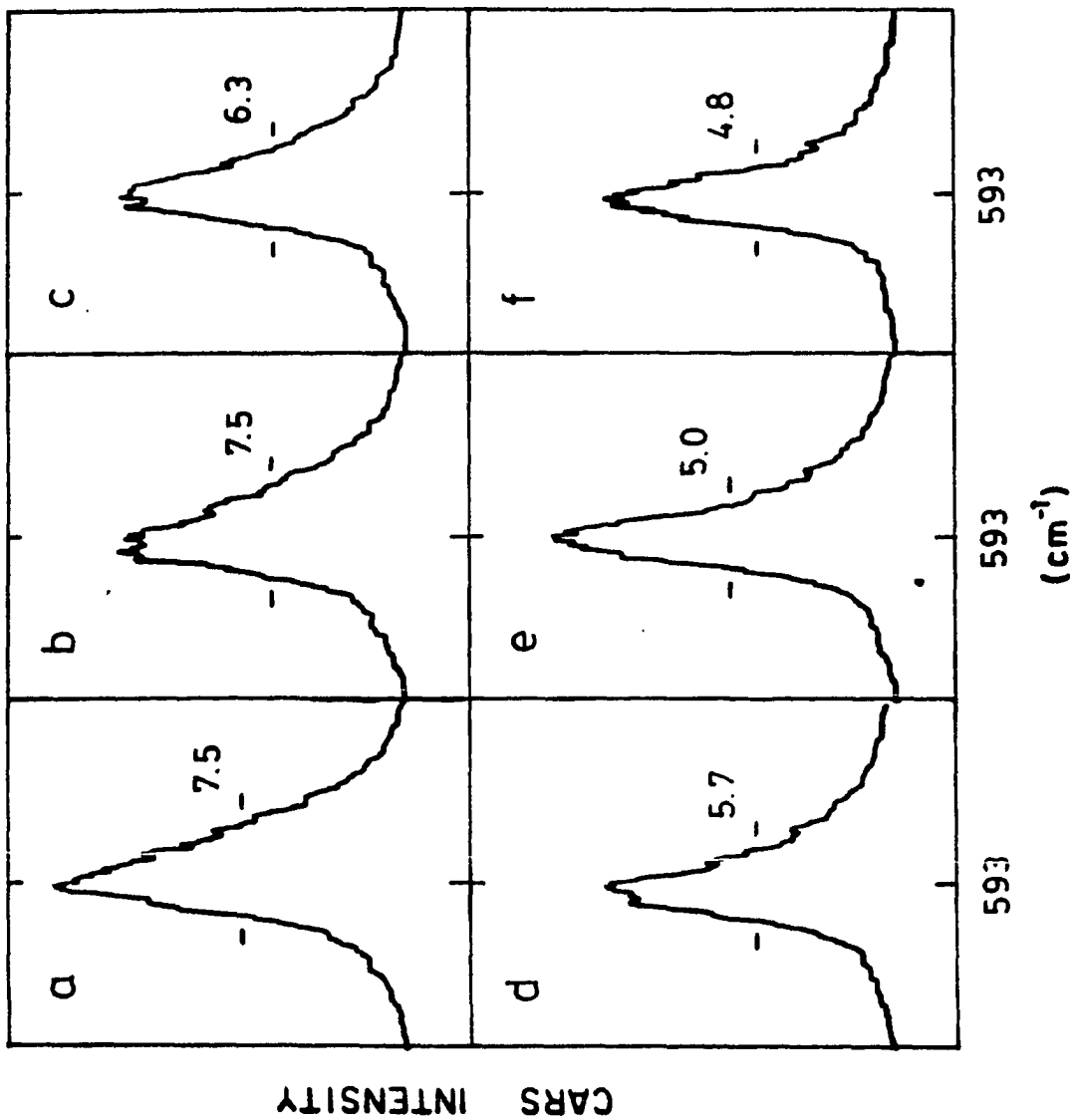
a
7.5
b
7.5
c
6.3
d
5.7
e
5.0
f
4.8
593
593
593
(cm⁻¹)
CARS INTENSITY

DISCUSSION

We begin by considering the data which suggest that the 585 cm^{-1} resonance is the excited state counterpart of the CV 593 cm^{-1} ground state mode. Of course, the observation of a prominent satellite hole at 585 cm^{-1} in the NPHB spectrum argues for this assignment. So do the data of the type shown in Fig. 3. These data were obtained with an average ω_1-intensity sufficiently high (75 mW/cm^2) to produce a deep (50% optical density change at saturation) zero-phonon hole coincident with ω_1 in several minutes [12,15]. Accompanying this hole is a broad pseudo-phonon sideband hole lying to the low energy side of ω_1, cf. Fig. 1. The peak intensity of the latter exceeds that of the saturated zero-phonon hole for sufficiently high burn fluences [14,15]. Thus, with the 585 cm^{-1} viewed as an excited state resonance one can understand why its intensity decreases with increasing ω_1-irradiation time, Fig. 3. It is a consequence of decreasing optical density at ω_1 due to hole burning which is reflected by a decreasing excited state population. The fact that the decrease in intensity of the 584 cm^{-1} resonance is not fully compensated by the increase in intensity of the 593 cm^{-1} ground state resonance is interesting, Fig. 3. It can be qualitatively understood by taking into consideration the following: the zero-phonon (at ω_1) and phonon sideband hole production is accom-

panied by production of a broad anti-hole to higher energy of ω_1 [14,15]. The same effect occurs in the vibronic satellite hole regions. Thus, by the very nature of NPHB there is no net loss in total absorption intensity; and the vibronic resonances associated with the multi-resonant CARS terms [5,6] which govern the ground state resonance intensity carry the inhomogeneous linewidths of the vibronic transitions (several hundred cm^{-1}). These two factors, together with the decrease in excited state population (with increasing ω_1-irradiation time), work in concert to counteract a reduction in intensity of the 593 cm^{-1} resonance due to the overall loss of resonant sites from hole burning. A quantitative understanding of intensity dependence on ω_1-irradiation time would be difficult to attain, in part because hole burning at ω_1 and the satellite regions occurs during the CARS scan (as well as hole filling at ω_1 due to the ω_2-laser, so-called laser induced hole filling effect [16]). We note that the type of behavior shown in Fig. 3 has also been observed for nile blue in PAA [17].

Not so apparent is the explanation for why the 585 cm^{-1} excited state resonance carries an intensity comparable to that of the 593 cm^{-1} ground state resonance, Fig. 3. This, perhaps, surprising result is also observed for nile blue. Given the severely inhomogeneously broadened nature of the optical absorption spectrum, the fact that the vibronic resonances associated with the usual CARS terms [5,6] (which

govern the intensities of the resonances) carry the large inhomogeneous linewidths (~500-1000 cm^{-1}) of the vibronic transitions and the extreme narrowness of the laser relative to the vibronic inhomogeneous linewidths, such a result was not anticipated. An explanation must take into account the results of Fig. 2 which show that the intensity of the 584 cm^{-1} resonance decreases as ω_1 is tuned from the absorption profile maximum to the low energy tail. In the tail region, ω_1 (and ω_2) is in resonance primarily with molecular origin (0,0) transitions while near the maximum, ω_1 (and ω_2) pump vibrationally congested regions. Indeed, Fig. 1 gives an accurate picture for the latter situation and shows that ω_1 pumps several different isochromats belonging to a corresponding number of vibronic transitions, 585 cm^{-1} being one of them. The vibronic transitions correspond to the zero-phonon satellite holes in Fig. 1. Considering only zero-phonon transitions, the zero-point (molecular) site energy distribution function for the excited electronic state is multi-peaked when ω_1 is tuned to a vibrationally congested region and single-peaked when ω_1 lies in the low energy tail. It is obvious then that the former situation can lead not only to a greater excited state population but also to a more egalitarian representation of the CV sites excited. But given that the intensities of the 585 and 593 cm^{-1} resonances are comparable when ω_1 is in the vicinity of the absorption maximum and that the

vibronic transitions have inhomogeneous linewidths of several hundred cm^{-1}, far greater egalitarianism would appear to be necessary. That is, one is attempting to arrive at a situation where the <u>total</u> excited state population is approximately the same as the ground state population [6]. One is far from this situation when only zero-phonon vibronic transitions are considered. To see this we ignore for simplicity but without loss of generality the DICE contribution to the excited state resonance. Then the pertinent term of $X^{(3)}(\omega_{as})$ for the intensity of this resonance can be written as

$$X^{(3)}(\omega_{as}) \propto \sum_{W'} \frac{\rho_{0'}^{W'}}{[d_{W'}-i(\Gamma_{0',0}+\alpha)][\omega_{v0}+d_{W'}-\Delta+i(\Gamma_{0',v}+\alpha)]} \times \frac{1}{[\omega_{v'0'}-\Delta+i(\Gamma_{v'0'}+\sigma)]} \cdot \qquad (1)$$

Here $\Delta = \omega_1 - \omega_2$ and we have extended the usual four-level equation [5,6] to take into account the complexity arising from the fact that ω_1 is in resonance with several different isochromats belonging to different vibronic transitions. The W' index labels these isochromats; the indicies 0' and 0 denote the ground and excited electronic state zero-point levels; and v and v' the ground and excited state vibrations of interest (here 593 and 585 cm^{-1}) with frequencies ω_{v0} and $\omega_{v'0'}$. The Γ's are the usual damping constants [5,6] while α and σ are the inhomogeneous linewidths of the vibronic and vi-

brational transitions. For CV/PAA we estimate $\alpha \sim 500 - 1000$ cm^{-1} and $\sigma \sim 4$ cm^{-1}. Eq. (1) is appropriate in the absence of line narrowing which is the case here, vide infra. The total excited state population probability, $\rho_{0'}$, equals $\sum_{w'} \rho_{0'}^{w'}$ with each zero-point contribution from mode w', $\rho_{0'}^{w'}$, centered at $\sim\omega_1 - \omega_{w'0'}$. The value of $\rho_{0'}^{w'}$ depends, in part, on the vibronic transition dipole for the $w' \leftarrow 0$ transition and the location of ω_1 in the inhomogeneously broadened absorption profile of one and the same transition (we ignore the contribution of the ω_2-field to the excited state population). Each $\rho_{0'}^{w'}$ is associated with an excited state zero-point site distribution function reflected in the detuning parameter $d_{w'}$. This parameter is given by $d_{w'} = d_w^0 + x$ where $d_w^0 = \omega_1 - \omega_{w'0'}$. If the distribution parameter x is represented by a Lorentzian with width β, residue theory can be used to obtain $\langle X^{(3)}(\omega_{as})\rangle$, the ensemble average. We do not give the expression here since we are not in a position to perform quantitative calculations. The point we wish to make with Eq. 1 is that $\rho_{0'}^{w'} < (FWHM)_{laser}/\alpha$ which is of the order 10^{-3}. Therefore, when w' is restricated to only several zero-phonon vibronic transitions as Fig. 1 mandates, we have $\rho_{0'} << \rho_0$ where ρ_0 is the total ground state population probability. Thus, we suggest that phonon sideband absorption must be considered as an important mechanism for production of significant values for $\rho_{0'}$. A precedent for this has been

established [6] for the mixed crystal pentacene in naphthalene. With an ω_1 pulse energy of 10 μJ and ω_1 coincident with the low energy tail of the phonon sideband building on the (0,0) transition of pentacene, the excited to ground state population ratio, ρ_0'/ρ_0 is 3.3:1. It is germane to note that the electronic transition dipoles for pentacene and CV are about 0.3 and 1.0 A, respectively. Further, the transition dipole for pentacene at the irradiated position of the phonon side band is only 0.04 A [6]. Now the appearance of phonon sideband holes in Fig. 1 (note the broad 32 cm^{-1} feature to the red of ω_B) shows that the linear electron-phonon coupling for CV/PAA is significant (also the case for nile blue in PAA). Therefore, the ω_1-field excites not only narrow zero-phonon isochromats but broad "isochromats" corresponding to the associated phonon sideband holes. Given their breadth (~100 cm^{-1}) and that the displacements between adjacent satellite holes are ~100 cm^{-1} (Fig. 1), it is clear that the linear electron-phonon coupling provides a mechanism for producing an egalitarian and potentially, therefore, a significant ρ_0' value. For ω_1 located in a sufficiently vibrationally region (as in Fig. 1, $\omega_1 = \omega_B$ or Fig. 3), a rough value for ρ_0' can be obtained by assuming that a ω_1 pumps single homogeneously broadened vibronic band with a FWHM of ~500 cm^{-1}, Fig. 1. For transition dipole of ~1.0 A, ω_1 pulse energy of 5 μJ and singlet lifetime of 1 ns we estimate a value for ρ_0'/ρ_0 of

unity for CV. We conclude, therefore, that phonon sideband pumping is a plausible explanation for the large ρ_0' values required. It should be pointed out that additional resonance enhancement for the excited state resonances can arise from CARS terms involving higher excited electronic states. Such states exist for CV at twice the ω_1 values used in our experiments.

If the 585 cm^{-1} CARS resonance is an excited state resonance resulting from ω_1-field induced excited state population, its intensity should exhibit a dependence on the peak power of the ω_1-field which is different from quadratic. In the absence of hole burning and in the regime where ρ_0' increases linearly with the ω_1-field intensity, the dependence is expected to be cubic. Unfortunately, the facile hole burning for CV/PAA prevents a simple interpretation of our intensity dependent data obtained at low temperatures. For this reason ω_1-dependent intensity studies were performed at room temperature where hole burning is not operative. The ω_1 frequency chosen was 16666 cm^{-1} (600.00 nm). A different problem was encountered -- photodegradation of the CV as evidenced by a decrease in time of the intensities both the 585 and 593 cm^{-1} resonances and discoloration of the irradiated spot. Photodegradation does not occur for T < 50K. Because of the photodegradation extensive studies of the ω_1-intensity dependence were not performed. Nevertheless, the data ob-

tained show that the 585 and 593 cm^{-1} behave differently. For example, for (ω_1,ω_2) pulse energies of $(7,4)_I$ and $(14,4)_{II}$ μJ and with a fresh spot used for each pulse energy pair the following results obtained: $I(585)_{II}/I(585)_I = 5$ and $I(593)_{II}/I(593)_I = 2$. The scan times were 4 min. The respective deviations of the ratios from 8 and 4 are presumably due to photodegradation and significant depletion of the ground state population. At the time, we are not able to say more. Still, the measured intensity ratios support the assignment of the 585 cm^{-1} resonance as an excited state mode.

We consider next the CARS profiles for the 593 cm^{-1} resonance shown in Fig. 4 which were briefly discussed in the previous section. A substantial narrowing of the resonance from 7.4 to 4.8 cm^{-1} occurs from 4.6 K to 74 K. No further narrowing is observed at higher temperatures. Again this narrowing is observed only for ω_1 values lying to lower energy of ~633.0 nm. A possible explanation is narrowing due to polymer motion in a restricted region of the polymer configuration space, i.e., the region for PAA which is associated with the low energy tail absorption of CV. If true, the implications for studying polymer configurational changes at low temperatures would be interesting. However, this does not appear to be the case. A comparable study was performed on PAA with a different probe molecule, oxazine 720. Oxazine 720 also exhibits an intense ground resonance at ~593 cm^{-1} since

its structure is similar to that of CV. Studies on this resonance were performed with ω_1 at 645.0 and 650.0 nm (low E tail of oxazine 720). For this region, the 593 cm^{-1} resonance exhibits a 4.6 K linewidth of close to 8 cm^{-1}. Furthermore, no narrowing is observed with increasing temperature (only a slight broadening). Therefore, it is more likely that the "motional" narrowing is associated with a coupled CV-PAA coordinate (perhaps associated with intermolecular H-bonding). The H-bonding between the $-NH_2$ groups of CV and carboxylic acid groups of PAA would, with oxazine 720, be sterically hindered due to the replacement of one of the hydrogens of $-NH_2$ by a bulky $-C_2H_5$ group.

The final point of discussion is concerned with the question of line narrowing. For fully resonant four-wave mixing of a four-level system, it has been shown that it is possible to achieve line narrowing for CARS or CSRS resonances provided the site excitation energy distributions for the vibrational and vibronic resonances are appropriately correlated [6,10,11]. Line narrowing in molecular solids has, however, only been reported for pentacene in benzoic acid [5] and in naphthalene [6]. In these fully resonant experiments, the four levels are 0, 0', v, and v' corresponding to the zero-point levels of the ground and excited electronic states and the ground and excited state counterparts of the same vibrational mode, respectively. We define $x = \omega_{v0} - \omega^0_{v0}$,

$y = \omega_{v'0} - \omega^0_{v'0}$ and $z = \omega_{0'0} - \omega^0_{0'0}$ as the shifts of the transition frequencies away from their mean values (labeled by superscript "0"). For complete correlation $y = \alpha x$ and $z = \beta x$, α and β constants. It follows then that another pertinent resonance is automatically correlated; $(\alpha-\beta)x = \omega_{v'0'} - \omega^0_{v'0'}$. For $|\alpha|$, $|\beta| > 1$ (a very reasonable assumption), the line narrowing possibilities are determined by the relative signs of α, β and $(\alpha-\beta)$ [6]. For example, if α, $\beta > 0$ (positive correlation) then the CARS resonance ω_{v0} (ground state mode) driven by ρ_0 would not be line narrowed while the CARS resonance $\omega_{v'0'}$ from ρ_0, would be. Further, the CSRS resonance ω_{v0} from ρ_0 would also be line narrowed. The other cases are discussed in ref. [6].

One of our motivations for studying four-wave mixing of dyes in polymers was to see whether the CARS and CSRS spectra would reveal line narrowing. We reported earlier [6] CARS and CSRS results for CV/PAA. In these experiments ω_1 was located at 630.0 nm (low E tail, Fig. 1) so as to minimize $\rho_{0'}$. No difference in the CARS and CSRS linewidths of the 593 cm^{-1} resonance was discernible. If the above four-level description for CV/PAA is appropriate, this result means that strong positive or negative ($\alpha,\beta < 0$) correlation does not exist [6]. We summarize now our findings for the 585 and 593 cm^{-1} excited and ground state CARS resonances. For ω_1 ranging between 614.0 and 588.0 nm, both resonances have, within experimental uncertainty ($\pm$ 0.3 cm^{-1}), the same linewidth at 4.6 K. The

FWHM has a slight dependence on ω_1, ranging between ~4.0 and ~4,5 cm^{-1}. Further, the 585 and 593 cm^{-1} linewidths do not broaden between 4.6 K and room T. These results, together with those of ref. 6, indicate that the 4.6 K linewidths are primarily determined by site inhomogeniety. The same picture has emerged for nile blue perchlorate in PAA [17].

Despite the absence of line narrowing, we would be reticent to conclude that site excitation energy correlations between the vibrational and vibronic transitions considered do not exist. The reason is that the large vibronic inhomogeneous linewidths of CV/PAA make the assumption of a four-level system questionable. That is, for example, one needs to consider the contribution of a large number of doubly resonant terms (in addition to those which are triply resonant) [6,10,11,18] to $X^{(3)}$ for the CARS and CSRS resonances. These would include terms involving excited electronic states higher than the S_1 state. With reference to the CARS 585 cm^{-1} excited state resonance driven by $\rho_{0'}$, we have already mentioned the possible importance of higher excited states.

In our opinion, the question of line narrowing in the fully resonant four-wave mixing spectra of molecules imbedded in amorphous hosts like polymers is deserving of further study. However, systems which exhibit optical absorption spectra with pronounced vibronic structure (in contrast with laser dyes in polymers) should be chosen for study.

ACKNOWLEDGEMENT

Ames Laboratory is operated for the U.S. Department of Energy by Iowa State University under Contract No. W-7405-Eng-82. This research was supported by the Director for Energy Research, Office of Basic Energy Science. Funding for the laser system was provided by NSF.

The assistance of T. P. Carter and B. L. Fearey with the hole burning experiments and sample preparation as well as useful discussions with them are gratefully acknowledged.

REFERENCES

1. P. L. DeCola, J. R. Andrews, R. M. Hochstrasser and H. P. Trommsdorff, J. Chem. Phys. 73, 4695 (1980).

2. J. R. Andrews, R. M. Hochstrasser and H. P. Trommsdorff, Chem. Phys. 62, 87 (1981).

3. J. R. Andrews and R. M. Hochstrasser, Chem. Phys. Lett. 82, 381 (1981).

4. J. R. Andrews and R. M. Hochstrasser, Chem. Phys. Lett. 83, 427 (1981).

5. R. Bozio, P. L. DeCola and R. M. Hochstrasser, in "Time Resolved Vibrational Spectroscopy", G. H. Atkinson, Ed., Academic Press: New York, 1983.

6. T-C. Chang, C. K. Johnson and G. J. Small, J. Phys. Chem. 89, xxxx (1985).

7. A. R. Bogdan, Y. Prior and N. Bloembergen, Opt. Lett. 6, 82 (1981).

8. Y. Prior, A. R. Bogdan, M. Dagenais and N. Bloembergen, Phys. Rev. Lett. 46, 111 (1981).

9. A. Bogdan, M. Downer and N. Bloembergen, Phys. Rev. A24, 623 (1981).

10. B. Dick and R. M. Hochstrasser, J. Chem. Phys. 78, 3398 (1983).

11. B. Dick and R. M. Hochstrasser, Chem. Phys. 75, 133 (1983).

12. B. L. Fearey, T. P. Carter and G. J. Small, J. Phys. Chem. 87, 3590 (1983).

13. T. P. Carter, B. L. Fearey, J. M. Hayes and G. J. Small, Chem. Phys. Lett. 102, 272 (1983).

14. T. P. Carter, B. L. Fearey and G. J. Small, unpublished results.

15. G. J. Small, in "Molecular Spectroscopy", V. M. Agranovich and R. M. Hochstrasser, Eds., North Holland Publishing Co.: Amsterdam, 1983.

16. B. L. Fearey, T. P. Carter and G. J. Small,"Spontaneous and Laser Induced Filling of Nonphotochemical Holes of Rare Earth Ions and Laser Dyes in Polymers", Chem. Phys., submitted.

17. Ta-Chau Chang, Ph.D. Dissertation, Iowa State University, 1985.

18. J. L. Oudar and Y. R. Shen, Phys. Rev. A22, 1141 (1980).

ADDITIONAL RESULTS AND DISCUSSIONS

The third-order nonlinear susceptibility of fully resonant CARS for PT/NPH can be adequately described by using a discrete four-level system. However, for the CV/PAA system, the polymer host presents a more complex situation because it imparts severe inhomogeneous broadening to vibronic transitions on the order of several hundred cm^{-1}. This contrasts with mixed crystals where the inhomogeneous broadening contribution to vibronic transitions is ~2 cm^{-1}. Comparing the CARS results between PT/NPH and CV/PAA, this feature is reflected by the presence of moveable peaks in PT/NPH and the absence of moveable peaks in CV/PAA. Under this condition with amorphous or disordered host like polymers, one cannot be sure that a well defined vibronic level is put in resonance by ω_1 (or ω_2), i.e., the simplicity of a discrete four-level system is lost. It is of interest to determine whether or not the excited state vibrational resonance in the CARS spectra obtained with polymer host can be probed. CARS spectra for CV/PAA and CV/PVK obtained at room temperature for ω_1 = 610.0 nm are shown in Fig. 1. The strong excited state vibrational resonance for CV/PAA is due to the phonon sideband absorption process populating the excited state population [58]. The absence of this band for CV/PVK may be due to different intermolecular interactions between CV and PVK.

Figure 1. Room temperature CARS spectra for (a) CV/PAA and (b) CV/PVK at ω_1 = 16390 cm^{-1} (near the center of $S_1 \leftarrow S_0$ cresyl violet absorption profile). See text for details.

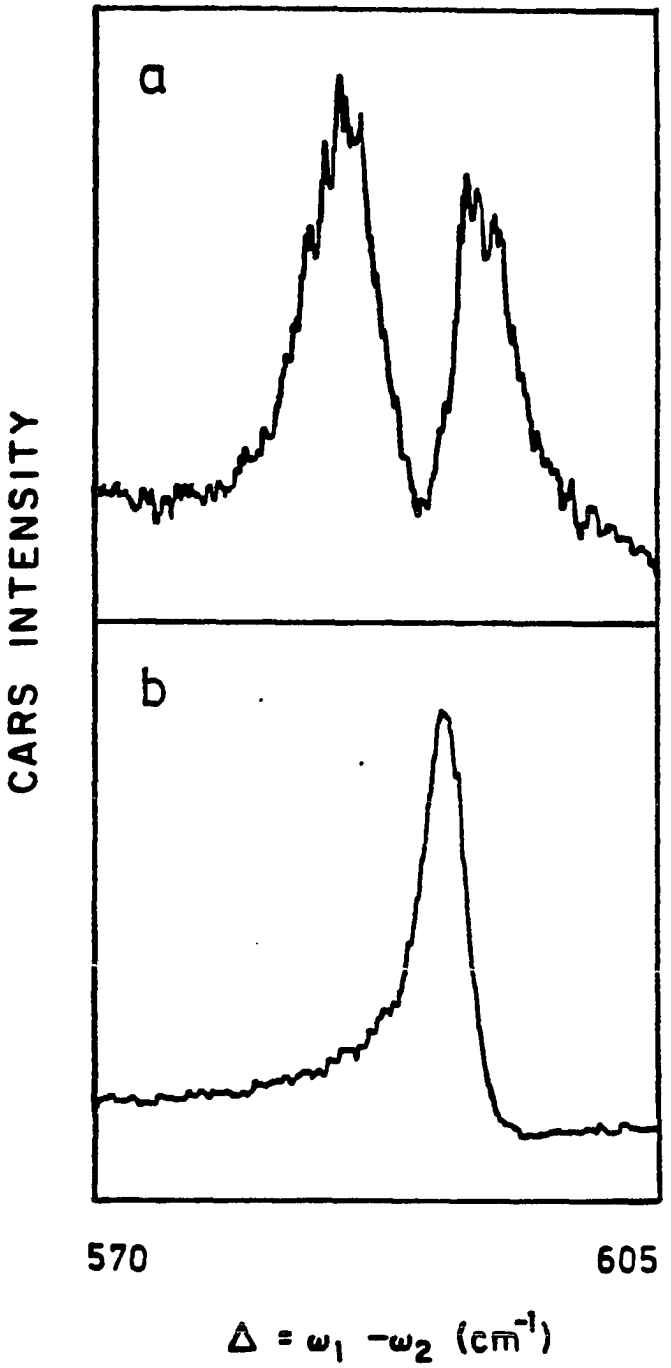
a
b
CARS INTENSITY
570
605
Δ = ω1 −ω2 (cm-1)

Nonphotochemical hole burning (NPHB) has been utilized to investigate the optical dephasing of impurities in polymer films in order to understand the dynamical properties of the host-guest systems [34-36,59-65]. The production of holes is due to site excitation energy selective photobleaching, which results from a narrow line laser pumping a subset of impurity sites isochromat. These impurity molecules may then interact with some isoenergetic configurations of host molecules which are generally described in terms of a distribution of asymmetric intermolecular double-well potentials or two-level systems (TLS), an example of which is shown in Fig. 2 [34-36]. Because of the phonon assisted tunneling (PAT) or thermally activated processes, some types of impurity-host "photoisomerization" processes deplete the population of these impurity sites whose excitation energies overlap the laser profile. For a detailed discussion of the NPHB mechanism and the theories of dephasing in amorphous solids, the reader is referred to the quoted references [34,35].

NPHB spectra of ionic dyes in polymers [36,59-61], for example nile blue perchlorate (NB) and cresyl violet perchlorate (CV) in polyacrylic acid (PAA), show extensive intramolecular vibronic satellite structure which yields accurate S_1 vibrational frequencies. However, it is difficult to induce NPHB in the CV/PVK system. Further, time dependent CARS spectra for CV/PAA and NB/PAA at T = 5 K show significant changes of the absolute intensities for excited state and

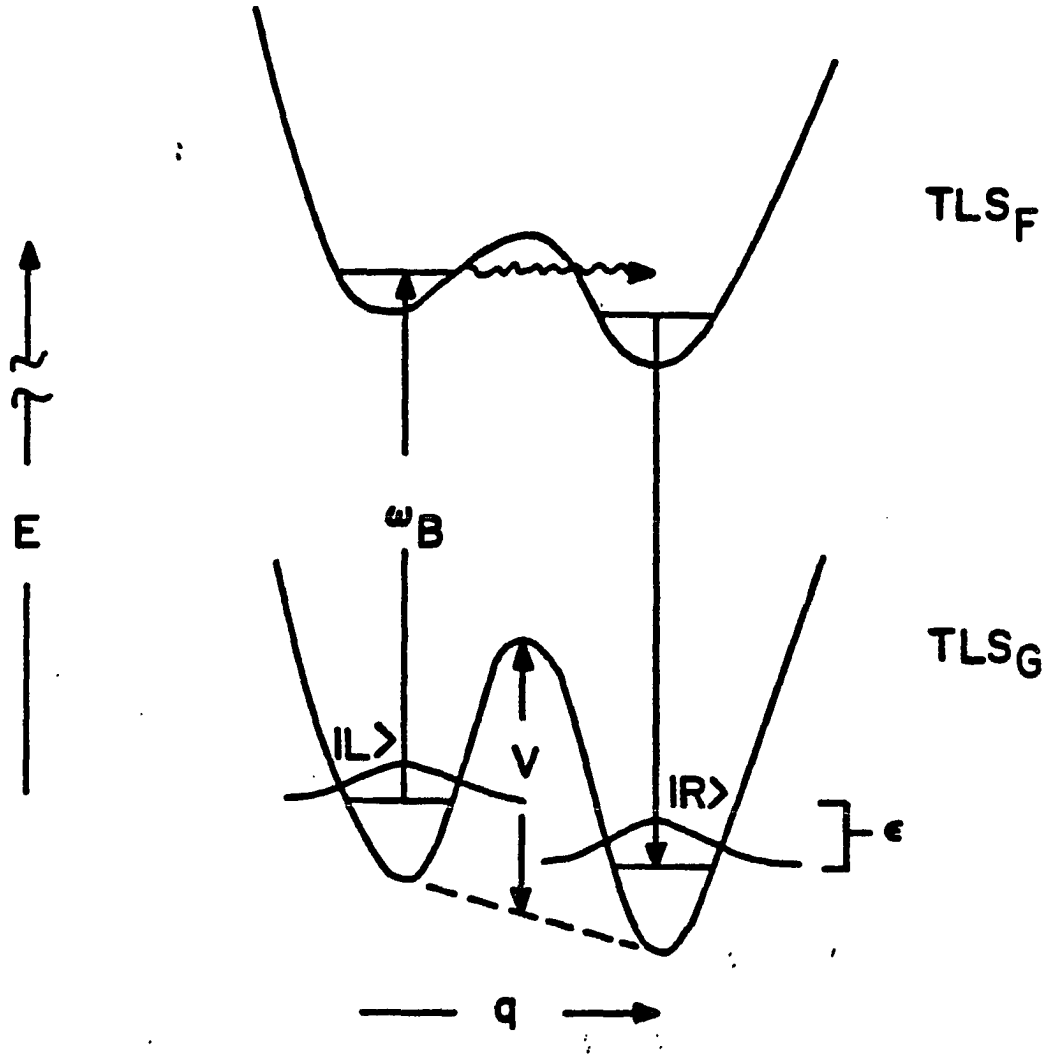

Figure 2. A schematic representation of the double well potential characteristic of two level systems. V: barrier height, ϵ: zero-point energy difference, E: energy, q: corrdinates, TLS_F: excited electronic state, and TLS_G: ground electronic state.

ground state vibrational bands. However, time dependent CARS signals for the ground state vibrational band of CV in PVK show no significant intensity dependence on time. This different behavior is suggested due to the hole burning effect. Two possible reasons for the absence of hole burning for CV/PVK are weak impuity-TLS coupling and/or fast TLS interconversion in the ground state [35].

It is noted that the nonresonant (NR) contribution as well as two-photon absorption (PTA) are not crucial in the fully resonant CARS spectra of PT/NPH [23]. If the simplicity of the discrete four-level system is lost in the polymer system, then processes from nonresonant contributions as well as two-photon absorption may interfere with the CARS process. However, in the absence of line narrowing, the CARS profiles of CV/PAA and NB/PAA can be described by a four-level model when the inhomogeneous linewidths are taken into account. Thus, the contributions from NR and TPA are not important for these systems.

CARS spectra for CV/PVK have been performed in the region of ω_1 = 16890 cm^{-1} ~ 15975 cm^{-1}. Illustrative spectra at 5 K showing the interference effect produced by nonresonant background are presented in Fig. 3 for various ω_1 values. The spectra were obtained with (ω_1, ω_2) pulse energies of about (20, -), (35, 4), (35, 4) and (30, 10) μJ corresponding to ω_1 = 16890, 16390, 16340, 16180 cm^{-1}, respectively. Based on the CARS spectra for CV/PAA, the very weak band at 586 cm^{-1} is

Figure 3. CARS spectra for CV in PVK as a function of tuning ω_1 at T = 5K. Spectra a-d correspond to ω_1 = 16890, 16390, 16340, 16180 cm^{-1} and were obtained with (ω_1, ω_2) pulse energies of (20, -), (35,4), (35,4), and (30,10) μJ, respectively.

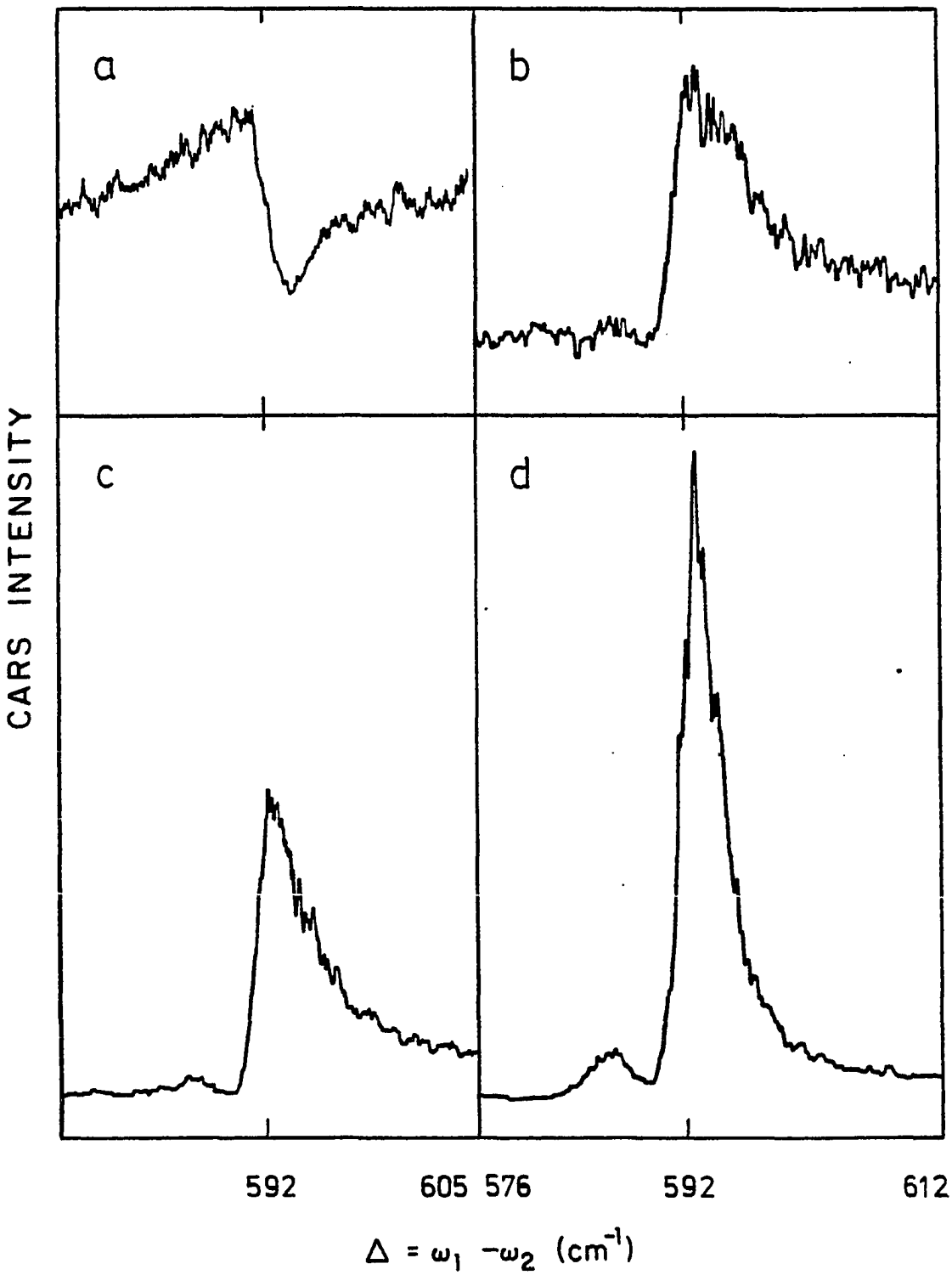
a
b
c
d
CARS INTENSITY
592
605
576
592
612
Δ = ω1 −ω2 (cm−1)

assigned as the excited state counterpart of the CV 593 cm^{-1} ground state mode. It is noted that the 586 cm^{-1} band is always weak in the low temperature spectra and is absent at high temperature, even when ω_1 is near the center of the absorption profile of CV. The dispersion profile in Fig. 3a was not observed for the CV/PAA and NB/PAA systems. We consider now a theoretical interpretation of the results in Fig. 3.

The interference between normal CARS and two-photon absorption resonances in $X^{(3)}$, other Raman resonances and the nonresonant background has been widely studied [12-14,66-72]. Most of the earlier experiments for examining the interference effect were performed by tuning ω_1 far away from a resonant transition. Thus, the third-order nonlinear susceptibility, $X^{(3)}(\omega_4)$, could be expressed as [16,71]

$$X^{(3)}(\omega_4) = X_{NR} + \sum_R \frac{A_R}{\omega_R - \Delta + i\Gamma_R} + \sum_T \frac{A_T}{\omega_T - 2\omega_1 + i\Gamma_T} \qquad (1)$$

where X_{NR} is assumed to be a real constant, ω_R is a Raman frequency close to $(\omega_1-\omega_2)$ and ω_T is a vibronic frequency in the vicinity of $2\omega_1$. The parameters A_R and A_T are defined as

$$A_R = N/24\hbar\, \alpha^R_{ij}\, \alpha^R_{kl}, \qquad (2a)$$

$$A_T = N/24\hbar\, \alpha^T_{jk}\, \alpha^T_{il} \qquad (2b)$$

where

$$\alpha_{ij}^{R} = \left(\frac{\hbar}{2\omega_R}\right)^{1/2} \left(d\alpha_{ij}^{R}/dQ_R\right), \tag{3a}$$

$$\alpha_{jk}^{T} = \frac{1}{\hbar} \sum_{b} \left[\frac{\langle g|u_j|b\rangle\langle b|u_k|T\rangle}{\omega_b+\omega_j} + \frac{\langle g|u_k|b\rangle\langle b|u_j|T\rangle}{\omega_b+\omega_k}\right]. \tag{3b}$$

N is the molecular number density. $d\alpha_{ij}^{R}/dQ_R$ is the derivative of the ij-th component of the polarizability tensor with respect to the normal coordinate of vibration Q_R. g and T refer to the ground and two-photon resonant states and b is an intermediate state.

With reference to Fig. 3, each spectrum corresponds to a fixed ω_1 so that the $(\omega_T-2\omega_1)$ in Eq. 1 is constant. For a fixed ω_1, TPA term may be included in the X_{NR} term. When $2\omega_1$ is close to a two-photon resonance, X_{NR} is not real but complex. Further, the severe inhomogeneous broadening to vibronic transitions makes resonant CARS similar to normal CARS. For simplicity, Eq. 1 can be rewritten as

$$X^{(3)}(\omega_4) = X_{NR} + \frac{A}{\omega_{v0}-\Delta+i\Gamma_{v0}} . \tag{4}$$

The measurement of the frequency difference between the maximum and minimum of the dispersion curve provides the relative strength of the nonresonant and Raman contributions when Γ_{v0}

is known [71]. Experimental spectra may be fit by Eq. 4 through variation of X_{NR} and A. This equation is appropriate for description of the resonant CARS spectra for CV/PVK as shown in Fig. 3a, for ω_1 = 16890 cm^{-1}.

Profiles b - d in Fig. 3 show more complicated features; an additional shoulder on the high frequency side of the resonance ~593 cm^{-1} is observed in the CARS spectra. The intensity of this shoulder is decreased when ω_1 is tuned from 16390 to 16170 cm^{-1}. It is suggested that this shoulder at ~595 cm^{-1} is a resonant mode. Three CARS spectra at ω_1 = 16390 cm^{-1} and T = 17 K, ω_1 = 16340 cm^{-1} and T = 32 K, and ω_1 = 16290 cm^{-1} and T = 51 K are shown in Fig. 4 as confirmation of this feature. A similar CARS profile for cytochrome C near the resonance mode 1362 cm^{-1} was observed when ω_1 was tuned to the peak center of a Soret band at ~24040 cm^{-1} [73]. No interpretation was given for this additional line for cytochrome C. In our work, it is obvious that the resonance at ~595 cm^{-1} is not a moveable peak because of enormous width of the vibronic transition and no changes of the frequency of this resonance while tuning ω_1. Further, since ω_1 is fixed during the scan of ω_2 for each spectrum, the denominator terms corresponding to one-photon and two-photon resonances in $X^{(3)}$ can change the CARS profile but cannot provide an additional band in the spectrum. If an additional Raman mode for the resonance at ~595 cm^{-1} is simply included in $X^{(3)}$, i.e., $X^{(3)}(\omega_4) = X^{(3)}_{NR}+X^{(3)}_{R1}+X^{(3)}_{R2}$, one is not able to explain

Figure 4. CARS spectra for CV/PVK ω_{vo} = 592 cm^{-1} and ω'_{v0} = 595 cm^{-1}. Profiles a-c correspond to ω_1 = 16390 cm^{-1} and T = 17K, ω_1 = 16340 cm^{-1} and T = 32K, and ω_1 = 16290 cm^{-1} and T = 51K, respectively. See text for details.

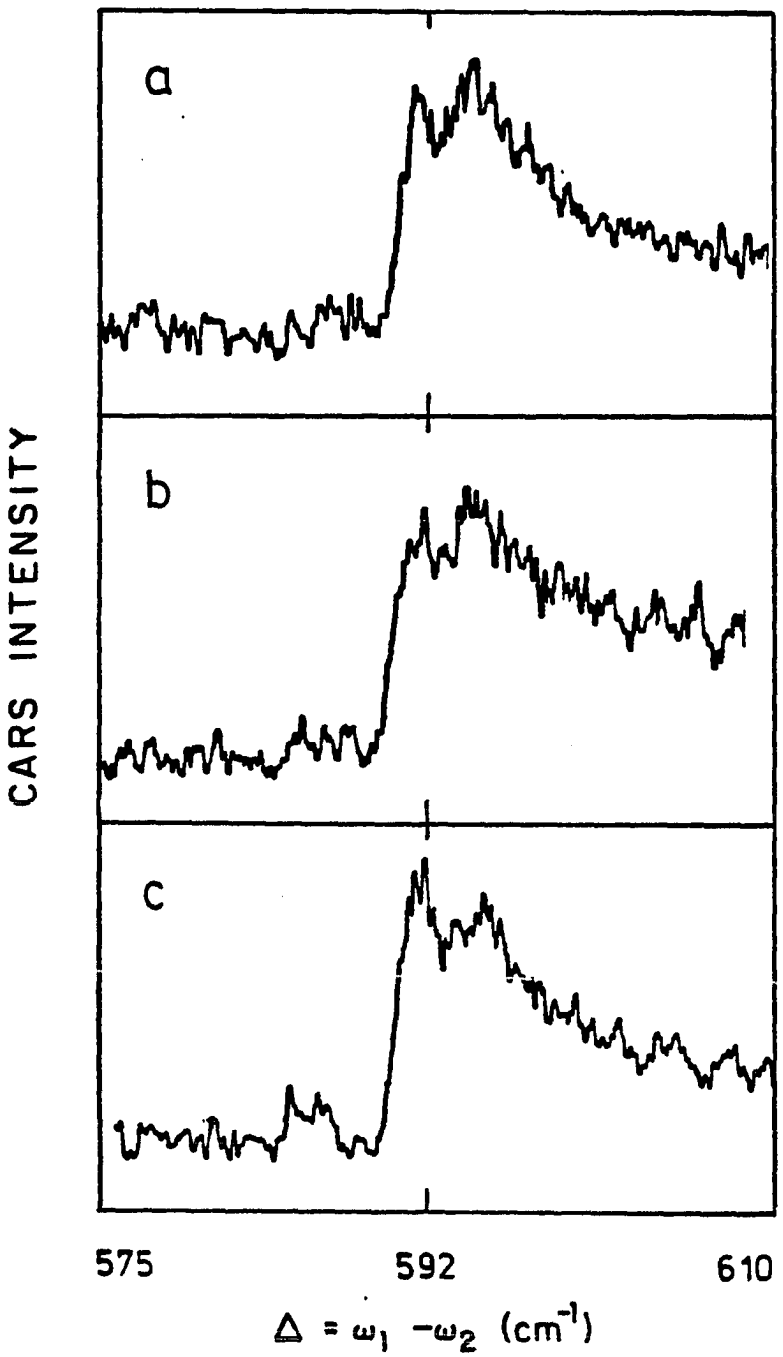
a
b
c
CARS INTENSITY
575
592
610
Δ = ω1 −ω2 (cm-1)

why the intensity of resonance at ~595 cm^{-1} changes as the ω_1-field is tuned.

An absorption spectrum for CV/PVK at T = 5 K is shown in Fig. 5. It appears that the inhomogeneously broadened absorption profile of CV in PVK may be the superposition of overlapping spectra due to two chemically distinct species. Rippen et al. [74] have studied the fluorescence spectra of both cationic and radicalic preparation of PVK films at 77 K. Fluorescence spectra from both films exhibit two components in their profiles. Judging from their spectra, one of the components is narrower than the other one by about 1/3. We assume that the additional resonance at 595 cm^{-1} is related to the sharper of the two absorption components. Further, We assume that the intermolecular interaction between CV and PVK causes about the same ratio for the two components in the CV absorption profile. In addition, we note that the weak excited state resonance at 586 cm^{-1} is observed in the region of ω_1 = 16340 ~ 15970 cm^{-1} at low temperature. This suggests that $\Delta = \omega_{v0}$ = 593 cm^{-1} is independent of tuning in the region ω_1 = 16340 ~ 16130 cm^{-1} and the additional resonance at $\Delta = \omega'_{v0}$ = 595 cm^{-1} is dependent on the tuning of ω_1 with respect to $\omega'_{0'0}$, where $\omega'_{0'0}$ is the peak frequency of the sharper absorption component. Then $X^{(3)}$ is given by

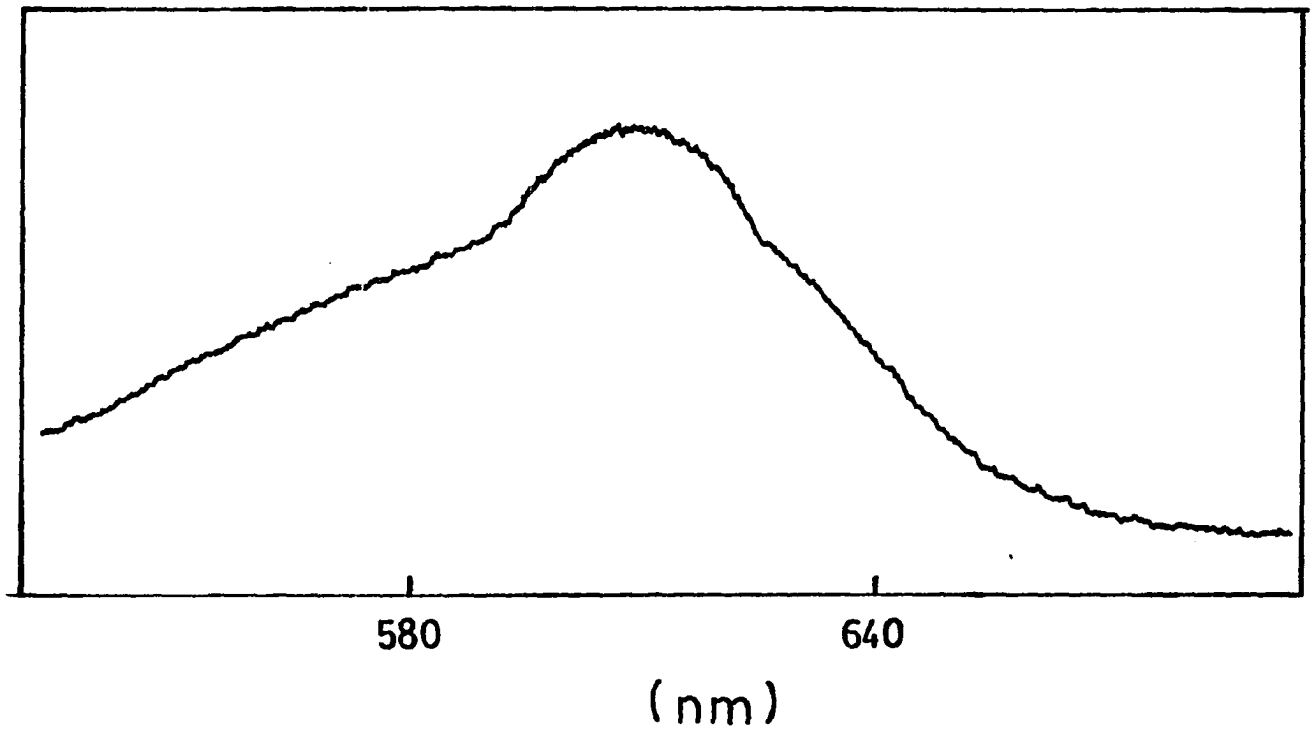

Figure 5. Absorption spectrum for CV/PVK at T = 5K.

$$X^{(3)}(\omega_4) = X_{NR} + \frac{A}{\omega_{v0}-\Delta+i\Gamma_{v0}} + \frac{B}{(\omega'_{v0}-\Delta+i\Gamma'_{v0})(\omega'_{0',0}-\omega_1+i\Gamma'_{0',0})}, \quad (5)$$

It is assumed that $\Gamma_{v0} = \Gamma'_{v0} = 1.5\ cm^{-1}$ and $\Gamma'_{0',0} = 100\ cm^{-1}$. The magnitude of B is suggested to be larger than the magnitude of A, because of the damping term $\Gamma'_{0',0}$. Simulated calculations with varying ω_1 to illustrate the tuning effect are shown in Fig. 6.

Temperature dependent spectra in Fig. 7 show that the intensity at ω'_{v0} increases as the temperature increases from 4.5 ~ 70 K and is absent for T > 100 K. In additional, it is noted that the observed linewidth at Fig. 7e is measured to be 2.5 cm^{-1}. This linewidth is much narrower than the observed linewidth for CV 593 cm^{-1} mode in PAA, which is 4.0 cm^{-1}. At the time we are not able to say more. In our opinion, this system deserves further study. First, CV/PVK CARS spectra did not show a photodegradation at high temperature and did not exhibit the hole burned effect at low temperature, which made the interpretation easier for CV/PVK then CV/PAA. Second, the interesting temperature dependent study, the weak excited state resonance at ~586 cm^{-1} and the narrower linewidth for the ground state resonance at 593 cm^{-1} remain unanswered, which may expose more fundamental information about intermolecular interaction for a polymer system.

Figure 6. Simulation of Eq. 5 to illustrate the CARS spectra when an additional resonance as a function of tuning ω_1 in $X^{(3)}$ is added. Profiles a - f correspond to $d = \omega_1 - \omega'_{0'0} = -400.0, -200.0, -100.0, 0.0, 100.0$ and $200.0\ cm^{-1}$, respectively.

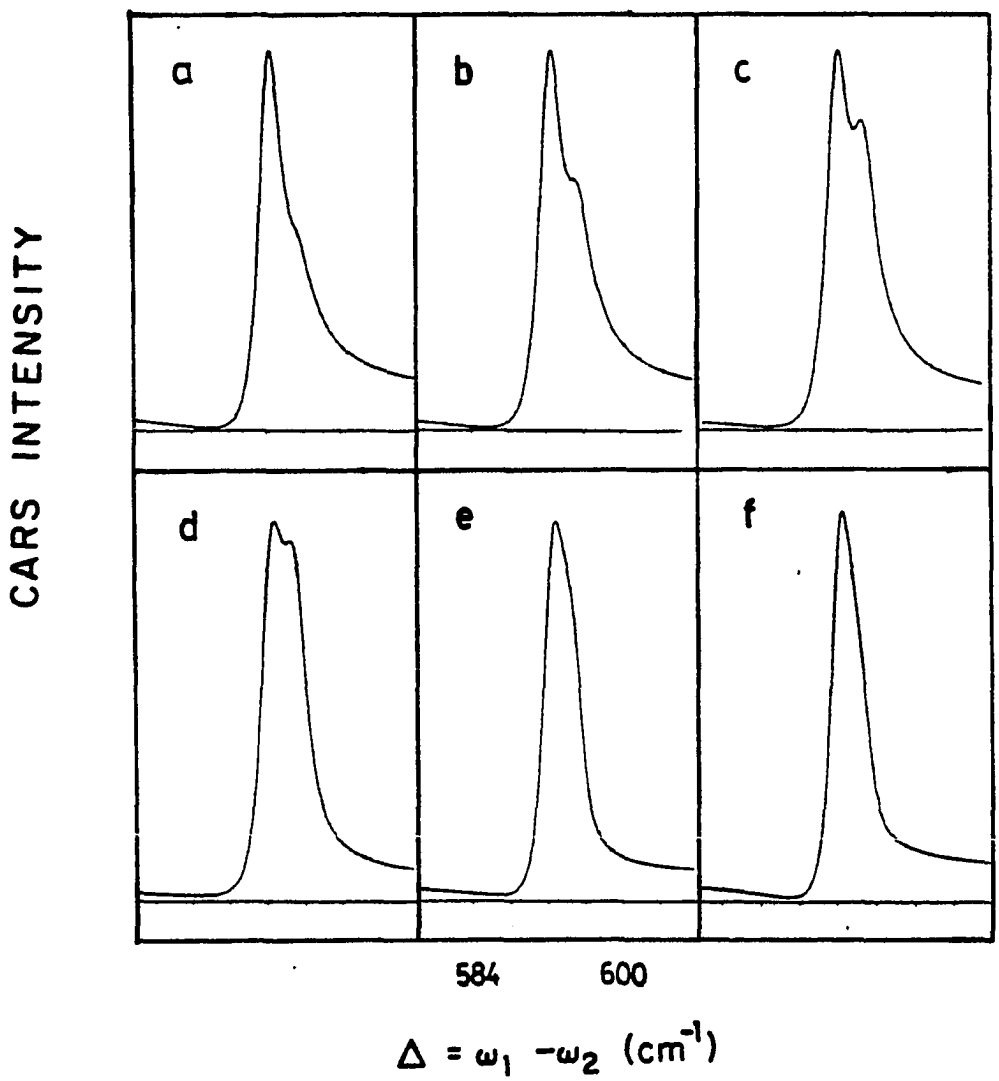
a
b
c
d
e
f
CARS INTENSITY
584
600
Δ = ω1 −ω2 (cm-1)

Figure 7. Temperature dependence of the CV/PVK for ω_1 = 16230 cm^{-1} and (ω_1,ω_2) pulse energies of (6,7) μJ (except profile e with pulse energies of (6,14) and profile f with pulse energies of (9,7) μJ). Spectra a-f correspond to T = 5, 17, 30, 50, 120, and 293 K, respectively.

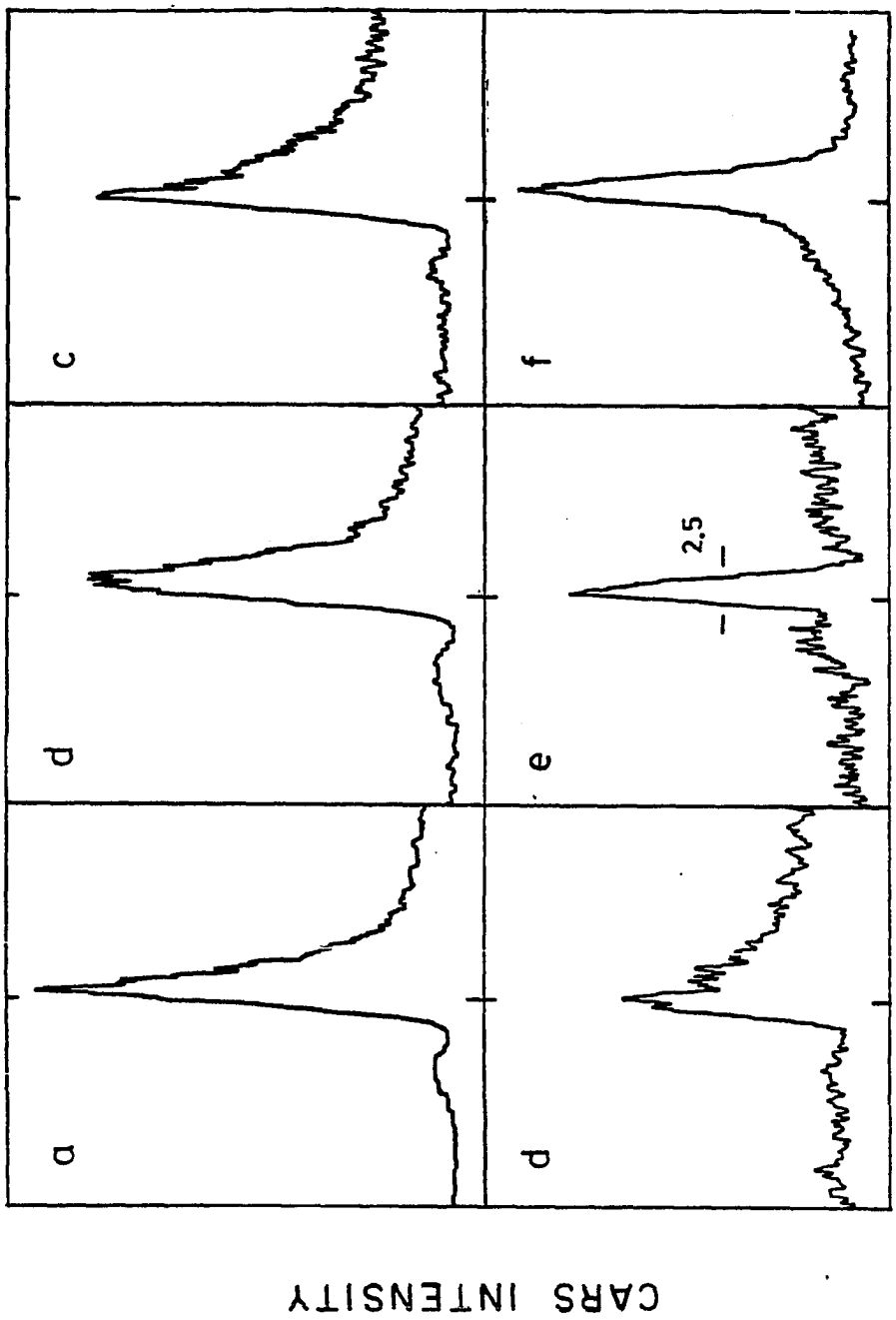
a
d
c
d
e
f
2.5
575
592
609
CARS INTENSITY
$\Delta = \omega_1 - \omega_2$ (cm^{-1})

CONCLUSION

A detailed description of dispersive four-wave mixing spectroscopy and its application to the study of the third order nonlinear susceptibility $X^{(3)}$ for pentacene doped in naphthalene and cresyl violet perchlorate embedded in polyacrylic acid or polyvinyl carbazole has been given. Theoretical examination of $x^{(3)}$ predicts that four resonances should be obtained for fully resonant FWM of a four-level system. Experimental results for the detuning of ω_1 in the PT/NPH system has demonstrated this feature. Two stationary peaks correspond to a ground state vibrational mode and its excited state counterpart and two moveable peaks, governed by the detuning of ω_1, are the partners of their stationary peaks, respectively. It is concluded that fully resonant CARS for PT/NPH can be theoretically understood in terms of a discrete four-level system.

The theoretical basis and experimental evidence for line narrowing have been established for fully resonant four-wave mixing of a four-level system. Theoretically, it is possible to achieve line narrowing for CARS and CSRS resonances when the inhomogeneous distributions for the vibrational and vibronic resonances are appropriately correlated. A careful line-narrowing study for the pentacene 755 cm^{-1} resonance in naphthalene has been examined. Under low power conditions the

observed linewidths (full width half maximum, FWHM) are 0.32 cm^{-1} for CARS and 0.28 cm^{-1} for CSRS at T = 4.5 K, which illustrates that line narrowing is operative. However, the laser bandwidths of 0.14 cm^{-1} utilized here are major contributors to the observed linewidths. Thus, we emphasize that the question of line narrowing for the ω_{v0} resonance deserves further study utilizing narrower linewidth lasers.

A surprising feature is that the excited state resonance $\omega_{v'0'}$ in the PT/NPH system has been observed with modest pulse energies for significant negative detuning. With reference to temperature dependent studies, we have proposed that the phonon hotband absorption is responsible for the excited state population mechanism. Theoretical calculations for the temperature dependence of ρ_0 and $\rho_{0'}$ based on this mechamism have been described. These determined values of ρ_0 and $\rho_{0'}$ are then used to calculate the intensity ratio $I_{v'0'}/I_{v0}$ as a function of temperature, which agrees with the experimental values within to 15%. This result leads to the conclusion that phonon hotband absorption is the mechanism for producing excited state population for negative detuning of the ω_1-field.

A significant excited state resonance $\omega_{v'0'}$ for PT/NPH has been observed in the positive detuning CARS spectra. A similar behavior was also observed in the pentacene in benzoic acid system [22]. It is suggested that phonon sideband

pumping is the excited state population mechanism. Further, temperature dependent CARS spectra for positive detuning have shown that the intensity ratio $I_{v'0'}/I_{v0}$ is suddenly decreased when the temperature is changed from T = 23 K to 34 K for PT/NPH. This behavior has been tentatively interpreted in terms of the interplay between DICE and the temperature dependence of the phonon sideband absorption building on the (0',0) band. Very recently, we have observed an unusual feature in the temperature dependent absorption spectra. We have noted that the (0',0) absorption band is significantly red-shifted when the temperature is raised from 30 K to 37 K. A further study is planned to illuminate this behavior since it is likely important for understanding the above temperature-dependent CARS data.

Power broadening data for the resonance at 755 cm^{-1} was observed in the CARS spectra. Line broadening was interpretated in terms of a distribution of dynamic Stark shifts resulting from the site inhomogeneous line broadening of vibronic transitions.

The application of four-wave mixing spectroscopy to the study of $X^{(3)}$ has been utilized to explore whether the FWM spectra would reveal line narrowing. No line narrowing was observed in the study of CARS and CSRS for the CV 593 cm^{-1} resonance in PAA, which may be due to the large inhomogeneous linewidths that make the assumption of a four-level system

questionable. In our opinion, the question of line narrowing in the fully resonant four-wave mixing spectra of molecules embedded in amorphous hosts, like polymer, is deserving of further study. However, systems which exhibit optical absorption spectra with pronounced vibronic structure (in contrast with laser dyes in polymers) should be chosen for this study.

Two bands at 593 cm^{-1} and 585 cm^{-1} were observed in the resonant CARS spectra for CV/PAA, which were characterized to be a ground state vibrational resonance and its counterpart, respectively. The higher intensity of the excited state resonance may be due to the linear electron-phonon interaction which produces an egalitarian distribution of excited dye sites and provides sufficiently high population in the excited state.

The manifestation of NPHB has been observed in the resonant CARS spectra of CV/PAA with increasing irradiation time of ω_1-field, the absolute intensities of the $\omega_{v'0}$ resonance is significantly decreased while that of the ω_{v0} resonance is increased. In the CV/PVK system, hole burning is not observed. Further, increasing of the irradiation time of laser pulse ω_1 did not change the intensity at ω_{v0} resonance. Thus, this difference in behavior between CV/PAA and CV/PVK can be satisfactively and qualitatively understood in terms of hole burning.

In the CV/PVK system, a significant interference from nonresonant contributions was observed in the CARS spectra when ω_1 was tuned to ~16890 cm^{-1}. Experimental results showed that this interference effect depended on the location of ω_1 within the absorption profile.

Two modes which interfere with nonresonant susceptibility were displayed in the CARS spectra when ω_1 was tuned to the region of 16390 ~ 16170 cm^{-1}. It is suggested that these two bands are due to the superposition of overlapping spectra due to two chemically distinct species characterized by their Raman modes. Several observations for the CV/PVK system remain unexplained. The unusual temperature dependent spectra were present. In addition, the observed linewidth at ω_{v0} = 593 cm^{-1} for CV/PVK is 2.5 cm^{-1} which is much narrower than the linewidths for other systems (for example : ~4.0 cm^{-1} for CV/PAA, ~8.0 cm^{-1} for OX720/PAA and ~7.5 cm^{-1} for CV/glycerol:H_2O). We suggest that they deserve further study to investigate the intermolecular interaction between CV and PVK.

ADDITIONAL REFERENCES

1. P. Franken, A. E. Hill, C. W. Peters and G. Weinreich, Phys. Rev. Lett. 7, 118 (1961).

2. J. A. Armstrong, N. Bloembergen, J. Ducuing and P. S. Pershan, Phys. Rev. 127, 1918 (1962).

3. N. Bloembergen, "Nonlinear Optics", Benjamin: New York, 1965.

4. L. D. Landan and E. M. Lifshitz, "Electrodynamics of Continuous Media", Pergamon Press: London and New York, 1960.

5 D. M. Faries, K. A. Gehring, P. L. Richards and Y. R. Shen, Phys. Rev. 180, 363 (1969).

6. E. J. Woodbury and W. K. Ng, Proc. IRE 50, 2347 (1962)

7. W. Kaiser and C. G. B. Garrett, Phys. Rev. Lett. 7, 229 (1961).

8. J. J. Hopfield, J. M. Worlock and K. Park, Phys. Rev. Lett. 11, 414 (1963).

9 R. W. Terhune, Bull. Am. Phys. Soc. 8, 359 (1963).

10. P. D. Maker and R. W. Terhune, Phys. Rev. 137, A801 (1965).

11. N. Bloembergen, "Nonlinear Spectroscopy" ed. N. Bloembergen, North-Holland Publishing Co.: Amsterdam, 1977.

12. M. D. Levenson, C. Flytzanis and N. Bloembergen, Phys. Rev. B6, 3962 (1972).

13. S. A. Akhmanov, V. G. Dmitriev, A. I. Kovrigin, N. I. Koroteev, V. G. Tunkin and A. I. Kholodnykh, JETP Lett. 15, 425 (1972).

14 J. J. Wynne, Phys. Rev. Lett. 29, 650 (1972).

15. I. Chabay, G. K. Klauminzer and B. S. Hudson, Appl. Phys. Lett. 28, 27 (1976).

16. R. M. Hochstrasser, G. R. Meredith and H. P. Trommsdorff, J. Chem. Phys. 73, 1009 (1980).

17. P. L. DeCola, R. M. Hochstrasser and H. P. Trommsdorff, Chem. Phys. Lett. 72, 1 (1980).

18. P. L. DeCola, J. R. Andrews, R. M. Hochstrasser and H. P. Trommsdorff, J. Chem. Phys. 73, 4695 (1980).

19. J. R. Andrews, R. M. Hochstrasser and H. P. Trommsdorff, Chem. Phys. 62, 87 (1981).

20. J. R. Andrews and R. M. Hochstrasser, Chem. Phys. Lett. 82, 381 (1981).

21. J. R. Andrews and R. M. Hochstrasser, Chem. Phys. Lett. 83, 427 (1981).

22. R. Bozio, P. L. DeCola and R. M. Hochstrasser, in "Time Resolved Vibrational Spectroscopy", G. H. Atkinson, Ed., Academic Press: New York, 1983.

23. T-C Chang, C. K. Johnson and G. J. Small, J. Phys. Chem. 89, xxxx (1985).

24. B. H. Hesp, and D. A. Wiersma, Chem. Phys. Lett. 75, 423 (1980).

25. F. Ho, W.-S. Tsay, J. Trout and R. M. Hochstrasser, Chem. Phys. Lett. 83, 5 (1981).

26. K. Duppen, B. Hesp and D. A. Wiersma, Chem. Phys. Lett. 79, 399 (1981).

27. F. Ho, W.-S. Tsay, J. Trout, S. Velsko and R. M. Hochstrasser, Chem. Phys. Lett. 97, 141 (1983).

28. E. L. Chronister and D. D. Dlott, J. Chem. Phys. 79, 5286 (1983).

29. C. L. Schlosser and D. D. Dlott, J. Chem. Phys. 80, 1394 (1984).

30. Y. R. Shen, "The Principles of Nonlinear Optics", Wiley-Interscience Publication: New York, 1984.

31. S. A. J. Druet, J.-P. E. Taran and Ch. J. Borde', J. Phys. (Paris) 40, 819 (1979).

32. J. L. Oudar and Y. R. Shen, Phys. Rev. A22, 1141 (1980).

33. N. Bloembergen, H. Lotem and R. T. Lynch, Indian J. Pure Appl. Phys. 16, 151 (1978).

34. J. M. Hayes, R. P. Stout and G. J. Small, J. Chem. Phys. 74, 4266 (1981).

35. G. J. Small, in Molecular Spectroscopy; V. M. Agranovich and R. M. Hochstrasser, Eds., North Holland Publishing Co.: Amsterdam, 1983.

36. B. L. Fearey, T. P. Carter and G. J. Small, J. Phys. Chem. 87,3590 (1983).

37. K. Duppen, D. P. Weitekamp and D. A. Wiersma, J. Chem. Phys. 79, 5835 (1983).

38. W. H. Hesselink and D. A. Wiersma, J. Chem. Phys. 74, 886 (1981).

39. W. H. Hesselink and D. A. Wiersma, J. Chem. Phys. 73, 648 (1980).

40. B. Dick and R. M. Hochstrasser, J. Chem. Phys. 78, 3398 (1983).

41. C. Flytzanis, "Quantum Electronics", Vol. A; H. Rabin, C. L. Tang, Eds., Academic Press: New York, 1975.

42. P. N. Butcher, "Nonlinear Optical Phenomena", Ohio State Univ. Press: Columbus, 1965.

43. R. N. Dewitt, A. B. Harvey and W. M. Tolles, NRL Memorandum Report 3260, Naval Research Laboratory, Washington, D.C., 1976.

44. W. Demtroder, "Laser Spectroscopy", Springer-Verlag: Berlin, 1981; p 65.

45. T. G. Schmalz and W. H. Flygare, in "Laser and Coherence Spectroscopy", J. I. Steinfeld, Ed., Plenum Press: New York, 1978.

46. A. R. Bogdan, Y. Prior and N. Bloembergen, Opt. Lett. 6, 82 (1981).

47. Y. Prior, A. R. Bogdan, M. Dagenais and N. Bloembergen, Phys. Rev. Lett. 46, 111 (1981).

48. A. Bogdan, M. Downer and N. Bloembergen, Phys, Rev. A24, 623 (1981).

49. N. Bloembergen and M. D. Levenson, in "High-Resolution Laser Spectroscopy", K. Shimoda, Ed., Springer-Verlag: Berlin, 1976.

50. W. H. Flygare, "Molecular Structure and Dynamics", Prentice-Hall Inc.: Englewood Cliffs, 1978.

51. A. Yariv, "Quantum Electronics", John Wiley and Sons Inc.: New York, 1975.

52. R. W. Boyd, M. G. Raymer, P. Narum and D. J. Harter, Phys. Rev. A24, 411 (1981).

53. F. Ouellette and M. M. Denariez-Roberge, Can. J. Phys. 60, 877 (1982).

54. B. Dick and R. M. Hochstrasser, Chem. Phys. 75, 133 (1983).

55. B. Dick and R. M. Hochstrasser, Chem. Phys. Lett. 102, 484 (1983).

56. L. A. Carreira, T. C. Maquire and T. B. Malloy, Jr., J. Chem. Phys. 66, 2621 (1977).

57. M. D. Levenson, "Introduction to Nonlinear Laser Spectroscopy", Academic: New York, 1982.

58. T-C. Chang and G. J. Small, Chem. Phys. to be published.

59. T. P. Carter, B. L. Fearey, J. M. Hayes and G. J. Small, Chem. Phys. Lett. 102, 272 (1983).

60. J. M. Hayes, B. L. Fearey and G. J. Small, to be published.

61. B. L. Fearey, T. P. Carter and G. J. Small, Chem. Phys., submitted.

62. R. Jankowiak and H. Bassler, Chem. Phys. Lett. 101, 274 (1983).

63. R. Jankowiak and H. Bassler, Chem. Phys. Lett. 95, 124 (1983).

64. J. Friedrich, J. D. Swalen and D. Haarer, J. Chem. Phys. 73, 705 (1980).

65. J. Friedrich, H. Wolfrum and D. Haarer, J. Chem. Phys. 77, 2309 (1982).

66. M. D. Levenson, IEEE J. Quantum Electron. QE-10, 110 (1974).

67. R. T. Lynch, Jr. and H. Lotem, J. Chem. Phys. 66, 1905

(1977).

68. H. Lotem, R. T. Lynch, Jr. and N. Bloembergen, Phys. Rev. A14, 1748 (1976).

69. R. T. Lynch, Jr., S. D. Kramer, H. Lotem and N. Bloembergen, Opt. Commun. 16, 372 (1976).

70. R. T. Lynch, Jr., H. Lotem and N. Bloembergen, J. Chem. Phys. 66, 4250 (1977).

71. M. D. Levenson and N. Bloembergen, Phys. Rev. B10, 4447 (1974).

72. S. D. Kramer and N. Bloembergen, Phys. Rev. B14, 4654 (1976).

73. P. K. Dutta, R. Dallinger and T. G. Spiro, J. Chem. Phys. 73, 3580 (1980).

74. G. Rippen, G. Kaufmann and W. Klopffer, Chem. Phys. 52, 165 (1980).

ACKNOWLEDGEMENTS

Many thanks to those who were part of this research either directly or indirectly.

I would like to express my sincere thanks to Professor Gerald J. Small for his expert guidance during the course of this research. The work described in this thesis could not have been completed without his helpful advice and patient discussion.

I would like to acknowledge and thank Dr. John Hayes for his valuable advice and help in the laboratory. A special thanks to Dr. Carey Johnson, who helped me get started with the initial experiments. I enjoyed the fellowship of the books of "Ephesians and Timothy" with Carey during the lunch time.

I owe thanks to the other members of the group, particularly Dr. Sylvia Stevenson Adelman and Maureen Connolly for providing the purified naphthalene, Bryan Fearey and Tom Carter for providing the NPHB spectra and most of polymer samples as well as useful discussions, and Mike McGlade for his help in the laboratory. A special thanks to Tom Carter, Mike Kenney and Bryan Isaac for their kind help in correcting my English.

I would like to thank my parents, Chen-Yu and Sin-Ju, and my parents-in-law, Ting-Chih and Hsiu-Chu, for their endless support and love. I also owe thanks to my two little kids,

Joshua and Joel. They have brought me many happy times, especially after I was exhausted from working in the laboratory.

My deepest gratitude goes to my wife, Yu-ching, not only for her skillful typing of this work but for her patient understanding and encouragement, and, most of all, her love.

"In returning and rest you shall be saved; in quietness and in trust shall be your strength," Isaiah 30-15. I appreciate God's guidance not only in the research here but throughout the many phases of my life.